On the Use of Modern Control Theory for Active Structural Acoustic Control

by

William R. Saunders

Dissertation submitted to the Faculty of the

Virginia Polytechnic Institute and State University

in partial fulfillment of the requirements for the degree of

Doctor of Philosophy

in

Mechanical Engineering

APPROVED:

Harry H. Robertshaw, Chairman
Mechanical Engineering Department

William T. Baumann
Electrical Engineering Department

John A. Burns
Mathematics Department

Chris R. Fuller
Mechanical Engineering Department

Yuan-Ning Liu
David Taylor Research Center

Alfred L. Wicks
Mechanical Engineering Department

December, 1991
Blacksburg, Virginia

On the Use of Modern Control Theory for Active Structural Acoustic Control

by

William R. Saunders

Committee Chairman: Harry H. Robertshaw

Mechanical Engineering Department

Abstract

A modern control theory formulation of Active Structural Acoustic Control (ASAC) of simple structures radiating acoustic energy into light or heavy fluid mediums is discussed in this dissertation. ASAC of a baffled, simply-supported plate subject to mechanical disturbances is investigated. For the case of light fluid loading, a finite element modelling approach is used to extend previous ASAC design methods. Vibration and acoustic controllers are designed for the plate. Comparison of the controller performance shows distinct advantages of the ASAC method for minimizing radiated acoustic power. A novel approach to the modelling of the heavy fluid-loaded plate is developed here. Augmenting structural and acoustic dynamics using state vector formalism allows the design of both vibration and ASAC controllers for the fluid-loaded plate. This modern control approach to active structural acoustic control is unique in its ability to suppress both persistent and transient disturbances on a plate in a heavy fluid. Numerical simulations of the open-loop and closed-loop plate response are provided to support the theoretical developments.

Acknowledgements

The completion of this dissertation was certainly a challenge for me in many ways. Alone, I could not have done it. I am grateful for the help and support of so many people. I would like to personally recognize everyone but it would quickly get overblown. Instead, I acknowledge a selected few for their assistance and to all the rest: Thank you.

First, I would like to acknowledge the members of my committee. Thanks Al, for always provoking the extra question and for playing a great third base. Thanks to John Burns and Gene Cliff for the humbling discussions back in the brainstorming phase of ASAC work at VPI. Thanks to Chris for believing something good would actually come from all that mathematical jumble. Thanks Liu, for keeping the conjugate consistent and for the encouragement in the early years. Many thanks to Bill (and his wonderful family) for the theory, the enthusiasm, and the support through it all. Finally, thanks to my mentor, Harry H. Robertshaw. My sincerest thanks and appreciation for the technical, administrative and worldly assistance through the entire program and beyond. Your example will always be an incentive to me.

A special thanks goes out to all my peers. Thanks to: Buddy and Laura, the pillars, Robert and Carol, for always being there, Ken, for always having an answer (which was almost always the right one), Steve R., for riding the seesaw we were on during the plate experiment, Jeff V., for everything you showed me, Rob C., for being a dedicated noise boy, Paul T., Bob S., Dan C. and lastly Tom, for (almost) always completing my assists and relating to the events that put us here today.

Thanks are also sent to my family of origin. Thanks Mom and Dad. I know it wasn't easy for you either. A special thanks for the support from all my brothers and sisters: Jackie, Bob (and Laurie), Don, Barb, and Liz. You were all there when I needed you.

To my own family, I express my sincere appreciation and regrets. It wasn't an even trade and I apologize for the hardships. To Connie, my most heartfelt appreciation for the support in the early years and my most sincere regrets that I asked you to weather this final academic voyage. May you find your bliss on that opposite shore. To Emily, Laura, and Ben, I offer my deepest thanks for playing a role which you cannot, perhaps will never, truly understand. I love you all.

Several other people were instrumental in helping me complete my requirements in a timely fashion. Thanks to Laurie Shea, an absolutely marvelous woman, all of the children from the IC group, and all the spirits at Cooper House. A special thanks also goes out to John Bradshaw for the Homecoming.

The work was sponsored under an ONR grant N0014-88-K-0721.

Last, I give thanks to the Lord. Only He knows what this really took from me and gave to me. I trust that the knowledge gained was worth the price of the pain.

Contents

List of Figures

List of Tables

Nomenclature

Roman letters

c_o	acoustic wave velocity
d	disturbance force vector
d_k	generalized disturbance force vector
f_k	generalized control force vector
h	thickness
j	$sqrt{-1}$
k_o	acoustic wavenumber
k_p	plate flexural wavenumber $(\sqrt{k_y^2 + k_z^2})$
m	modal index in z direction
m_p	plate mass density
n	modal index in y direction
p	farfield acoustic pressure
p^s	acoustic surface pressure
p_k	generalized surface pressure
q	structural displacement, physical coordinates
s	Laplace variable $(j\omega)$
t	time
u	control force vector
w	structural displacement, modal coordinates
y	modal acceleration
C	generalized damping matrix
C_p	damping differential operator
D	flexural rigidity
E	Young's modulus
$G(\omega)$	radiation filter matrix
K	generalized stiffness matrix
L_y	length in y direction
L_z	length in z direction
M	generalized mass matrix

$M(\omega)$	radiated power operator matrix
N	fluid loading parameter - farfield approximation
Q	state cost weighting matrix
R	control cost weighting matrix
S	area
W_a	augmented state vector
Z_{rad}	fluid loading impedance matrix
Z	fluid loading force vector

Greek letters

ρ_p	structural density
ρ_o	acoustic fluid density
δ	delta function
ϵ	intrinsic fluid loading parameter
ω_g	coincidence frequency
ω_k	in vacuo resonant frequency
ω_k^f	fluid-loaded resonant frequency
ν	Poisson ratio
ψ	plate eigenvectors
ζ	viscous damping parameter
Ψ	velocity potential
Π	radiated power
Φ	eigenvector weighting matrix for control signal
Γ	eigenvector weighting matrix for disturbance signal

General

∇	del operator, cartesian coordinates
$<>$	space-time averaged value
i, j	matrix element index
$\hat{}$	Fourier transformed variable
$\dot{}$	first time derivative
$\ddot{}$	second time derivative
^{T}	transpose of a matrix or vector
$*$	hermitian of a matrix or vector

Chapter 1

Introduction

Active Structural Acoustic Control (ASAC) is an extension of active vibration control technology. ASAC is different from existing active vibration control techniques in that the acoustic controllers are designed to modify only the radiating portion of a structure's velocity field. Obviously, this might be accomplished easily if the output of microphones (or hydrophones, for a submerged structure) were made available to the control system. However, it should be clear that the availability of farfield acoustic sensors is not practical in a variety of ASAC applications. This report proposes ASAC designs, intended to minimize farfield radiated acoustic power, which do not require farfield measurements.

It is important to distinguish the objective of ASAC among several closely related control approaches. Active noise control, designed to reduce acoustic pressure or power in a specified domain, does not attempt to modify the velocity field on the source boundary. Noise control strategies attempt to reduce acoustic levels by altering the acoustic velocity potential primarily with external acoustic sources. Active vibration control minimizes some measure of the vibrational energy in a structure with no particular regard to the accompanying change in radiated sound. A nearly inevitable consequence of modifying the structural vibration is a change in the sound

pressure radiated away from the structure. However, the modified acoustic radiation may be higher or lower. It is possible to use active vibration controllers to lower the structural acoustic response if proper weighting of the cost function is employed. However, this approach requires an iterative process. The designer monitors the change in closed-loop radiated pressure and adjusts the controller after each observation, until the desired acoustic response is achieved. An example of this type of design approach was presented by Meirovitch and Thangjitham [1, 2]. The attractive feature of ASAC is the controller's ability to optimally reduce farfield acoustic power output from a structure using sensors and actuators located on the structure itself. This approach relies on proper modelling of the structural acoustic dynamics.

The intention of this research is to design ASAC compensators and to assess numerically the performance of the resulting closed-loop plants. A relatively simple geometry is chosen for the investigation. The structural-acoustic plant examined here is a rectangular plate with simply-supported boundary conditions and mounted in an infinite baffle. One side of the baffle is assumed to be in vacuo; the other side is exposed to a compressible fluid medium of some specified acoustic impedance. The purpose of choosing the simply-supported plate is twofold: to facilitate the acousticians' understanding of the closed-loop dynamics introduced by feedback control systems and to allow verification of the structural-acoustic modelling required for the ASAC design. Additionally, a testbed experiment for control law validation exists at the Smart Structures Laboratory at VPI & SU. The experiment is a simply-supported steel plate which may be used to verify any ASAC results suggested by this research.

This research investigates modern control approaches to minimize acoustic radiation

from a simply-supported plate excited by mechanical disturbances of arbitrary waveform. The disturbances may be steady-state (i.e. harmonic), persistent stochastic (e.g. broadband) or transient in nature. Two distinct cases are considered: ASAC of the plate under light fluid loading (i.e. in air) and ASAC of the plate under heavy fluid loading (i.e. submerged in water). From the acoustics perspective, the two cases are quite different. If we examine the equation of motion for the general problem, using a linear operator form, we have

$$\mathbf{Z_p} w(y,z,t) = d(y,z,t) - \mathbf{Z_{rad}} w(y,z,t) \tag{1.1}$$

where

$$\begin{aligned} w(y,z,t) &= \text{plate normal velocity} \\ d(y,z,t) &= \text{general disturbance input} \\ \mathbf{Z_p} &= \text{plate impedance operator} \\ \mathbf{Z_{rad}} &= \text{(fluid) specific acoustic impedance.} \end{aligned}$$

It will be shown in the following chapters that the fluid impedance Z_{rad} is negligible for relatively low density fluids. The presence (or not) of this term in equation 1.1 changes the dynamics of the fluid-structure system substantially. This is because of the substantial surface pressure created by acoustic radiation into a dense fluid (e.g. water). The surface pressure introduces dynamic feedback of the acoustic response to the structural response, as shown in figure 1.1.

When the fluid may be considered light, in terms defined later in this report, the feedback path from the acoustic pressure to the elastic structure is insignificant and may be considered to be "open". However, for the case of intermediate to heavy fluid loading the "closed-loop, open-loop" form of figure 1.1 produces an additional force on the structure. It is then required to account for the structural feedback

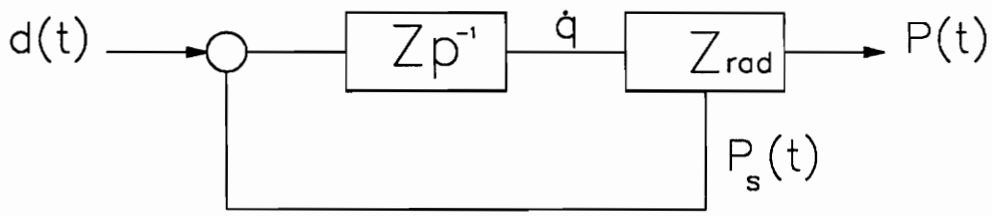

Figure 1.1: Open-loop block diagram of structural radiation in a heavy fluid

forces caused by the surface pressure in the dynamic model used for the control law. In principle, the addition of a force input to the plate is straightforward. However, examination of the form of the acoustic feedback force indicates that the force is a function of excitation frequency. For a harmonic disturbance on the submerged plate, the realization of a state-space control law for vibration suppression, with acoustic considerations, follows directly and was recently posed by Meirovitch [2]. The work proposed here seeks to remove the harmonic restriction, and introduce the fluid-loaded acoustic dynamics directly to the controller. The impact of the fluid-loaded plate's acoustic dynamics on the controller form and performance will be of principal concern throughout.

The bandwidth of the controller will be designed for subsonic acoustic control only. Here the notion of subsonic is referenced to the relative Mach numbers of wave propagation in the fluid and structural mediums. It is recognized that acoustic radiation from a structure is related to the supersonic region of the wavenumber spectrum even for the subsonic bandwidth of the chosen definition. From a control perspective, it is helpful to refer to relative phase speed variables (i.e. M) because the acoustic radiation in the subsonic region is highly proportional to modal amplitudes of the structural response. This enables a modified modal control approach for the ASAC application. A wealth of knowledge about modal control systems is available, thus the development of ASAC control laws in the modal coordinate system seems appropriate and will be explored in this research.

A primary contribution of this work will be to pose the equations for vibration/ASAC control of a submerged, simply-supported plate in a state-space LQ framework. Of principal importance is the ability of the controller to provide tran-

sient suppression for the heavy fluid-loaded situation. A review of the literature indicated that state-space control of transient acoustic radiation from submerged structures has not been addressed. The fundamental problems associated with transient control of submerged structures will be reviewed in Chapter 4. A method to provide the controller with the ability to minimize the acoustic radiated power for either transient or persistent disturbances on the structure will be derived and illustrated using numerical analysis.

Additional contributions include a similar ASAC formulation for a plate in a light acoustic medium, with these results providing a control law which may be implemented on the testbed in the lab. Previous analysis showed that ASAC of a clamped-clamped beam is realizable using LQ theory [3]. That analysis introduced the radiation filter matrix, a significant contribution to ASAC research. Radiation filters provide the controller with the ability to minimize only the radiated acoustic power. A complete discussion of radiation filters is provided in Chapter 3. The results of the clamped beam analysis indicated that a similar formulation could be extended to the 2-d structure. The emphasis here will be the design of realistic radiation filters for the experimental setup.

Final introductory comments on the organization of this report will be helpful. A literature review surveys a broad variety of publications which are relevant to the research presented here. Important developments in the fields of structural acoustics, active vibration control, and active structural acoustic control are discussed in Chapter 2. A brief summary of similar control theory research being pursued by the aeroelastic community is included, also. The remainder of the dissertation follows two distinct themes: ASAC of a lightly fluid-loaded plate and ASAC of a heavy

fluid-loaded plate.

ASAC control of a lightly fluid-loaded plate is the subject of Chapter 3. First, the dynamic model of the simply-supported plate is reviewed analytically and developed using a finite element approach. Next, radiation filters are calculated using the numerical model results. The design of the ASAC controller is presented and simulations of the closed-loop performance for the plate are provided. Three different disturbance waveforms are examined: a harmonic disturbance at the second mode frequency, a broadband disturbance whose bandwidth excites all of the controlled modes and an impulsive disturbance. Simulation results are shown in both frequency and time domain format. A comparison of the ASAC control approach to a vibration control approach is provided via the simulation results.

The development, design and performance of an ASAC controller for the heavy fluid-loaded plate is presented in Chapter 4 and Chapter 5. A detailed discussion of the structural acoustic modelling is given in Chapter 4. An analytical approach, based on the in-vacuo modes of the system, is used to determine the radiation impedance matrix. A method is presented which allows formulation of a time invariant state matrix for the coupled fluid-structure dynamics equations in state-space notation. State equations for the open-loop and closed-loop systems are derived in Chapter 5. The control law for the vibration and acoustic active control schemes are included in the closed-loop equations. Simulation results of a vibration controller and an ASAC controller are presented using a similar format to that for the light fluid plate simulation work. Finally, a discussion of the conclusions and recommendations which result from this dissertation is included in Chapter 6.

In closing these introductory remarks, the author would like to highlight the fact that development of modern control theory ASAC design methods is quite new in the literature. It is expected that there are a large number of structural acousticians who know, or care to know, little about modern controls. Similarly, the lack of ASAC theory to date indicates that there is an equal percentage of control theorists who have never worked with a structural acoustic plant. This research strives to remain straightforward in its approach from both the acoustics and controls perspectives. The author has attempted to include sufficient references throughout for both types of readers to become integrated. Controls is a science which does not exist of itself, but relies on some physical science which describes the dynamics of a plant to be controlled. The ideas proposed in this research are intended to promote a feedback system between acousticians and control theorists for the further development of ASAC.

Chapter 2

Literature Review

Control theory is typically concerned with regulating the flow of a physical system variable (such as energy, information, etc.) such that the regulated system behaves in a manner specified by the design engineer [4]. This definition implies that it is necessary to have knowledge of the pertinent system dynamics and mastery of the specific branches of control theory required to perform the desired regulation. The following summary highlights previously published technical literature discussing the relevant system dynamics for ASAC of a steel plate (in air or water) and various controller designs for vibration and structural acoustic control.

Three separate discussions are included. First, the physics of the plate acoustics are reviewed by examining appropriate studies spawned by the subject of classical acoustics. Second, the applied field of active control is summarized by introducing the reference material most applicable to the problem investigated in this research. Finally, a discussion of existing ASAC studies is provided.

2.1 Classical acoustics

For this investigation, the system is a vibrating elastic body in a compressible fluid medium of arbitrary density. This type of system gives rise to time-dependent pressure fluctuations around the static pressure in the fluid. The general study of structural vibration and the subsequent generation of sound was originated nearly a century ago in Lord Rayleigh's **Theory of Sound** [5]. The broad field of classical acoustics, defined here as the study of solutions to the inhomogenous wave equation in a stationary fluid medium, has received a great deal of attention. Approximately fifty years ago, dynamics of the structure-fluid interaction were introduced to the acoustics problem. The original work in this area is generally attributed to Lax [6] who investigated the effect of resistive and reactive radiation loading on the mode shapes of a vibrating diaphragm. This important step provided the ability to distinguish efficient versus inefficient velocity distributions for varying regimes of frequency. Today, structural acoustics has become an important branch of classical acoustics. Several excellent texts are available which examine the physics of the structure-fluid-acoustic interaction [7, 8, 9]. Next, a few brief comments on the acoustic boundary value problem will be provided followed by a discussion of relevant past work in the structural acoustics discipline.

2.1.1 Structural Acoustics

The differential equation relating the temporal and spatial fluid parameter fluctuations about their ambient (static) values is called the wave equation. A derivation of the linear wave equation is generally straightforward and typically follows from the equations of fluid mechanics. Derivations are included in most acoustic textbooks,

such as Ross [10] and Kinsler and Frey [11]. It is important for the control design engineer to understand the underlying assumptions built into the system dynamics which describe this plant. Since the structural acoustic dynamics introduced later are subject to the wave equation, a complete derivation of the wave equation is included in Appendix A.

A description of the pressure field radiated by an elastic body in free or forced vibration is determined by solving the homogenous wave equation in conjunction with the boundary condition prescribed over the radiating surface. The two equations are:

- *Acoustic wave equation in a stationary fluid*

$$\nabla^2 p(x,y,z,t) - (\frac{1}{c_o^2})\frac{\partial^2 p(x,y,z,t)}{\partial t^2} = 0 \tag{2.1}$$

where $p(x,y,z,t)$ is the acoustic pressure and c_o is the phase speed of the acoustic medium.

- *Conservation of momentum at solid-fluid interface*

$$\frac{\partial p(0,y,z,\omega)}{\partial x} = -\rho_o \frac{\partial v(0,y,z,t)}{\partial t} \tag{2.2}$$

where ρ_o is the fluid density and $v(x,y,z,t)$ is the acoustic particle velocity. The structure is assumed to be planar, lying in the y,z plane. These two conditions, along with the imposition of the kinematic condition at the solid-fluid interface, comprise the boundary value problem of a radiating elastic body.

Solutions of the boundary value problem described above can be posed in the time

domain or frequency domain. Once the appropriate structural dynamics are coupled into the problem, the radiated acoustic pressure may be described for both transient and steady-state excitation. It is possible to determine transient signatures of radiated noise by convolving the acoustic radiation impulse response with the applied force time history [12, 13]. However, this approach will not be addressed here. Instead, traditional steady-state analysis methods will be employed to calculate acoustic quantities such as pressure, power, radiation impedance, etc. As suggested by Baumann et.al. [3], if the resulting expressions can be approximated by rational transfer functions between relevant inputs and outputs, then the system will be completely specified. This is a natural consequence of the relation between a system's transfer function and impulse response function. By "building" filters having the calculated transfer functions, the response of the system to transient, as well as steady-state, excitations can be computed by applying the desired input waveform to the filter and observing the output. Note that filtering the input in the time domain is a causal operation and thus can be implemented in real time. Finally, cascading the transfer function representations into a state-space description will provide time histories of all system states.

For steady-state (harmonic) conditions, equation 2.1 becomes the homogeneous Helmholtz equation:

$$(\nabla^2 + k_o^2)p(x, y, z, t) = 0 \tag{2.3}$$

with the wavenumber defined by $k_o = \frac{\omega}{c_o}$. Solution of equation 2.3 provides the acoustic pressure radiated from the structure. An excellent discussion of the general formulation of the pressure field of arbitrary source configurations is given by Junger and Feit [8]. They show that by manipulation of equation 2.3, the pressure field can

be represented by a surface integral of a linear combination of surface pressure and acceleration. Without detail, the resulting linear integral equation, known as the Helmholtz integral equation, will be stated as

$$p(x,y,z,t) = \int_{S_o} \left(p(0,y,z,t)\frac{\partial g}{\partial z} + \rho_o \dot{v} g \right) dS(0,y,z) \tag{2.4}$$

where g is the Green function of the problem and the integration is over the surface S_o.

The difficulty in solving equation 2.4 arises from the fact that only the acceleration distribution on the boundary is specified. For arbitrary source configurations and general solutions over a broad frequency range, the surface pressure distribution must be obtained numerically. Significant research has been completed in this area, resulting in sophisticated numerical codes [14, 15]. Fortunately, the integral equation can be avoided under certain circumstances. First, if the fluid loading is insignificant, the surface pressure will be negligible. Second, for certain source geometries, the surface pressure term in equation 2.4 disappears. A planar source, mounted in an infinite baffle, is one of those. For both cases, the simplification of equation 2.4, in conjunction with an assumption that the pressure is defined in the farfield, results in the well-known Rayleigh integral

$$p(x,y,z,t) = \frac{\rho}{2\pi R} \int_{S_o} exp(ik\,|R - R_o|)\dot{v}(R_o) dS(R_o) \tag{2.5}$$

For the light fluid-loaded problem discussed in the Chapter 3, the Rayleigh integral will be sufficient to develop the structural-acoustic plant dynamics. However, when the fluid density becomes significant relative to the structural density, a slightly different approach will be introduced to solve the specified boundary value problem.

That approach employs Fourier transform methods and will be discussed in Chapter 4.

Next, a very important physical concept in structural acoustics is stated because of its relevance to the ASAC approach given in this paper. For an infinitely extended radiator, it can be shown that there is a coincident frequency where acoustic radiation "cuts on." There are various ways to show this. For example, consider the infinite plate which has a steady-state velocity ($exp[-i\omega t]$ is implied) given by

$$v(x) = V\ exp[-ik_B x] \tag{2.6}$$

where k_B is the flexural wavenumber of the plate vibrations. Then, an expression for the sound pressure in the half-space above the plate is [7]

$$p(x,y) = \frac{V\rho_o c_o}{(1-\frac{k_B^2}{k_o^2})^{\frac{1}{2}}}\ exp[-ik_B x]\ exp[-i(k_o^2 - k_B^2 y)^{\frac{1}{2}}. \tag{2.7}$$

Equation 2.7 shows the two fundamentally different regimes for radiation from an infinite plate. For wavelengths of plate vibration which are larger than the acoustic wavelength, the radical in the denominator of equation 2.7 is real and the plate radiates sound. On the other hand, when the wavelength of the plate vibration is smaller than that in the acoustic medium, the radical is imaginary and no sound is radiated. Because of this relationship between wavenumbers, and subsequently phase speeds, of the structure and fluid, the farfield region of silence is called subsonic and the farfield region of sound pressure generation is called supersonic.

This feature of radiating versus non-radiating wavenumbers carries over somewhat to the finite plate. The primary distinction is that an effective cut-on frequency is

spread over a fairly large bandwidth for the finite case. Although there remains a precise value of the coincident frequency for the plate, the wave scattering associated with the finite structure produces radiated acoustic energy even for subsonic excitation. The amount of radiation is proportional to the mach number. This gives rise to the concept of radiation efficiency for specific wavenumbers of the plate. In the subsonic region, finite plate vibrations do not radiate sound efficiently. As the sonic ratio $\frac{k_o}{k_B} = 1$ is approached, the efficiency increases gradually, reaching unity in the supersonic regime.

Low-frequency excitation of finite plates, defined as excitation confined to a bandwidth covering the first n modes of the plate, will be subsonic for the plate dimensions treated in this dissertation. In this regime, the modal radiated pressure is determined mostly by the amplitude of modal vibration. *The ASAC control laws developed later in this paper are designed for subsonic acoustic control.* More will be said about the importance of this statement later in this work.

This concludes the general acoustics background necessary to set up the ASAC plant dynamics. Now, a discussion of the acoustics literature for radiation of a finite plate in a light or heavy fluid medium is provided. First, we deal with the light fluid loading, or plates in air.

Light fluid loading

The acoustic coupling of rectangular radiators in free or forced vibration has received much attention in the literature for the past thirty years. Some of the early benchmark studies of the acoustic response of panels were by Smith [16] and Maidanik

[17]. They defined the radiation resistance by

$$\Pi(\omega) =< v^2 > R_{rad}(\omega), \tag{2.8}$$

where the radiated power $\Pi(\omega)$ is based on the time-space average plate velocity. Using this radiation resistance concept, Maidanik described a radiation classification of panel modes according to their effective source characteristics. It was shown that the subsonic radiation efficiency of different panel modes varied according to the symmetry of the standing wave patterns. Terms such as edge modes and corner modes were defined to describe the physical significance of different plate mode radiation characteristics. These terms will be used throughout this study but will not be re-defined here. The interested reader is referred to the mentioned reference.

Wallace reported on the radiation resistance of a baffled, rectangular panel for varied aspect ratios [18]. He chose simply-supported boundary conditions and used the Rayleigh integral to develop an analytical expression for the plate radiated pressure in the far-field. This allowed a calculation of the radiation resistance, according to equation 2.8.

Later, Wallace extended the results discussed above to provide an estimate of the radiation damping of the plate modes in air [19]. Analytical expressions for the radiation damping were provided which will be used in Chapter 3 to support the assumption of negligible fluid loading for the in-air case. Next, a review of the available literature for finite plates radiating into dense acoustic mediums is given.

Heavy fluid loading

Two metrics of the fluid loading may be used to evaluate the significance of the acoustic radiation on the structural dynamics of a flat plate. The first metric is based on a ratio of the structural mass and the entrained mass of the fluid-loaded structure:

$$N = \frac{\rho_p h}{\frac{\rho_o}{k_p}} \tag{2.9}$$

where the structural mass density is $\rho_p h$ and the layer of fluid "added-mass" is $\frac{\rho_o}{k_p}$. When the fluid density ρ_o is large, the metric N is smaller than unity, indicating significant fluid loading. This is to say that the added mass is significant and must be included in the dynamic formulation of the structural acoustic problem. A second measure of fluid loading was introduced by Crighton and Innes [20]. Two dimensionless parameters were specified to characterize fluid loading at any frequency. An intrinsic fluid loading parameter

$$\epsilon = \frac{\rho_o c_o}{\rho_p h \omega_g} = \left(\frac{\rho_o}{\rho_s}\right)\left[\frac{E}{12\rho_p c_o^2(1-\nu^2)}\right]^{\frac{1}{2}} \tag{2.10}$$

and the phase Mach number

$$M = \frac{k_o}{k_p} = \left(\frac{\omega}{\omega_g}\right)^{\frac{1}{2}} \tag{2.11}$$

may be related to classify the degree of fluid loading according to the regimes identified by Crighton and Innes:

$$\begin{array}{lcccl} \text{Light} & \sim & M & = & O(1) \\ \text{Significant} & \sim & M & = & O(\epsilon) \\ \text{Heavy} & \sim & M & \ll & \epsilon \end{array}$$

For example, the fluid loading parameters for the steel plate which will serve as the structural plant for this research are calculated below for an operational frequency of $60Hz$:

Medium	M		ϵ
air	.126	$\gg$	$7.15e-4$
water	.027	$\ll$	0.133

As expected, in-air vibration corresponds to light fluid loading while in-water vibration must be considered as heavy fluid loading.

Various researchers have reported on the behavior of submerged plates for simply-supported boundary conditions. Junger and Feit discussed a general formulation of expressions for vibration response and sound radiation from a submerged rectangular plate (Section 8.7). It is stated clearly that "... *when such a plate is submerged, each mode may generate an acoustic pressure in the plane of the plate. The resulting pressure distribution due to a single mode is not orthogonal to the other modes. Therefore, if one attempts to formulate the problem in terms of the in-vacuo normal modes, these modes become coupled.*" Their subsequent analysis does pose the problem using the in-vacuo modes as a basis. Analytical expressions for the specific acoustical impedance are presented. The modal coupling on the plate is represented by this fluid-loaded impedance matrix. It is important to note that the self (diagonal) and mutual (off-diagonal) terms in that matrix are known, rational functions of frequency.

The form of the fluid-loaded impedance equations, in transform space, have been examined in some detail by different authors. First, Davies [21] presented asymptotic (low frequency) solutions of the impedance equations. He showed that the

impedance terms describe the important modal coupling due to both fluid inertia and radiation damping effects. The approximate results showed that the effective coupling depends on both wavenumber matching and resonance frequency proximity, and hence on the relative magnitudes of the widths of the resonant peaks and the frequency spacing of the resonances. The work by Davies showed that the inertial coupling terms play a somewhat minor role. It is stated that "*the slight changes in resonance frequencies caused by the inertia coupling are overshadowed by the large changes in frequency caused by the modal self inertia.*"

Mutual radiation coupling terms were shown to be important in certain situations. When the structural damping is small, the resonance peaks are very narrow and separated. Thus the energy of the system is contained in very narrow, separate bands of energy. This prevents any modal interactions. As the structural damping is increased, the widths of the resonance peaks increase. The subsequent modal overlap provides an energy transfer mechanism. The input power to any one mode may be dissipated in the vibrations of many modes, and the relative amount of power dissipated by the plate is increased. This is an interesting comment from an active control perspective. It may be possible that the increased damping introduced by feedback control will lead to increased coupling between the plate modes; the additional power dissipation from the modal coupling would essentially be "free." This concept needs to be examined during the analysis.

The experimental and theoretical dynamics of fluid-loaded plates were investigated by Sandman and Vieira [22]. Again, their approach was to generate the solutions in terms of the in-vacuo normal modes. A numerical solution for relatively low-mode response was presented and shown to be in good agreement with experimental results.

The results indicated that the inertial coupling terms mattered little to plate-fluid resonance frequencies. However, a significant impact on the amplitudes of resonant response was observed because of the cross-modal pressures induced by the fluid. Since the authors did not include damping in their numerical model, it is not possible to comment on the interaction of structural damping and modal coupling discussed previously.

A comparison of the low frequency approximations (by Davies) with numerical results for the modal coupling factors was presented in an analysis of vibration and acoustic radiation of elastically supported rectangular plates by Lomas and Hayek [23]. Consistently, their analysis showed that close proximity of two modes causes significant coupling via the radiation impedance matrix. Examination of the inertial impedance matrix showed that for low frequencies, where the modes are corner modes, the self coupling terms are essentially constant. This fact will be used to simplify the controller design discussed in Chapter 5.

Finally, it is worthwhile to question whether active control may be beneficial in reducing structural acoustic radiation of sound. The active control method proposed in this research uses two mechanisms to reduce the power radiated from the structure. The first mechanism is direct suppression of the any persistent disturbances entering the plant. Clearly, it is helpful to reduce the forced response of the structure. The second mechanism is mechanical damping resulting from modifying the system eigenvalues. The question might be asked, can the introduction of increased mechanical damping by active control be expected to reduce radiated noise from vibrating structures? A qualitative answer to this question may be obtained by discussing the results obtained by Laulagnet and Guyader [24]. They discuss a modal

analysis of an elastic cylinder in a heavy fluid in terms of structurally damped, evenly damped, and radiation damped modes. It is shown that the evenly damped modes, represented by an equal amount of structural damping and radiation damping, radiate the most power. In contrast, the structurally damped modes radiate the least power. Thus, it seems possible to "convert" efficient, evenly damped modes to less efficient, structurally damped modes by adding structural damping through active control strategies.

2.2 Active control

Active control of the structural plant dynamics has been the focus of extensive research for the past thirty years. A wide variety of subjects within the topic of active control may be examined. For example, active control of noise, vibration, attitude of space structures, and airfoil flutter has been investigated by many researchers. This review concentrates on those aspects of active control which are most relevant to this research. The important topics are identified as active vibration control, active flutter suppression, and active structural acoustic control. The inclusion of active flutter control is because of some similarities in the design approach for flutter suppression and the design approach presented for the heavy fluid-loaded plate.

2.2.1 Active vibration control

The active vibration control technology discussed in this section may be categorized according to two different theoretical approaches. Classical control theory is a frequency domain approach to control design and is applicable for low order plants. Franklin et.al. [25] and Takahashi [26] introduce the fundamentals of classical con-

trols. Modern control theory is based in linear systems theory and relies on state vector differential equations to cast the controller design. The resulting matrix equations are more suited for multi-input, multi-output systems; however, the physical insight to the design may be lost along the way. Representative texts which discuss modern control fundamentals are by Dorf [27] and Elgerd [28].

Modern control theory supplies most of the horsepower for the methods discussed in the later chapters. In particular, linear quadratic optimal control theory derives using state-space constraints on the associated variational problem. Kirk [29] and Anderson [30] discuss the optimal control formulation. Generally, the LQ problem results in a matrix Ricatti equation which may be solved for the optimal controller gains. The dual problem may be solved to calculate an optimal state estimator, first proposed by Kalman [31] and Bucy [32]. The results of their studies have become very popular and will be used in the compensator designs presented in this research.

The field of active vibration control includes both feedforward and feedback methods. Feedforward control refers to the placement of a compensator or filter in the forward path of the actuator signal. Typically, the filter is adapted in real time to minimize some error signal specified by the design engineer. An excellent discussion of the feedforward approach is given by Widrow and Stearns [33]. Modern control theory is typically associated with feedback control although the state vector formulation certainly does not prevent the use of feedforward "prefilters". An important distinction between feedback and feedforward controllers is the ability of the feedback controller to suppress both transient and persistent disturbances. Presently, state-of-the-art techniques in feedforward control encounter difficulty in suppressing transient inputs. Another important distinction for the different approaches is

the amount of apriori modelling required by the controller. Modern control design methods must have a reasonably accurate plant model during the design process. It is possible to quantify the accuracy requirements given a specific plant and control objectives. Design of robust controllers may be pursued in future research but will not be covered in this dissertation. Feedforward controller design is less sensitive to modelling error for harmonic or narrowband disturbance compensation. For example, the filtered-X LMS control law requires the transfer function between the error signal and the actuators at the frequencies of interest. However, it is sufficient to know only the correct quadrant for the phase and still obtain excellent closed-loop results. As the bandwidth of the disturbance forces increases, the modelling requirements become more stringent. Finally, either control approach may be designed to suppress structural modes, waves propagating in the structure, power flow, radiated power, etc. This dissertation is devoted to feedback control design. A review of the literature on modal control using feedback methods is discussed next.

Modal Control

Modal control is a popular tool in a great variety of active vibration control applications. Any controller design which is formulated in modal coordinate space is referred to as modal control. An introductory discussion of various types of dynamic systems which may be transformed to a modal coordinate space is given by Inman [44]. A modal description of the system can be posed algebraically or using state vector formalism. The general process of transforming the physical plant coordinates to modal coordinates in the state-space is summarized in Chapter 3. Details of the method are widely known and have been presented by numerous authors. For example, see Chen or Meirovitch [45, 66].

Modal control has a number of advantages in vibration control design. The structural modes are a natural basis and have been the subject of thousands of research articles in the broad field of system identification. For relatively simple structures, it is possible to experimentally determine a structure's modal parameters with enough accuracy for a reliable controller design. State matrices in modal coordinates are in a nice form which allows the designer to retain some physical insight to the problem. Finally, the measurements required to provide state information to the controller are relatively easy as compared to wave propagation or power flow control concepts [34, 35]. Modal control also has some disadvantages. A conversion of the physical coordinates of the output measurements to modal coordinates is required and this conversion introduces potential uncertainties related to observation spillover. Meirovitch and Baruh [36, 37] formally introduced the use of modal filters as a procedure for extracting modal states from distributed measurements. A discrete approach to modal filtering was demonstrated by Rubenstein et.al. [38]. Their results indicated that least-squares solutions to the modal filtering problem serve a useful purpose for vibration control strategies. Another distinct disadvantage of modal control is the requirement for relatively accurate identification of the structure's modal parameters. This may be difficult for complex structures or structures subject to heavy damping, either mechanical or acoustic in origin.

A recent experiment in active vibration control by Rubenstein [46] successfully demonstrated the use of modal coordinates for vibration suppression. Significant reductions in modal vibration were achieved for both transient and persistent disturbances. The modal control experiment used the LQG control law which underlies the light fluid ASAC design presented in Chapter 3. Only the choice of cost function

will change for the acoustic controller versus the vibration controller. Thus, a timely experimental validation of ASAC for light fluid loading should follow the analytical development presented in this research.

2.2.2 Active flutter suppression

A collection of research literature published by the aircraft community during the past fifteen years provides important insight to the general approach of the research reported later in this dissertation. The publications report on the effort to use modern control theory for gust alleviation (i.e. disturbance compensation) and active suppression of flutter. Karpel [39] summarizes the work of previous researchers [40, 41, 42] and the efforts to model the unsteady aerodynamic loads for active controller designs. The difficulty in the aeroelastic design approach is remarkably similar to the difficulty which will be discussed in relation to the ASAC design in the presence of heavy fluid loading. Examining the aeroelastic system equations of motion reveals the open-loop equation in modal coordinates

$$\left([M]\,s^2 + [C]\,s + [K]\right) X(s) = q\,[A(s)]\,X(s) \tag{2.12}$$

where

M = structural mass matrix

C = structural damping matrix

K = structural stiffness matrix

$A(s)$ = aerodynamic influence matrix

q = dynamic pressure

The representation of the unsteady loads for the influence matrix $[A(s)]$ presents the main difficulty in the subsequent controller design. The researchers in the field report on a design technique to overcome this difficulty. It is based on a rational approximation of the unsteady loads in the entire Laplace domain. This yields matrix equations of motion with constant coefficients. Stated otherwise, additional states representing the aerodynamic influence matrix are augmented to the structural system states to form open-loop plant equations with constant coefficient matrices. This is the approach which will be used to design the ASAC controller for the heavy fluid.

It is worthwhile noting that the present emphasis in the active flutter research reported very recently is on minimal realizations for the augmented systems. The system order may grow significantly, and prohibitively, for realistic controller designs. Karpel [43] reports on recent techniques to optimally reduce the system order and maintain the accuracy of the full-order compensator. It is expected that the modern control approach to ASAC will require a similar model reduction effort in future research.

2.2.3 Active structural acoustic control

Active structural acoustic control refers to the active suppression of far-field acoustic power, or some related acoustic variable, through the use of force inputs to the structure. This may be accomplished with or without the use of far-field acoustic measurements. By this definition, the study of ASAC was inititated very recently. Because of the limited amount of literature available, the following discussion will include both feedforward and feedback control approaches to ASAC. An emphasis, of course, will be placed on the existing literature on feedback ASAC design approaches.

The use of structural force actuation to modify a structure's radiated pressure field was initially proposed by Fuller and Jones [47, 48]. This early work was concerned with the development and experimental investigation of an active vibration control system designed to reduce interior sound levels in elastic vibrating cylinders by point force inputs. Microphones were used to supply error signals for a LMS adaptive controller. The experimental results showed that vibration inputs could successfully reduce interior acoustic levels. Later, Fuller discussed and demonstrated the use of structural control of sound transmitted through an elastic plate. As before, the control was applied directly to the plate by point force inputs while the error information was produced by radiated acoustic field measurements. Recently, a large number of ASAC studies have been published by Fuller et.al [49, 50, 51, 52]. Most of the references discuss adaptive LMS control schemes in conjunction with acoustic field measurements. It is worth noting that a very important result was identified in the ASAC research just cited. It was demonstrated that ASAC control accomplished the optimal minimization of radiated sound pressure or power

through two distinct mechanisms. First, direct suppression of the vibration modes proportionately reduced the acoustic output. Second, the acoustic output was also minimized via modal restructuring. This refers to the destructive interference which may take place between two or more vibration modes under persistent excitation. Their research showed that the controller might actually increase certain modes of vibration if the net vibration, and subsequent radiation, might be suppressed through the destructive interference of the participating modes.

Very limited research has been reported on the use of modern control theory for ASAC. Meirovitch and Thangjitham discussed an approach to active control of radiated pressure from a simply-supported plate, for a case of light fluid loading and a submerged plate (presumably heavy fluid loading) [1, 2]. For the in-air case, the authors used an in-vacuo modal basis and LQ theory to minimize a vibration cost function. A Rayleigh integral formulation of the pressure was used to evaluate the closed-loop radiated pressure field produced by a simply-supported plate for different combinations of actuators and sensors. The number and locations of actuators were iteratively modified by the designer to minimize the resulting radiated pressure at a single point in the far-field. It is important to note that the controller did not have the ability to target efficiently radiating modes; this lack of discretion might be expected to increase the number of actuators required. In addition, they did not evaluate the far-field pressure at field points away from the minimized pressure. It is intuitive that the pressure may go up or down at these locations. An overall acoustic power cost function would eliminate this uncertainty. For the submerged plate, a state-space realization of the plate dynamics for harmonic excitation was described which was valid for the acoustic far-field. The analysis presented later in this report will remove this restrictive harmonic assumption and include the rele-

vant acoustic dynamics in the plant. This extension will allow a minimization of the global acoustic power without far-field measurements.

Based on the definition of ASAC stated above, only one group of researchers has published studies of a modern control theory approach to ASAC. Baumann et.al. discussed a LQ optimal approach to minimize the radiated power from a baffled, clamped beam subject to either impulsive loads or stochastic steady disturbances [3, 53]. The general approach in both studies is a modal coordinate formulation of the structural-acoustic plant through the use of the beam equation, a Rayleigh integral representation of the farfield pressure, and augmentation of new acoustic state variables. This is the general approach for the ASAC design discussed in Chapter 3.

Finally, it is emphasized that there exists very little literature reporting on active control of structures in a heavy fluid. Gu and Fuller [54, 55, 56] present feedforward controller designs and results for baffled, infinite and finite rectangular plates radiating into a fluid filled half-space. Presently, to the author's knowledge, no documentation of a feedback active control strategy to suppress transient vibration or acoustic radiation of a fluid-loaded structure is available in the literature. The results presented in this research offer a strategy for both objectives, as the vibration suppression is simply a less restrictive case than the ASAC objective.

Chapter 3

ASAC of a Simply-Supported Plate: Light Fluid Loading

An ASAC design approach for a baffled, rectangular plate radiating sound into a relatively light acoustic medium is presented in this chapter. The controller design relies on a truncated model derived from finite-element analysis, although the model might have been determined from experimental measurements, also. This approach is intended to provide an easy transition of ASAC design methods for simple structures, i.e. a plate, to more complex structures.

The ASAC design discussed here extends the work of Baumann et.al. [3]. First, a structural model is developed using the in-vacuo modes as a basis. This basis may be generated using analytical functions or numerical approximations from a finite-element representation. A choice to use a finite-element approach was made as a precursor of design methods for more complex structures. Next, an estimate of the power radiated to the farfield by the structure for harmonic velocity patterns is described in the Laplace domain. A Hermitian transfer matrix, called the radiated power operator matrix, results from the estimation method. The factor of the transfer matrix is the radiation filter which provides the controller with the neces-

sary information about the efficiently radiating velocity patterns. Augmenting the acoustic information to the state-space model for the structure provides the plant equations required for controller design.

A full development of the plant and controller equations is discussed next. The modelling of the structural dynamics and the acoustic dynamics are provided first. Then the control law is developed and simulated for the simply-supported plate. The acoustic modelling follows the method of Baumann, however the basis for this work derives from FEM analysis.

3.1 Open-loop structural model

Description of the open-loop plant (i.e. the plate) dynamics requires the accurate modelling of three parameters:

1. Plate resonant frequencies
2. Plate damping values
3. Plate modeshapes

Two distinct mathematical approaches, analytical or numerical, may be used to determine these parameters. Additionally, system identification methods may be employed if the plant is physically real. For the theoretical development presented in this dissertation, a blended analytical-numerical approach will be adopted. First, a brief description of the boundary value problem being solved here is presented for clarity. The solution of the equations is then presented in numerical format, using the NASTRAN finite-element solver. Finally, the mechanics of assembling the plant parameters into state-space form is described.

3.1.1 The structural boundary value problem

The bending wave equation for a homogeneous thin plate adequately describes the structural plant. A rectangular coordinate system is used, with the plate taken to lie in the $y, z-$plane. The transverse displacement is parallel to the $x-$axis. A schematic of the plate geometry is shown in figure 3.1. The effects of rotatory inertia and shear deformation are not included in the model. Previous experimental work by Rubenstein [29] indicated good agreement between the eigenstructure of this type of model and a rectangular steel plate.

Without derivation, we can write the differential equation for the plate as

$$m_p \frac{\partial^2 q(y,z,t)}{\partial t^2} + C_p \frac{\partial q(y,z,t)}{\partial t} + D\nabla^4 q(y,z,t) = u(y,z,t) + d(y,z,t) \qquad (3.1)$$

where

$$\begin{aligned} m_p &= \rho_s h \\ D &= \frac{Eh^3}{12(1-\nu^2)} \end{aligned}$$

and a velocity-dependent damping term C_p has been included. The damping is assumed to be proportional. The forcing terms $u(y,z,t)$ and $d(y,z,t)$ correspond to a control force vector and a disturbance force vector. A description of the simply-supported boundary conditions completes the boundary value problem:

$$q(y,z) = \frac{\partial^2 q(y,z)}{\partial y^2} = 0, \quad y = 0, L_y \qquad (3.2)$$

$$q(y,z) = \frac{\partial^2 q(y,z)}{\partial z^2} = 0, \quad z = 0, L_z \qquad (3.3)$$

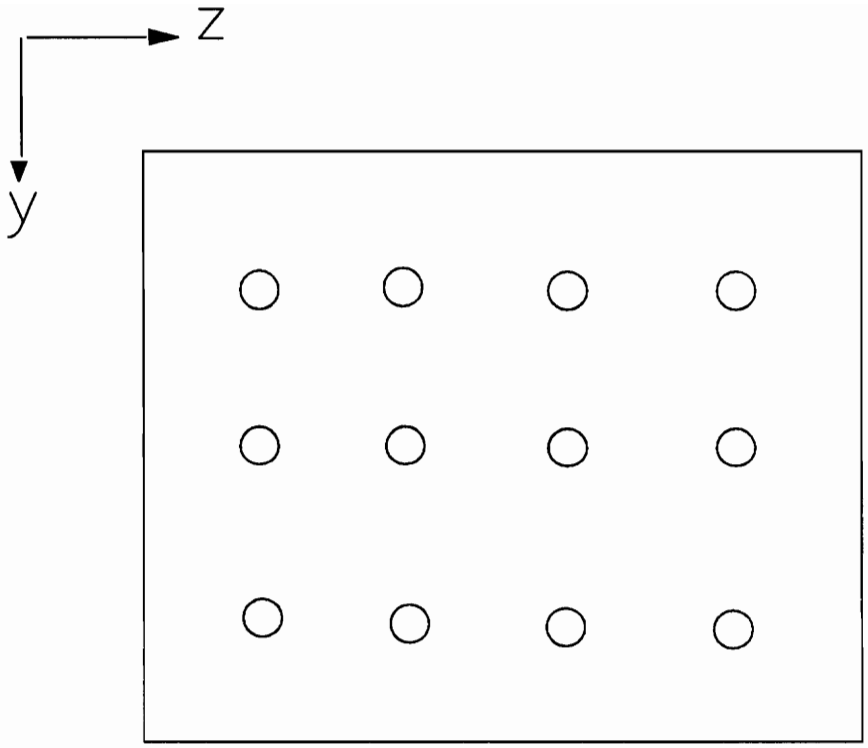

Figure 3.1: Plate geometry in rectangular coordinate system

The functions which satisfy the boundary conditions given by equations 3.2 and 3.3 and the homogeneous solution of equation 3.1 are

$$q_k(y,z) = W_k sin\frac{n\pi y}{L_y} sin\frac{m\pi z}{L_z}, \tag{3.4}$$

where

$$\begin{aligned} m &= 1,2,3.... \\ n &= 1,2,3.... \end{aligned}$$

are the indices of the number of modes which make up the expansion. This analytical approach will also yield eigenvalues of free vibration, or the natural resonances of the plate system.

It is possible to diagonalize the system of equations which result from the modal expansion of equation 3.1 using the shape functions of equation 3.4 if the differential operators of equation 3.1 satisfy certain conditions. The diagonalization is actually a transformation of coordinates to a modal space and is discussed in detail in chapter 5. Because the focus of this chapter is the use of finite-element output to describe the open-loop plant, only the desired form of the plant model will be given here. It is stated that the goal of the finite element analysis is to describe the coefficient matrices for the equation

$$[\mathcal{M}]\,\ddot{w} + [\mathcal{C}]\,\dot{w} + [\mathcal{K}]\,w = P^T u + P^T d, \tag{3.5}$$

where $[\mathcal{M}]$, $[\mathcal{C}]$, and $[\mathcal{K}]$ are diagonal, generalized (i.e. modal) matrices for the mass, damping, and stiffness of the structure, w is the modal position, and $P^T u$ and $P^T d$ represent the corresponding generalized forces on the structure. (The brackets on the matrix quantities will be omitted for the rest of this development.) Of course,

the transformation matrix P is required for this approach.

A practical approach to the development of the simply-supported plate equations may be achieved using NASTRAN. The general approach to develop the modal form of the structural plant equation 3.5 is well-known [4, 44, 66] but is included here for completeness. The following section summarizes the steps required to generate the open-loop state-space equations for some structural model using NASTRAN output.

3.1.2 NASTRAN methodology

The similarity transform of system equations is used for various reasons. For this work, it is desirable to pose the controller in modal form. It is possible to use NASTRAN to perform the transformation of the simply-supported plate equation to modal coordinates. This method was developed during this research and is presented next.

We begin with the matrix form of the the vibration equation, assuming that the damping matrix is proportional to the mass and/or stiffness matrix (see the discussion in chapter 4):

$$M\ddot{q} + C\dot{q} + Kq = u + d. \tag{3.6}$$

where M, C, and K are the physical mass, viscous damping, and stiffness matrices defined by the bulk data entries for the structural model. The displacement vector q consists of translations and rotations for all unconstrained grid points in the model. The force vectors u and d are control forces and disturbance forces, as before. We need the modal matrix P, whose columns are the eigenvectors normalized by the

square root of the generalized mass. These are available in NASTRAN by specifying the MASS option on the *eig* card in the bulk data deck. Thus, the following transformation is sought:

$$q = Pw. \tag{3.7}$$

Substituting equation 3.7 and premultiplying by P^T, we produce the following generalized matrices:

$$\mathcal{M}\ddot{w} + \mathcal{C}\dot{w} + \mathcal{K}w = P^T u + P^T d. \tag{3.8}$$

where

$$\begin{array}{rcll} \mathcal{M} & = & I & \\ \mathcal{C}_{i,j} & = & 2\zeta\omega_n & i = j = n \\ & = & 0 & i \neq j \\ \mathcal{K}_{i,j} & = & \omega_n^2 & i = j = n \\ & = & 0 & i \neq j \end{array}$$

This is the desired form of the matrix equation for the structure's dynamics. The normal modes analysis (e.g. solution sequence 3) in NASTRAN provides the transformation matrix, the generalized mass, and the generalized stiffness for the structure. The generalized damping follows from specification of the value of viscous damping ζ. Next, we can write the state equations for the generalized coordinates as follows:

$$\begin{bmatrix} \ddot{w} \\ \dot{w} \end{bmatrix} = \begin{bmatrix} 0 & I \\ -\mathcal{K} & -\mathcal{C} \end{bmatrix} \begin{bmatrix} w \\ \dot{w} \end{bmatrix} + \begin{bmatrix} 0 \\ P^T \end{bmatrix} u\delta(y-y_j)\delta(z-z_k) + \begin{bmatrix} 0 \\ P^T \end{bmatrix} d\delta(y-y_j)\delta(z-z_k)$$

The form shown above implies that the forces are weighted by the eigenvectors at the respective grid points (y_j, z_k) of application. If we expand the expression $P^T u\delta(y - y_j)\delta(z - z_k)$, assuming, for now, only one applied force at grid point

(y_j, z_k), we get

$$P^T u \delta(y - y_j)\delta(z - z_k) = \phi_{1jk}u_{jk} + \phi_{2jk}u_{jk} + \cdots + \phi_{njk}u_{jk}.$$

Now let u_{jk} be an element in the control vector $u \in \mathcal{R}^m$, define $\Phi \in \mathcal{R}^{n\times m}$ as the eigenvector weighting matrix for the control signal and $\Gamma \in \mathcal{R}^{n\times v}$ as the weighting matrix for the disturbance inputs. Then we can write the state equation as:

$$\begin{bmatrix} \ddot{w} \\ \dot{w} \end{bmatrix} = \begin{bmatrix} 0 & I \\ -\mathcal{K} & -\mathcal{C} \end{bmatrix} \begin{bmatrix} w \\ \dot{w} \end{bmatrix} + \begin{bmatrix} 0 \\ \Phi \end{bmatrix} u \begin{bmatrix} 0 \\ \Gamma \end{bmatrix} d \tag{3.9}$$

Now the output equation depends on how we choose our measured variables. As discussed previously, the testbed experiment relies on measurements of acceleration at chosen grid points of the model. The truncation and transformation of the grid point accelerations to modal coordinate accelerations was discussed in detail by Rubenstein [55]. For an output vector of modal coordinate accelerations

$$\ddot{w} = -\mathcal{C}\dot{w} - \mathcal{K}w + \Phi u + \Gamma d \tag{3.10}$$

the output equation takes the form

$$y = \begin{bmatrix} -\mathcal{K} & -\mathcal{C} \end{bmatrix} \begin{bmatrix} w \\ \dot{w} \end{bmatrix} + \begin{bmatrix} \Phi \end{bmatrix} u + \begin{bmatrix} \Gamma \end{bmatrix} d \tag{3.11}$$

Equations 3.9 and 3.11 form the structural model necessary for the state-space controller design presented in Section 3.3. The order of the various matrices or vectors is summarized below for clarity. $w \in \mathcal{R}^{2n}$ $u \in \mathcal{R}^m$ $y \in \mathcal{R}^{n\times 2n}$ $d \in \mathcal{R}^v$ $\mathcal{K} \in \mathcal{R}^{n\times n}$ $\mathcal{C} \in \mathcal{R}^{n\times n}$ $\Phi \in \mathcal{R}^{n\times m}$ $\Gamma \in \mathcal{R}^{n\times v}$ This completes the development of the state equations via NASTRAN modelling. Notice that we need only the generalized damping matrix, generalized stiffness matrix, and

the modal matrix from NASTRAN. Also notice that there is no requirement to manipulate matrices with dimensions equal to the degrees of freedom of the FEM. The designer may choose to retain the rotational coordinates of the FEM, however truncation of the rotations is desirable. This is because they are not required to describe the normal plate motion, thus they increase the system order unnecessarily. It is possible that generalized moments may need to be described for some other application. Then the retention of the rotational information would be required. Next, the acoustic dynamic modelling will be described in the manner of Baumann et.al. [3].

3.2 Radiation filters

Acoustic dynamics for the simply-supported plate may be derived which describe the farfield radiated pressure and/or power. For the case of light fluid loading, the in-vacuo modes may be used to represent a complete set of radiating velocity patterns on the plate. It will be shown that some of the modes radiate power independently, some of the modes interact in the acoustic farfield, and some of the modes radiate sound more efficiently than others. First, a matrix quantity which represents the farfield acoustic power radiated over some sector of the half-space on one side of the baffle is calculated. It is shown that this matrix may be factored, the factored term representing a transfer function which provides the ability to map modal velocities to farfield power. A state-space representation of the radiation filter is then developed and augmented to the structural model to form a plant whose outputs may be either modal amplitudes or radiated power.

3.2.1 Analytical development

Following the development of section 3.1.2, the plate is modelled by a first-order ordinary differential equation of the form

$$\dot{w} = Fw + Gu + Ld \tag{3.12}$$

where $w \in R^{2n}$ is the state of the system, $u \in R^m$ is a vector of actuator inputs that can be used to control the structure, and $d \in R^v$ is disturbance input of arbitrary waveform. The approximate velocity of the structure at position (y, z) and time t is given by

$$v(y, z, t) \cong \sum_{i=1}^{N} \Phi_i(y, z) w_{2i}(t). \tag{3.13}$$

where the Φ_i functions are the structural modeshapes. It is assumed that equation 3.13 approximates the actual velocity to the desired accuracy.

The pressure in the farfield at the point (R, θ, ϕ) in a fixed spherical coordinate system, due to a harmonic input of frequency ω, can be computed from the Rayleigh integral as

$$p(t) = \frac{j\omega\rho_o}{2\pi} \int_S \frac{v(S,t)e^{jk(R-Ro)}}{(R - R_o)} dS \tag{3.14}$$

where S is the surface area domain (y, z) of the structure. The pressure resulting from the velocity distribution associated with the $i^{\underline{th}}$ spatial function on the structure

$$v(y, z, t) = w_{2i}(t)\Phi_i(y, z) \tag{3.15}$$

where

$$w_{2i}(t) = w_{2i}e^{j\omega t} \tag{3.16}$$

can be written as

$$p(t) = w_{2i}\left[\frac{j\omega\rho_o e^{j\omega t}}{2\pi}\int_S \Phi_i(S)e^{-jkr_s}dS\right]\frac{e^{jkR}}{R}. \tag{3.17}$$

where the factor of e^{jkR} accounts for the propagation delay and the factor of R in the denominator accounts for the spherical spreading loss.

From a system-theoretic point of view, we can consider the input of the system to be the time variation of the $i^{\underline{th}}$ mode, $w_{2i}(t)$, and the output to be the pressure, $p(t)$, at a given point (R, θ, ϕ). For a harmonic input of the form in equation 3.16, equation 3.17 shows that the output can be written as

$$p(t) = \hat{h}(\omega)w_{2i}e^{j\omega t}, \tag{3.18}$$

which is in the form of the steady-state response of a linear system with transfer function $\hat{h}(\omega)$, where $\hat{h}(\omega)$ is the Fourier transform of the system impulse response $h(t)$. (In the remainder of this dissertation, the Fourier transform of a variable will be denoted by a carat, $\hat{}$.) We can characterize the transfer function of a system from steady-state (i.e. harmonic) considerations. This knowledge of the transfer function completely specifies the system since it is equivalent to knowing the impulse response. By building (i.e. specifying a differential equation for) a filter having the desired transfer function, the response of the system to transient, as well as steady-state, excitations can be computed by applying the desired input waveform to the filter and observing the output. Note that filtering the input in the time domain is

a causal operation, and thus can be implemented in real time. The output pressure could also be computed by taking the Fourier transform of the input and then taking the inverse Fourier transform of the product $\hat{h}(\omega)\hat{w}_{2i}(\omega)$, but this cannot be done causally.

We will write the transfer function between the time variation of the velocity, $w_{2i}(t)$, of the $i^{\underline{th}}$ spatial function Φ_i and the pressure in the far field at the point (R, θ, ϕ) as

$$\frac{\hat{p}_i(R, \theta, \phi, \omega)}{\hat{w}_{2i}(\omega)} = \frac{\hat{h}_i(\theta, \phi, \omega)e^{jkR}}{R}. \tag{3.19}$$

where the spatial dependence has been included explicitly and, for notational convenience, the delay and loss terms of the transfer function have been written separately.

Using the real-valued pressure and fixing R, the total energy per unit area radiated into the farfield in direction (θ, ϕ) is given by the integration of the instantaneous power per unit area with respect to time, that is

$$\frac{1}{\rho_o c_o} \int_0^\infty \left[\sum_{i=1}^{N} p_i(R, \theta, \phi, t) \right]^2 dt. \tag{3.20}$$

Comparing equation 3.20 to equation 11 of Mann, et.al. [57] we recognize the expression as a summation of the instantaneous intensity for some spatial segment over time. This time-domain formulation of the radiated power indicates the quadratic cost which will be minimized by the ASAC controller. For the radiation filter design, the expression is desired in the frequency domain.

By Parseval's theorem, this may be expressed as

$$\frac{1}{\pi\rho_o c_o}\int_0^\infty \left|\sum_{i=1}^{N}\hat{p}_i(R,\theta,\phi,\omega)\right|^2 d\omega \tag{3.21}$$

$$= \frac{1}{\pi\rho_o c_o R^2}\int_0^\infty |H(\theta,\phi,\omega)W(\omega)|^2\, d\omega \tag{3.22}$$

$$= \frac{1}{\pi\rho_o c_o R^2}\int_0^\infty W^{T*}(\omega)H^{T*}(\theta,\phi,\omega)H(\theta,\phi,\omega)W(\omega)d\omega \tag{3.23}$$

where

$$W = \begin{bmatrix} \hat{w}_2 \\ \hat{w}_4 \\ \vdots \\ \hat{w}_{2n} \end{bmatrix}; \quad H = \left[\hat{h}_1\ \hat{h}_2\ \ldots\ \hat{h}_n\right]. \tag{3.24}$$

For the above, the complex conjugate is denoted by *, and the units of equation 3.21 are energy per area ($\frac{J}{m^2}$) as expected.

To compute the total radiated energy, integrate equation 3.23 over the surface of a sphere of radius R such that $kR \gg 1$. This yields

$$\int_0^\infty W^{T*}(\omega)\left[M(\omega)\right]W(\omega)d\omega. \tag{3.25}$$

where

$$M(\omega) = \frac{1}{\pi\rho_o c_o}\int_0^{2\pi}\int_0^{\pi} H^{T*}(\theta,\phi,\omega)H(\theta,\phi,\omega)sin\theta d\theta d\phi \tag{3.26}$$

$M(\omega)$ has units corresponding to those of radiation resistance ($\frac{kg}{s}$). Thus the diagonal entries represent, up to a constant term, the self-radiation efficiencies of the

'modes' Φ_i. The off-diagonal terms similarly are the mutual-radiation efficiencies. A discussion of the mutual terms in the matrix is given later.

It is possible to approximately factor the matrix in equation 3.26, to any desired accuracy, as

$$M(\omega) \approx G^{T*}(\omega)G(\omega) \tag{3.27}$$

To see this, note that $H^*(\theta,\phi,\omega) = H(\theta,\phi,-\omega)$ and that $M(\omega)$ can be written as

$$\frac{1}{\pi\rho_o c_o}\int_0^{2\pi}\int_0^{\pi} H^T(\theta,\phi,-\omega)H(\theta,\phi,\omega)sin\theta d\theta d\phi. \tag{3.28}$$

In the Laplace transform domain consider the matrix

$$M(s) = \frac{1}{\pi\rho_o c_o}\int_0^{2\pi}\int_0^{\pi} H^T(\theta,\phi,-s)H(\theta,\phi,s)sin\theta d\theta d\phi \tag{3.29}$$

where $H(\theta,\phi,s)$ is the Laplace transform associated with $H(\theta,\phi,\omega)$ and $M(s)$ agrees with equation 3.28 when $s = j\omega$. The matrix $M(s)$ is real ($M^*(s) = M(s^*)$), para-conjugate, hermitian ($M^{T*}(s) = M(-s^*)$), and non-negative on the real-frequency axis $s = j\omega$ ($b^{T*}M(j\omega)b \geq 0 \quad \forall\ b \in \mathcal{C}^{n\times 1}$). This positive semi-definiteness of the matrix is implied by its physical interpretation as a radiated energy operator. Approximating $M(s)$ to any desired accuracy by a rational matrix $\tilde{M}(s)$ allows us to write

$$\tilde{M}(s) = G^T(-s)G(s) \tag{3.30}$$

where $G(s)$ is a real, rational matrix that is analytic in $Re(s) > 0$. Substituting $s = j\omega$ produces the desired factorization. (A formal proof that the spectral factorization of the matrix quantity exists was presented by Youla (16). A constructive

proof in state-space form can be found in Francis [60]. In general, $M(s)$ will be of rank n and $G(s)$ will be an $n \times n$ matrix. For certain degenerate cases it may happen that $M(s)$ will be of normal rank $r < n$, in which case $G(s)$ will be of dimension $r \times n$. In the following, it will be assumed that M is not degenerate, but the degenerate case follows immediately.

The total radiated energy may be expressed as

$$\Pi = \int_0^\infty W^{T*}(\omega) G^{T*}(\omega) G(\omega) W(\omega) d\omega \tag{3.31}$$

and by Parseval's theorem this is equivalent to

$$\Pi = \int_0^\infty z^T(t) z(t) dt \tag{3.32}$$

where $z(t) = \mathcal{L}^{-1}[G(s)W(s)]$. That is, $z \in R^n$ is the result of passing the vector of modal (velocity) amplitudes w_{2i} through a filter with transfer function $G(s)$. Thus, by computing the filter transfer function $G(s)$ to the desired accuracy and measuring the modal amplitudes, it is possible to approximate the total farfield radiated power by equation 3.30.

It was stated by Baumann et.al. [3] that the 'radiation filter', $G(s)$, is a causal operator on the input (modal velocity) signal. This is a consequence of the fact that the spectral factorization produces a $G(s)$ with no poles in $Re(s) > 0$. Interpreting $G(s)$ as a bilateral Laplace transform, which has a region of convergence including the $j\omega$ axis, the absence of right-half plane poles means that the inverse transform, which is the impulse response of the filter, is zero for $t < 0$ [58]. Hence, the filter is causal. Thus, we have designed a physically realizable frequency/spatial filter to produce

system states which can be used to generate a radiated power cost function. The squared magnitude of the state $z(t)$ can be viewed as the energy radiated through the given sphere at time $t + \frac{R}{c}$ due to the velocity field up to time t. The transfer function $G(s)$ does not contain a propagation delay, e^{jkR}, as this term canceled out in equation 3.23.

Note that the form of the radiation resistance matrix, $M(s)$, determines whether the power radiated by the various modes is coupled. For no coupling, equation 3.26 is a diagonal matrix. However, non-zero expressions for the off-diagonal elements of $M(s)$ indicate an interaction of the power radiated by the corresponding $(i^{\underline{th}}, j^{\underline{th}})$ modes. In the manner of Yousri and Fahy [59], we refer to the diagonal terms as self-radiation resistances and the off-diagonal terms as mutual-radiation resistances.

3.2.2 Numerical calculation

Numerical calculation of the radiated power matrix, $M(s)$, is accomplished by calculating the in-vacuo modeshapes of a simply-supported plate and performing the integration defined in equation 3.29. The resulting matrix may then be factored according to equation 3.30. The results of the numerical procedures are presented next.

A numerical model was developed for the simply-supported plate testbed experiment using a pre-processor code from MSC PAL2 and the standard solution sequences in NASTRAN (ver 66a). The model contained 360 degrees of freedom, an excessive number chosen simply to facilitate the coincidence of accelerometer locations with model grid points. A normal modes solution was used to generate mass-normalized

eigenvectors for the plate.

A comparison of two representative analytical modeshapes and FEM modeshapes for the plate shows that the mass loading of the accelerometers had minimal impact on the eigenvectors. Visual inspection of the modeshapes shown in figures 3.2 and 3.3 indicates nearly insignificant perturbation of the $sin - sin$ modeshapes by the accelerometer array. As a result, it is expected that the radiation resistances of the FEM plate modes will be very similar to radiation resistance values predicted using the analytical modeshapes.

Numerical calculation of the radiated power operator matrix using equation 3.29 was performed using a AT-486 computer and MATLAB software. Five modes were included in the calculations. The results of the calculations for $M(s)$ are shown in figure 3.4. The different curves shown on the plot represent the radiation resistances of the first five modes for the simply-supported plate. As a reminder, the self-radiation resistance curves correspond to the diagonal terms of $M(s)$ and the mutual radiation resistances result from the off-diagonal terms. Notice that there are non-zero mutual radiation resistances between mode one and mode five only. The monotonically increasing value of the M(1,5) term at the higher frequencies is simply a result of the frequency cutoff used for the calculation. The presence of mutual resistances for the light fluid loading problem is dependent on the order of the effective radiation sources of the various modes as explained by Maidanik [17]. As expected, units of the curves are $\frac{kg}{sec}$. Now, a rational approximation of each curve is required for the factorization.

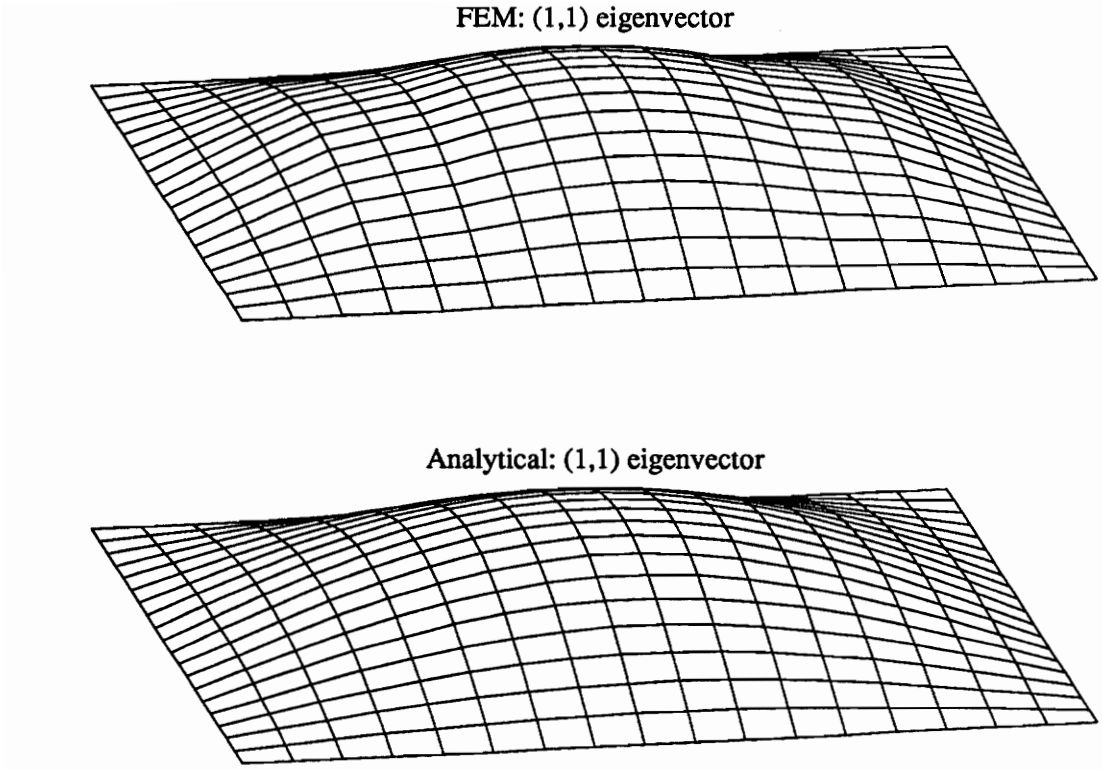

Figure 3.2: A comparison of the analytical and FEM modeshape for mode 1

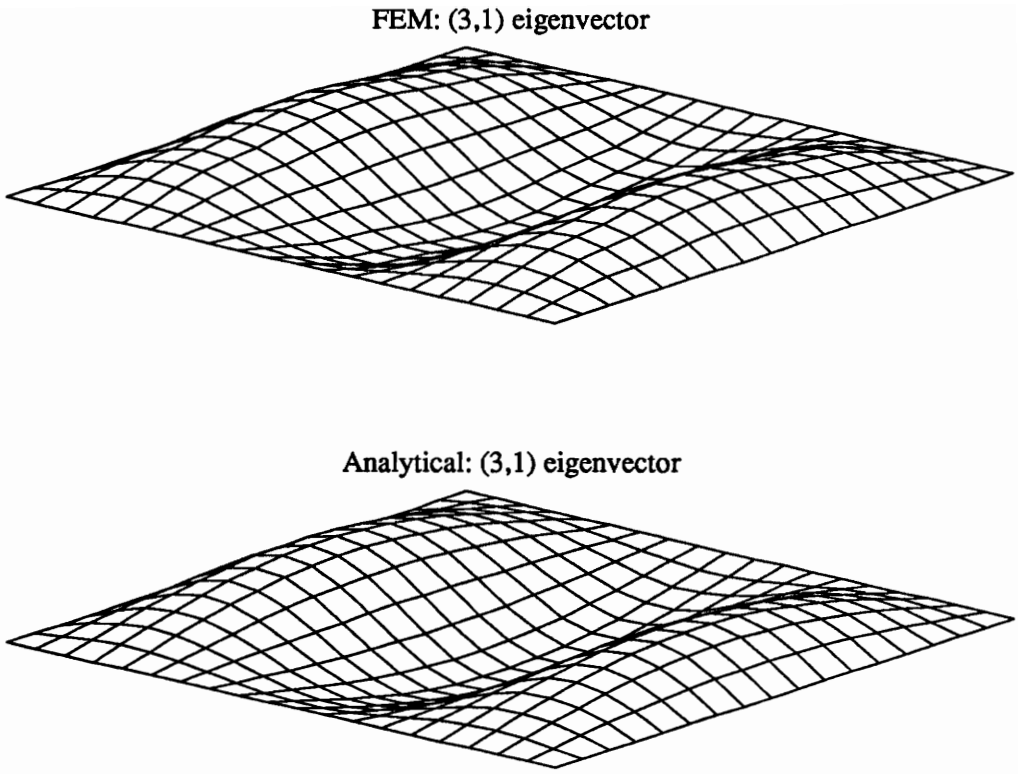

Figure 3.3: A comparison of the analytical and FEM modeshape for mode 5

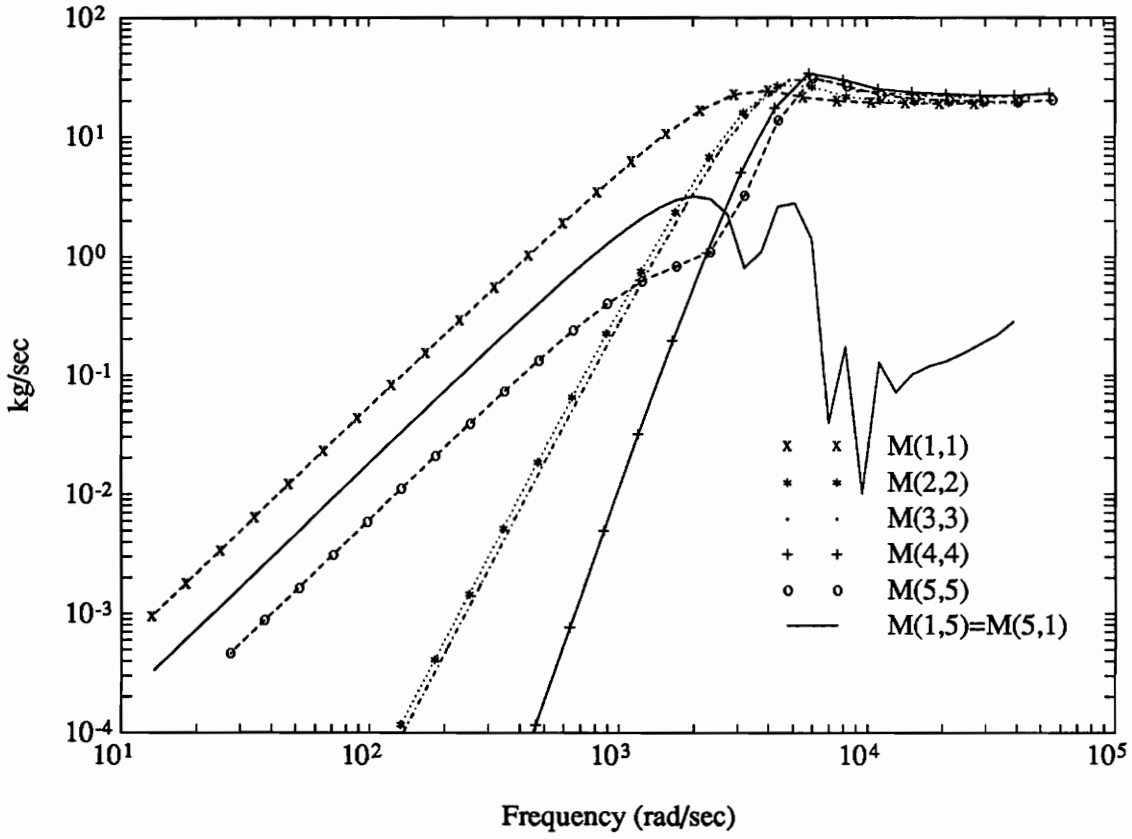

Figure 3.4: $M(s)$: The radiated power operator matrix for the simply-supported plate.

3.2.3 Rational approximations and factorization

A rational function describing the behavior of each term in $M(s)$ is required before factorization of the matrix into the radiation filters. Each curve will be modelled by a proper transfer function and assembled to represent the radiated power operator matrix. The resulting multi-input, multi-output system may be realized in state-space form. A state space factorization scheme from Francis [60] will then be used to calculate the state-space description of the stable factored matrix $G(s)$ which is the radiation filter matrix.

Generally, each magnitude curve shown on figure 3.4 behaves like a highpass filter. Because the $M(s)$ matrix is hermitian, the phase is zero as a result of the conjugate poles implied by the matrix. Thus we expect any approximation of the curves to include both stable and unstable poles. The curvefits of the radiation resistances for the first two modes are shown in figures 3.5 and 3.6. The fits are within 2 percent error in the control bandwidth ($10 - 500$Hz) but are not as accurate above the break of the high pass. This will not affect the controller performance in the control bandwidth. Of course, it may be required to extend the accuracy of the radiation filter models to higher frequencies in some situations. The design engineer needs to consider the spectral description of the disturbance(s), characterization of modal spillover, etc. to determine an adequate truncation frequency for accurate filter design. Next, the pole-zero form of the transfer function descriptions for the rational approximations of the non-zero terms in the $M(s)$ matrix are provided in table 3.1. Notice that this Laplace domain representation of $M(s)$ has the required symmetry about the imaginary ($s = j\omega$) axis. The symmetry of the zeros and poles provides the zero-phase characteristic of the real para-conjugate matrix. A spectral

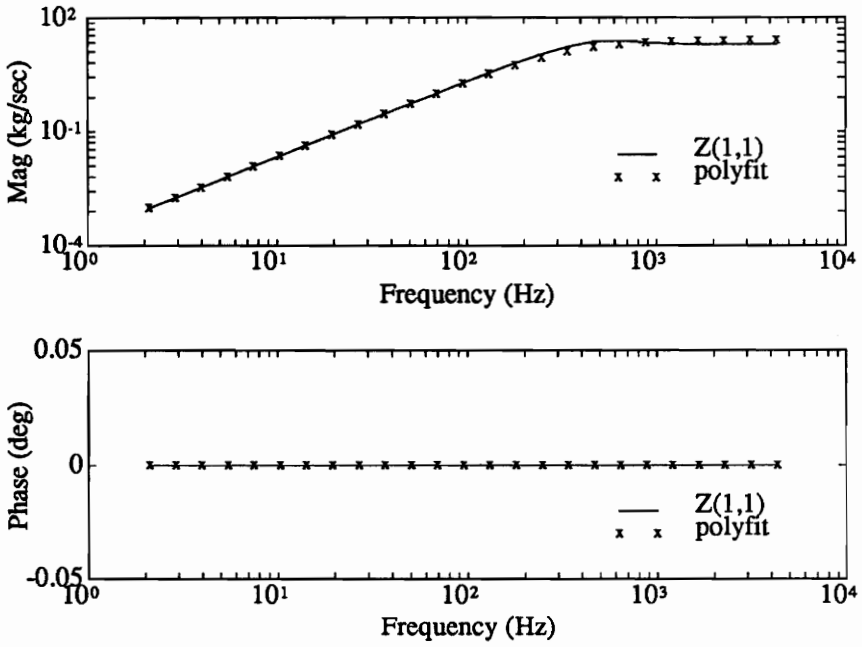

Figure 3.5: Rational approximation of the mode 1 radiation resistance, $M(1,1)$.

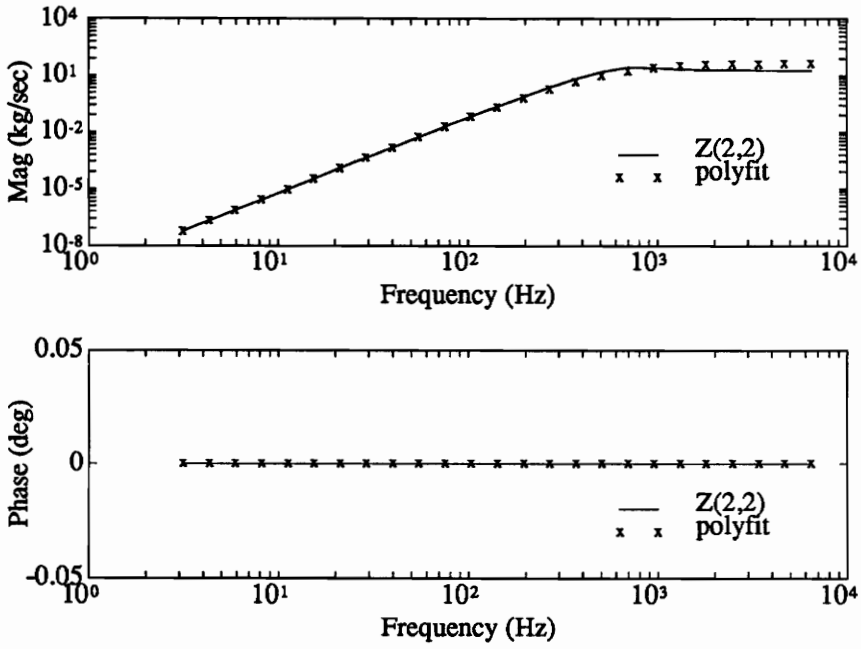

Figure 3.6: Rational approximation of the mode 2 radiation resistance, $M(2,2)$.

Table 3.1: Rational approximations for the radiated power operator matrix, $M(s)$

$$
\begin{aligned}
M(1,1) &= \frac{(s \pm 0.1)}{(s \pm 2142)} \\
M(2,2) &= \frac{(s \pm 0.1)(s \pm 0.2)}{(s \pm 3240)(s \pm 3340)} \\
M(3,3) &= \frac{(s \pm 0.1)(s \pm 0.2)}{(s \pm 3240)(s \pm 3340)} \\
M(4,4) &= \frac{(s \pm 0.1)(s \pm 0.1 \pm j0.15)}{(s \pm 3900)(s \pm 4100)(s \pm 4200)} \\
M(5,5) &= \frac{(s \pm 1320 \pm j2280)}{(s \pm 2930)(s \pm 6140)(s \pm 6180)} \\
M(1,5) = M(5,1) &= \frac{(s \pm 1320 \pm j2280)}{(s \pm 3520)(s \pm 3550)(s \pm 3580)}
\end{aligned}
$$

factorization of $M(s)$, defined by $G^*(s)G(s) = M(s)$ will produce the stable factor $G(s)$. (The symbol * is the complex conjugate transpose, or hermitian.) As mentioned previously, this stable factor is called the *radiation filter* for the plate. The design of radiation filters is the key element of the ASAC approach for the light fluid loading problem.

A state-space method from Francis was employed to factor $M(s)$. A brief summary of the technique is discussed next. For a square matrix $M(s)$ having the following properties, it can be shown that a spectral factorization defined by $M = G_-^* G_-$ exists:

$$M, M^{-1} \in \mathbf{RL}_\infty \tag{3.33}$$

$$M^* = M \tag{3.34}$$

$$M(\infty) > 0 \tag{3.35}$$

Of course, the goal is to realize G_- which is the stable spectral factor. Starting with a state-space realization of $M(s)$ shown in table 3.1 and doing a similarity transformation

$$M(s) = \left[\begin{bmatrix} A_1 & 0 \\ 0 & A2 \end{bmatrix}, \begin{bmatrix} B_1 \\ B_2 \end{bmatrix}, \begin{bmatrix} C_1 & C_2 \end{bmatrix}, D \right] \tag{3.36}$$

where A_1 is stable and A_2 is antistable. After a minimal realization of the stable part

$$M_1(s) = [A_1, B_1, C_1, 0] \tag{3.37}$$

and using Liouville's theorem the matrix becomes

$$M(s) = \left[\begin{bmatrix} A_1 & 0 \\ 0 & -A_1^T \end{bmatrix}, \begin{bmatrix} B_1 \\ -C_1^T \end{bmatrix}, \begin{bmatrix} C_1 & B_1^T \end{bmatrix}, D.\right] \tag{3.38}$$

A quantity is defined

$$A^x = A - BD^{-1}C \tag{3.39}$$

$$\tag{3.40}$$

$$= \begin{bmatrix} A_1 - B_1 D^{-1} C_1 & -B_1 D^{-1} B_1^T \\ C_1^T D^{-1} C_1 & -(A_1 - B_1 D^{-1} C_1)^T \end{bmatrix} \tag{3.41}$$

$$\tag{3.42}$$

which is a Hamiltonian matrix. The solution of the associated Ricatti equation, say $[X]$ provides a transformation matrix

$$T = \begin{bmatrix} I & 0 \\ X & I \end{bmatrix}. \tag{3.43}$$

Now a transformation of equation 3.37 with equation 3.43 gives the final result for the factored radiation filter:

$$G_-(s) = \left[A_1, B_1, D^{-\frac{1}{2}}(C_1 + B_1^T X), D^{\frac{1}{2}}\right] \tag{3.44}$$

A few comments on the factorization process are included to provide caution and stimulate research for anyone interested in repeating this design approach. First, the approach used here can lead to poorly conditioned matrices during the intermediate calculations required by the factorization. The companion form blocks of the $M(s)$ state-space realization produced by MATLAB software very often leads to poor conditioning because of the relatively high break frequencies used to model

the high pass shapes. The condition numbers may be the source of significant errors in the factorizations, particularly when the Hamiltonian is solved by an eigenvalue method. If this method must be used, balancing may be required to achieve factorizations without corruption by substantial numerical noise. A more numerically reliable solution of the Hamiltonian may be accomplished using the Schur decomposition approach in MATLAB.

The results of the numerical factorization are shown in figure 3.7. Magnitudes of each non-zero element of the radiation filter matrix $G_{-}(s)$ are plotted against radian frequency. The relative importance of the cross-terms is easy to distinguish from the figure.

3.3 Control law development

The equations for the ASAC controller are described in this section. An optimal control approach is developed which uses a LQG control law in such a way that both transient and persistent disturbances may be rejected. Detailed discussion of the LQG control equations will not be provided but the reader may refer to any of the following references on optimal control theory [29, 61, 62].

State space representations of the dynamics described in sections 3.1.2 and 3.2.1 will be combined in this section. The state equations for the various components of the system dynamics (e.g. structural dynamics, acoustic dynamics, etc.) were generated independently. These equations and the state equations for additional dynamics in the system will be used to define an augmented state vector for the entire system. The resulting augmented state space equations will then become constraints in a Linear Quadratic optimal control law to reduce farfield radiated power.

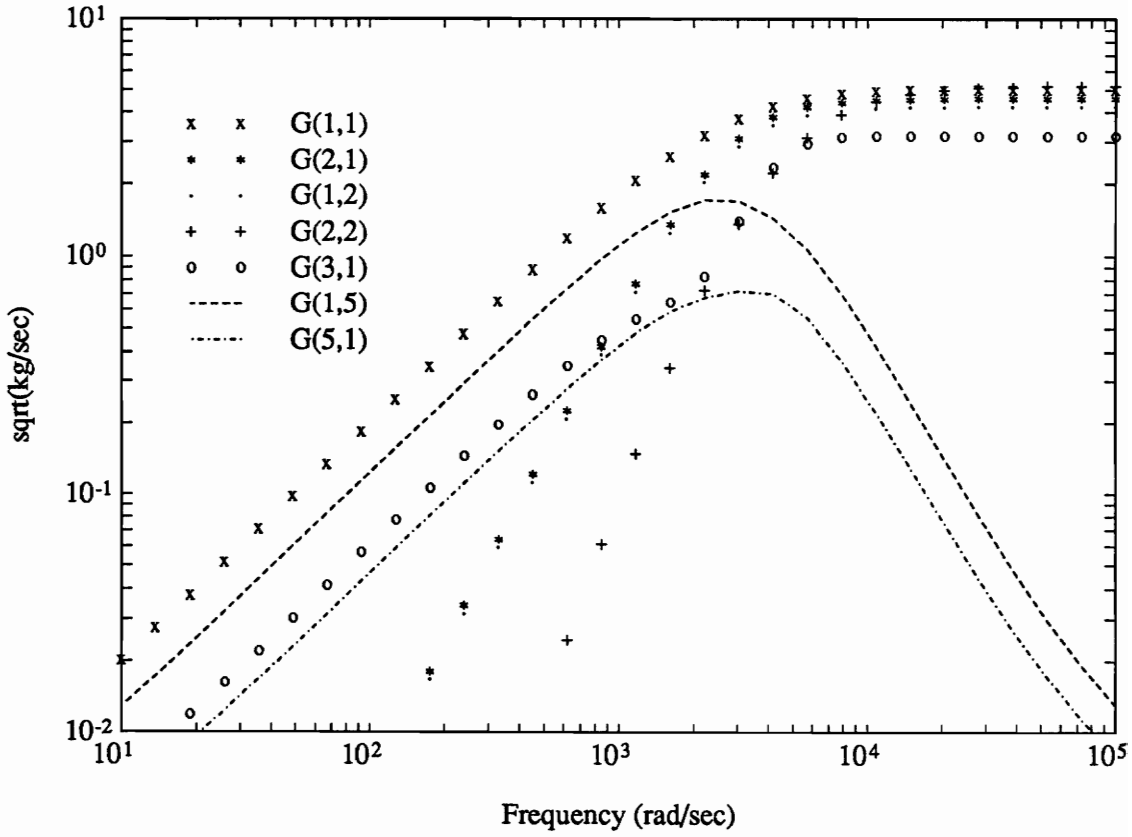

Figure 3.7: Radiation filters for the simply-supported plate.

Following the results of section 3.1.2 the state-space description of the structural dynamics may be written in condensed form:

In-vacuo plate dynamics:

$$\dot{w} = Fw + Gu + Ld \tag{3.45}$$

$$y = Cw + D_c u + D_d d + \Xi \tag{3.46}$$

where $w \in R^{2n}$ is the state of the system in modal coordinates, $u \in R^m$ is the actuator input used to control the structure, and $d \in R^t$ is the disturbance input. The waveform of the disturbance is arbitrary in equation 3.45. In the output equation, $y \in R^n$ is a vector of measured modal accelerations and $\Xi \in R^n$ is zero mean Gaussian measurement noise. Direct feedthrough of the applied control and disturbance forces is present because of the choice of acceleration outputs.

Following the results of section 3.2, the dynamics of the radiation filters may be written in state-space form. The following equations result from the factored matrix $G_{-}(s)$ in equation 3.44:

Radiation filter dynamics:

$$\dot{p} = F_{rad}p + G_{rad}w \tag{3.47}$$

$$Z = C_{rad}p + D_{rad}w \tag{3.48}$$

where $p \in R^v$ represent the acoustic states of the radiation filters, w are the plate velocities which drive the filters, and $Z \in R^n$ is the output vector of the filters. There is one output for each of the modelled modes. The units of Z correspond

to the radical of watts. Thus, this signal is in some sense simply an artifact of the design procedure and has little physical significance on its own.

Two additional sets of dynamics must be defined before the augmented system is created. These dynamics are required for two different reasons. First, an analog filtering of the control signal needs to take place before it is passed to the actuator. This step is necessary for any vibration or structural acoustic controller designed using digital systems. The difficulty lies in the zero-order hold implicit in the digitally synthesized control signal. This introduces a sequence of steps to the structure. The spectrum of the discrete sequence depends on the sampling period of the digital control loop, but generally will be of sufficient bandwidth to excite either uncontrolled or unmodelled modes, or both. Smoothing the signal with an active or passive network (nearly) eliminates the pulse and provides an opportunity to roll off the control actuator input above the frequency of the controlled modes. Typically, simple low-pass filters will suffice for this objective. The final set of dynamic equations model any external disturbances which enter the plant. This approach is widely known in modern control theory and is discussed by Ackermann [63] and Sievers and vonFlotow [64]. Simply stated, if a plant is subjected to a deterministic or band-limited disturbance (i.e. not white noise) a disturbance observer may be used to estimate the disturbance entering the plant. Of course, if the estimate is relatively accurate, the disturbance may be suppressed by the controller. For the ASAC design, a standard approach will be taken where the disturbance model may be described by a low-order filter driven by Gaussian, zero-mean noise.

The dynamic equations for the smoothing filter and the disturbance model may be written in state-space form:

Smoothing filter dynamics:

$$\dot{s} = F_f s + G_f \tilde{u} \tag{3.49}$$

$$u = C_f s \tag{3.50}$$

Disturbance dynamics:

$$\dot{r} = F_d r + G_d \eta \tag{3.51}$$

$$d = C_d r \tag{3.52}$$

where $s \in R^{2m}$ is the state of the smoothing filter, $\tilde{u} \in R^m$ is the control actuator signal directly from the digital-to-analog converter, $u \in R^m$ is the control actuator signal after passing through the filter, $r \in R^{2t}$ is the disturbance model state vector assuming simple second-order dynamics, and the associated state matrices for both sets of dynamics are companion form matrices for second-order state equations of the general form

$$\begin{bmatrix} x \\ \dot{x} \end{bmatrix} = \begin{bmatrix} 0 & I \\ -\omega^2 & -2\zeta\omega \end{bmatrix} \begin{bmatrix} x \\ \dot{x} \end{bmatrix} + \begin{bmatrix} 0 \\ 1 \end{bmatrix} f \tag{3.53}$$

$$y = \begin{bmatrix} 0 & 1 \end{bmatrix} \begin{bmatrix} x \\ \dot{x} \end{bmatrix} \tag{3.54}$$

The equations 3.45 through 3.52 may be augmented using the state vector

$$W_a = \begin{bmatrix} w \\ p \\ s \\ r \end{bmatrix} \tag{3.55}$$

with $W_a \in R^{\alpha}$ ($\alpha = 2n + v + 2m + 2t$) so that the augmented system equations become

$$\dot{W}_a = \begin{bmatrix} \dot{w} \\ \dot{p} \\ \dot{s} \\ \dot{r} \end{bmatrix} = \begin{bmatrix} F & 0 & GC_f & LC_d \\ G_{rad} & F_{rad} & 0 & 0 \\ 0 & 0 & F_f & 0 \\ 0 & 0 & 0 & F_d \end{bmatrix} \begin{bmatrix} w \\ p \\ s \\ r \end{bmatrix} + \begin{bmatrix} 0 \\ 0 \\ G_f \\ 0 \end{bmatrix} \tilde{u} + \begin{bmatrix} 0 \\ 0 \\ 0 \\ G_d \end{bmatrix} \eta \quad (3.56)$$

$$y = \begin{bmatrix} C & 0 & D_c C_f & D_d C_d \end{bmatrix} \begin{bmatrix} w \\ p \\ s \\ r \end{bmatrix} + \Xi \quad (3.57)$$

or

$$z = \begin{bmatrix} D_{rad} & C_{rad} & 0 & 0 \end{bmatrix} \begin{bmatrix} w \\ p \\ s \\ r \end{bmatrix} + \Xi \quad (3.58)$$

It will be shown next that the choice of output equation 3.57 or 3.58 distinguishes the vibration controller from the ASAC controller. First, the LQG formulation is introduced briefly.

The controller described in the following discussion was introduced by Baumann, et.al. [3] and [53]. It uses an LQG paradigm in conjunction with the acoustics modelling described earlier to generate a feedback controller capable of minimizing modal vibration or radiated acoustic power. This formulation will be applied to the numerically generated, augmented, simply-supported plate equations.

A LQG controller combines the LQR optimal control problem with an optimal filtering method for state estimation. Briefly, the design of the controller starts with

the augmented state equations 3.56 through 3.58, which will be written in condensed form as follows:

$$\dot{X}_a = F_a X_a + G_a \tilde{u} + L_a \eta \tag{3.59}$$

$$y = C_a X_a + \Xi \tag{3.60}$$

$$z = C_a^a X_a + \Xi. \tag{3.61}$$

The LQR problem may be solved using these augmented equations and a quadratic function of some specified cost. In general, the cost is a quadratic function of the state and the control according to

$$J = \int_0^\infty (X_a^T Q X_a + \tilde{u}^T R \tilde{u}) dt \tag{3.62}$$

where Q is a positive semi-definite weighting matrix on the regulation of the state and R is a positive definite matrix which specifies the amount of control effort expended. A cost function is defined for the vibration control effort or the ASAC priority using this minimum-energy cost relationship. For vibration control, the quadratic cost function to be minimized is

$$J_v = \int_0^\infty (y^T y + \tilde{u}^T R \tilde{u}) dt \tag{3.63}$$

For active structural acoustic control, the quadratic cost function to be minimized is

$$J_a = \int_0^\infty (z^T z + \tilde{u}^T R \tilde{u}) dt. \tag{3.64}$$

The only apparent difference between the two cost functions is the choice of out-

put variable in the minimization. However, it is emphasized that the acoustic cost corresponds to a frequency-weighted vibration cost. The frequency weighting is implicit in equation 3.64 via the radiation filters. Referring back to equation 3.32, it becomes clear that minimizing the acoustic cost of equation 3.64 is equivalent to minimizing the radiated power balanced by some penalty on the control effort. *The acoustic cost function J_a distinguishes the ASAC controller from active vibration control approaches in that it suppresses the efficiently radiating modes of the structure preferentially among the entirety of modes in the control bandwidth. A second method of acoustic power reduction is provided by the acoustic cost. Modal restructuring may occur whereby relative phase between the modes is used to reduce the overall sound power without significant suppression of the participating modes. This was demonstrated by Baumann et.al [53] and will not be re-emphasized in this research.*

When the disturbances entering the plant are not deterministic, the state values will not be known for the calculation of the control signal. However, a stochastic optimal control problem may be posed using the expected values of the costs given by equations 3.63 and 3.64. The stochastic optimal control design will not be repeated here but it should be understood that the following comments on the control and estimation design procedure may be applied for deterministic or stochastic time histories.

The optimal compensator derived from equations 3.59 through 3.64 is state feedback. Thus the control law is

$$\tilde{u} = -K_c X_a \tag{3.65}$$

where $K_c \in R^{mx\alpha}$. The control gains K_c are calculated from the Hamiltonian of the variational problem. Details may be found in Kirk [29]. Equation 3.65 assumes that all states are available in the feedback loop. However, the two measurement variables y and z are not states. Thus, an estimator is required to construct values of the states. This will be achieved using an optimal filtering technique.

A stochastic optimal filtering technique may be used to minimize the mean-squared value of the measurement residual $(y - \hat{y})$. As the residual approaches zero, *the estimate of the state $\hat{X}_a$ approaches the actual values of the state.* The details of the derivation are well-known so that only the resulting equations are included here. The Kalman-Bucy filter equations are

$$\dot{\hat{X}}_a = F_a\hat{X}_a + G_a\tilde{u} + K_f(y - \hat{y}) \tag{3.66}$$

$$\hat{y} = C_a\hat{X}_a \tag{3.67}$$

where K_f results from solving the dual optimal control problem [29]. Now, the control law may be written using the accurate estimates of the state, so that

$$\tilde{u} = -K_c\hat{X}_a \tag{3.68}$$

3.4 Simulation results

A nine-mode model of the simply-supported plate was developed to provide a simulation testbed for the ASAC controller developed in Section 3.3. It was mentioned previously that the control simulations correspond to an experimental testbed in the Smart Structures Lab at VPI &SU which may be used to verify the predicted

results. No experimental validation was included here but will be published separately. A description of the numerical experiment is discussed next.

A simply-supported plate of the parameters shown in table 3.2 is the testbed experiment and the open-loop plant used for the simulations presented here. Accelerometers were placed on the plate at the locations indicated in table 3.3. It will be assumed that one disturbance force and one control force enter at non-collocated discrete points (y, z) of the plate. A single disturbance force and a single control force is adequate to illustrate the ASAC controller, although it may be expected that more actuators will improve the performance of the closed-loop system. Quantitative comparisons for various numbers of control actuators is straightforward and will not be investigated here. For the simulation results presented next, the disturbance force entered the structure at the same coordinates as accelerometer location five and the control force was located at the coordinates of accelerometer location eight. This corresponded to a separation distance of approximately $0.1m$.

A comparison will be made between the vibration controller and the ASAC controller for the experiment described above. The vibration amplitudes before and after control will be sufficient to highlight the advantages of ASAC controllers. Radiated pressures will also be presented for the case of harmonic excitation. Now, recall that the selection of the cost function, equation 3.63 or equation 3.64 distinguishes between the vibration and acoustic control law. For the vibration control law, the weighting matrix Q is determined by expanding the inner product of the output vector:

$$y^T y = (C_a X_a)^T (C_a X_a)$$

Table 3.2: Properties and dimensions of the simply-supported plate

dimensions	$z = 0.6m, \quad y = 0.5m$
thickness	$h = 2.9mm$
density	$7798\frac{kg}{m^3}$
Young's Modulus	$E = 207GPa$
Poisson ratio	$\nu = 0.292$

Table 3.3: Measurement locations for the simply-supported plate

acc no.	$y(m)$	$z(m)$
1	0.12	0.12
2	0.24	0.12
3	0.39	0.12
4	0.12	0.25
5	0.24	0.25
6	0.39	0.25
7	0.12	0.35
8	0.24	0.35
9	0.39	0.35
10	0.12	0.47
11	0.24	0.47
12	0.39	0.47

$$= X_a^T C_a^T C_a X_a$$

$$= X_a^T \, Q \, X_a$$

Selection of the control weighting R for the vibration cost determines the amount of control effort expended. The value of R is best determined by balancing the amount of control authority available from the actuators and the performance specifications placed on the closed-loop system. For this research, R was chosen to provide "good" control results and to assure that equal control effort was expended for the vibration cost and the acoustic cost.

There are also weighting matrices which must be selected for the dual problem. For the estimator design, the weighting matrices essentially scale the covariance of the stochastic process noise driving the disturbance dynamics and the covariance of the measurement noise present on the output measurements. The details of the selection process for these matrices is covered at a fundamental level by Ellis [68]. It is relatively important that the design engineer understand, at least qualitatively the effect of the weight selections on the closed-loop system. For example, it is possible to degrade the closed-loop performance of the plant away from the disturbance bandwidth. An example of the degradation which can occur from poor system design is shown in figure 3.8. Although significant damping has been added to the resonant peak, the magnitude in the stiffness region of the mode 1 accelerance is substantially higher than the open-loop magnitude over the same frequencies. Sys-

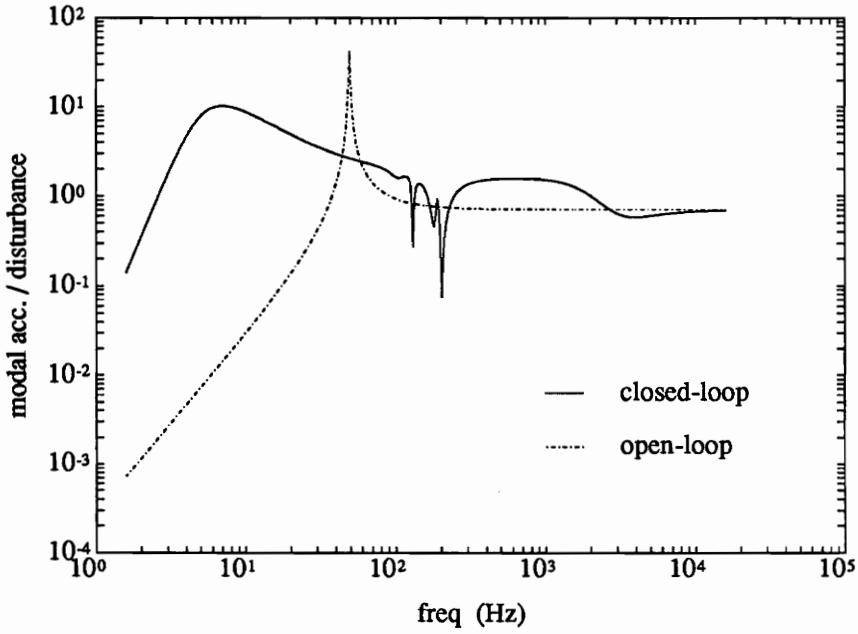

Figure 3.8: Closed-loop transfer function of modal acceleration to 105 Hz disturbance, Mode 1, Poor gain selection.

tem analysis during the design stage will help guide the selection of LQ weighting matrices to avoid the problems depicted in figure 3.8. After the weighting matrices are defined for the entire compensator, control gains K_c and estimator gains K_f are calculated. The MATLAB Control Toolbox was used to solve the Ricatti equations for the two gain matrices.

Simulated closed-loop performance may be illustrated using frequency-domain or time-domain concepts. For frequency-domain analysis, bode plots of the continuous-time compensator equations were calculated. The compensator equations for the simply-supported plate may be written in state-space form. The derivation follows from equations 3.59, 3.60, and 3.66 through 3.68. Only the final result will be given here:

$$\begin{bmatrix} \dot{X} \\ \dot{\hat{X}}_a \end{bmatrix} = \begin{bmatrix} F & -GK_c \\ K_f C & F_a - G_a K_c - K_f C_a \end{bmatrix} \begin{bmatrix} X \\ \hat{X}_a \end{bmatrix} + \begin{bmatrix} L & 0 \\ K_f D_d & K_f \end{bmatrix} \begin{bmatrix} \eta \\ \Xi \end{bmatrix} \quad (3.69)$$

$$y = [C - D_c K_c] \begin{bmatrix} X \\ \hat{X}_a \end{bmatrix} + [D_d I] \begin{bmatrix} \eta \\ \Xi \end{bmatrix} \quad (3.70)$$

Note that the form of the compensator equations 3.69 and 3.70 are the same for the vibration compensator and the acoustic compensator. The augmented radiation states are not required for the vibration controller but their presence does not affect the compensator as they are unobservable. Of course, the gain matrices will be different for the two cases. The outputs of equation 3.70 are the individual modal accelerations and the inputs are the process and measurement noise, respectively. Thus, the closed-loop response of the i_{th} mode to the disturbance input may be examined across the bandwidth of the controller by calculating the transfer function of the compensator equations.

Simulations in the time-domain were calculated for the vibration and acoustic costs, also. The time-domain simulations were performed using the sampled-data representation of the control equations discussed in section 3.3. Rubenstein [46] provides the details of modifying the continuous-time control equations for digital implementation. The time-domain analysis approach provides one particularly important advantage compared to the frequency-domain analysis. Simulation of the real-time controller may be performed using constraints on the control actuator forces which meet practical hardware limitations. Next, simulated results for the vibration and ASAC control of the simply-supported plate will be presented using both analysis approaches.

Comparison of ASAC to vibration control will be examined for three different cases. First, a harmonic disturbance at 105 Hz enters the plant. The first plate mode is 49 Hz and the second mode of the plate is 108 Hz. Second, a broadband persistent disturbance is used to excite the plant. The disturbance is formed by passing Gaussian noise through a low-pass filter with a pass band from 0 to 250 Hz. Finally, a pulse is applied to the plate. The bandwidth of the pulse covers the entire control bandwidth 0 to 250 Hz. For all three cases, it will be assumed that actuator authority is not a limitation. Of course, this is not true in practice. However, the issue being investigated is controller performance without regard to actuator specifications. Limiting the control signal amplitude allowed by the controller is a straightforward addition to the simulation code and will not be addressed here.

Case 1: $105Hz$ harmonic disturbance

A composite transfer function illustrating the modal accelerance of all nine modelled modes relative to the disturbance force is shown in figure 3.9. The frequency of the disturbance force is indicated on the figure. The dominance of modes 1 and 5 for the chosen disturbance location are obvious in the composite plot. Figure 3.10 shows the spectral shape of the narrowband disturbance model included in the compensator. The disturbance estimator is robust enough to provide an estimate of a disturbance anywhere within the bandwidth of the disturbance model. The bandwidth may be defined by the half-power points. Recall for this case, the disturbance is a harmonic input at $105Hz$.

Transfer functions of the closed-loop response for vibration control of modes 1 through 5 are shown in figures 3.11 through 3.13. Several important observations can be made about the bode plots. First, the closed-loop system has a "notch" at the frequency of the disturbance. The notch occurs in the closed-loop transfer function of the second mode. For one control actuator, the notch is typically placed in the transfer function of the mode in closest proximity to the frequency of the disturbance. This notch in the transfer function is the disturbance compensation which the LQG controller provides. It may be shown that the depth of the notch is controlled by the selection of the weighting matrices in the controller design, discussed earlier. However, a tradeoff must be made when choosing the weights because the "out-of-band" frequencies of the closed-loop transfer function may be increased above the open-loop transfer function if too much cancellation is required at the disturbance frequency. For this work, the weights of the compensator were iteratively chosen to provide good performance at the frequencies of interest without serious

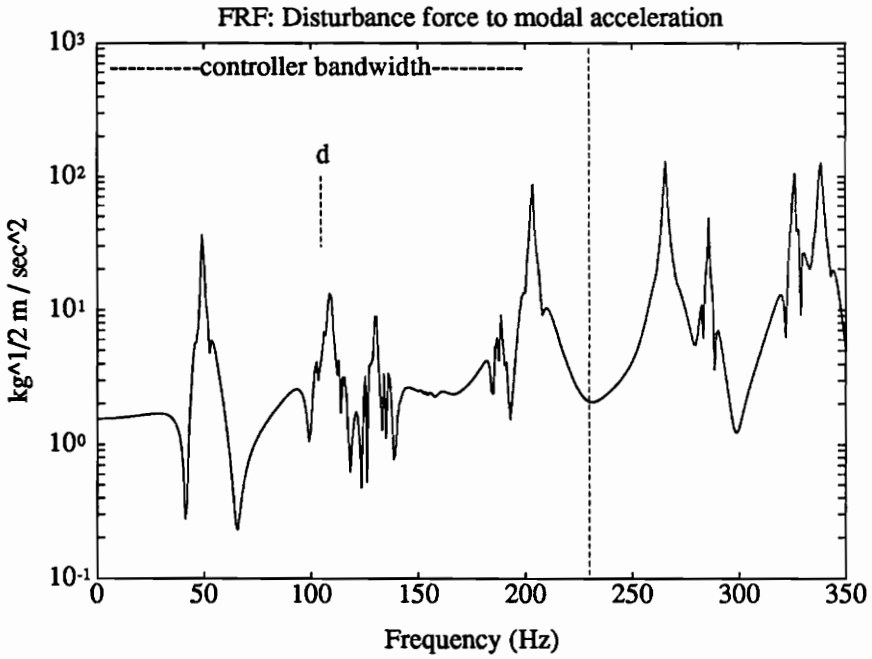

Figure 3.9: Composite open-loop accelerance plot of nine-mode plant model for the simply-supported plate, disturbance at $y = 0.24m, z = 0.25m$.

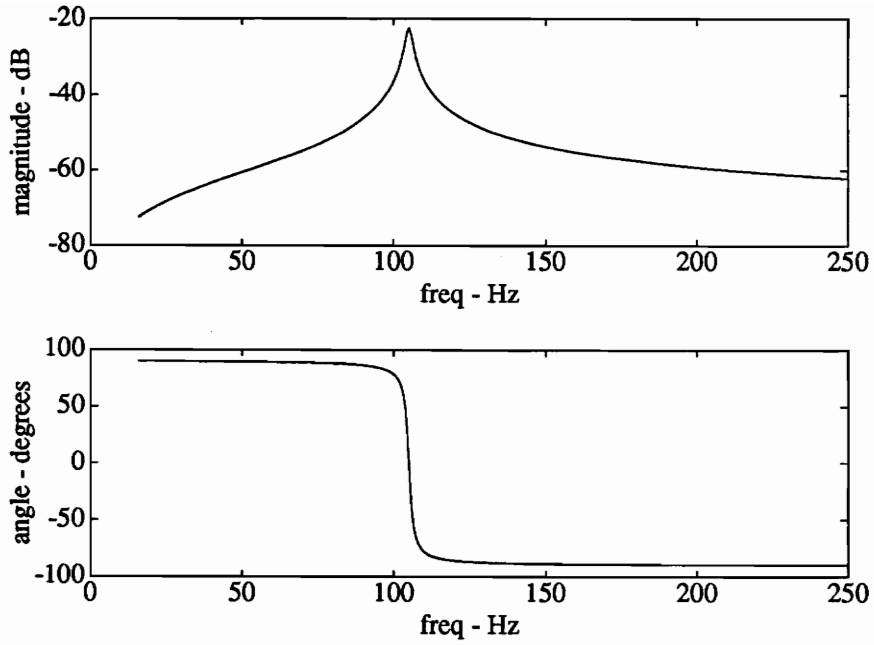

Figure 3.10: Narrowband disturbance spectrum, center frequency of $105Hz$.

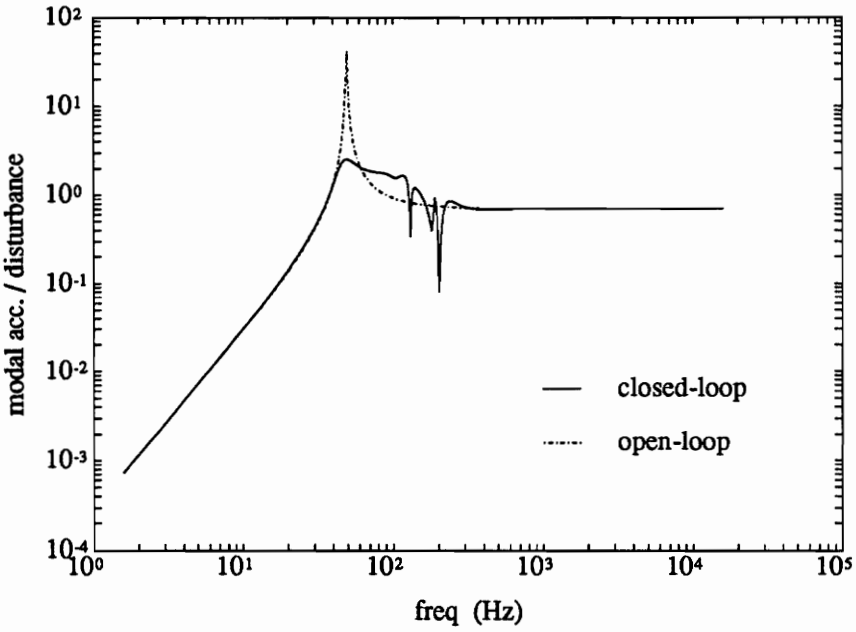

a. Mode 1 : 47 Hz

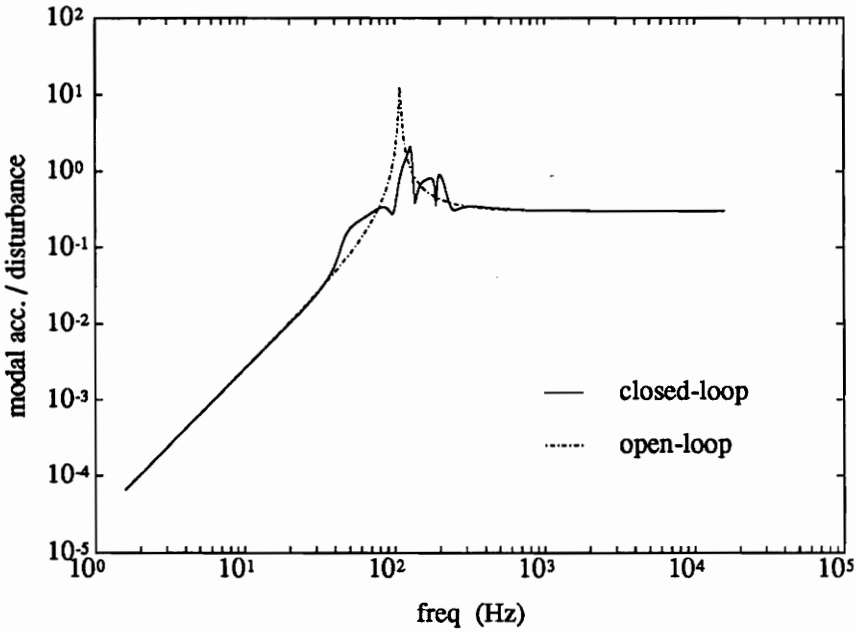

b. Mode 2 : 108 Hz

Figure 3.11: Closed-loop transfer function of modal acceleration to 105 Hz harmonic disturbance, modes 1 and 2, vibration control.

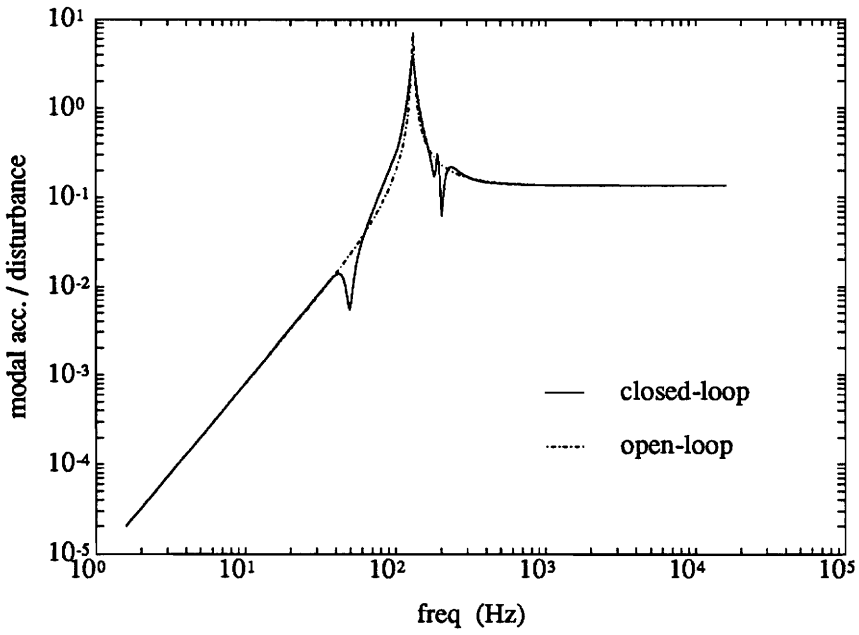

a. Mode 3 : 130 Hz

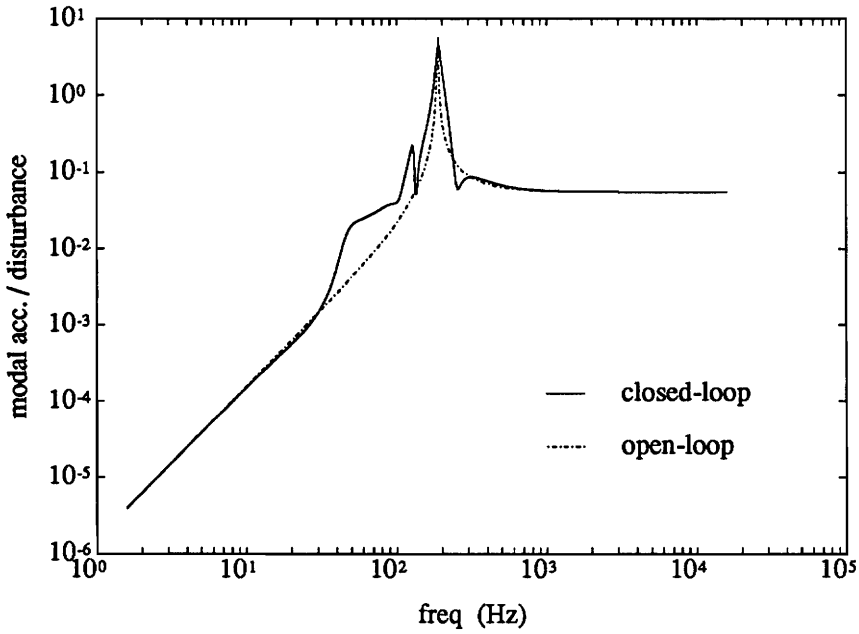

b. Mode 4 : 188 Hz

Figure 3.12: Closed-loop transfer function of modal acceleration to 105 Hz harmonic disturbance, modes 3 and 4, vibration control.

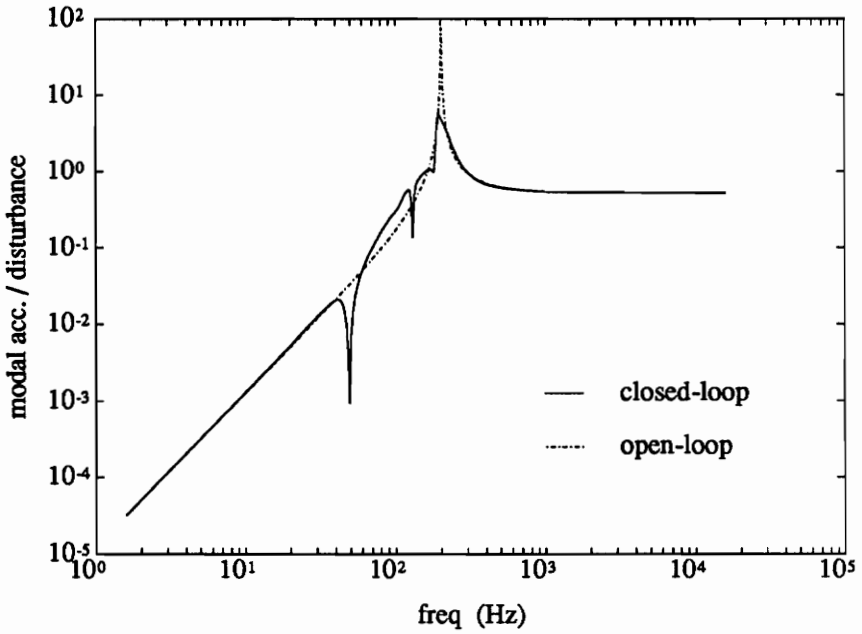

a. Mode 5 : 203 Hz

Figure 3.13: Closed-loop transfer function of modal acceleration to 105 Hz harmonic disturbance, mode 5, vibration control.

degradation elsewhere. Now, referring back to figures 3.11 through 3.13 a second point of interest for the vibration control results. Significant damping is added to several of the modes. This damping provides the transient suppression. To summarize the results, the vibration controller reduces the mode 2 vibration response more than 40 dB and adds significant damping to the first mode.

Similar plots are shown in figures 3.14 through 3.16 for the ASAC controller. A noticeable difference in the closed-loop response of mode 2 is apparent for the ASAC versus vibration control. The ASAC control, through its effort to minimize only the most important radiating modes, hardly penalizes the mode 2 vibration. Recall that the radiation filter for mode 2 is approximately 20 dB lower than the mode 1 filter at this frequency. This feature is more clearly demonstrated in the time-domain results shown next.

A discrete-time controller was designed to generate the time-domain results. The assumed sample frequency was $2000Hz$. It is expected that this sample frequency will be possible for a real demonstration of the ASAC controller. Figures 3.17 through 3.21 show the time response of the plate during closed-loop simulations of vibration control and ASAC control. Each figure compares the closed-loop modal acceleration for the vibration and the ASAC controllers. The results show the plate response before, during and after the control is applied to the plate. The controller was turned on at $t = 5$ seconds. The weights for the gain calculations were chosen to provide equal control effort expended by the vibration and ASAC controllers. Comparing the vibration and ASAC results clearly indicates the ability of the ASAC controller to target the efficiently radiating modes as discussed above. For equal control energy, the radiated power from the plate during ASAC was forty-five percent less

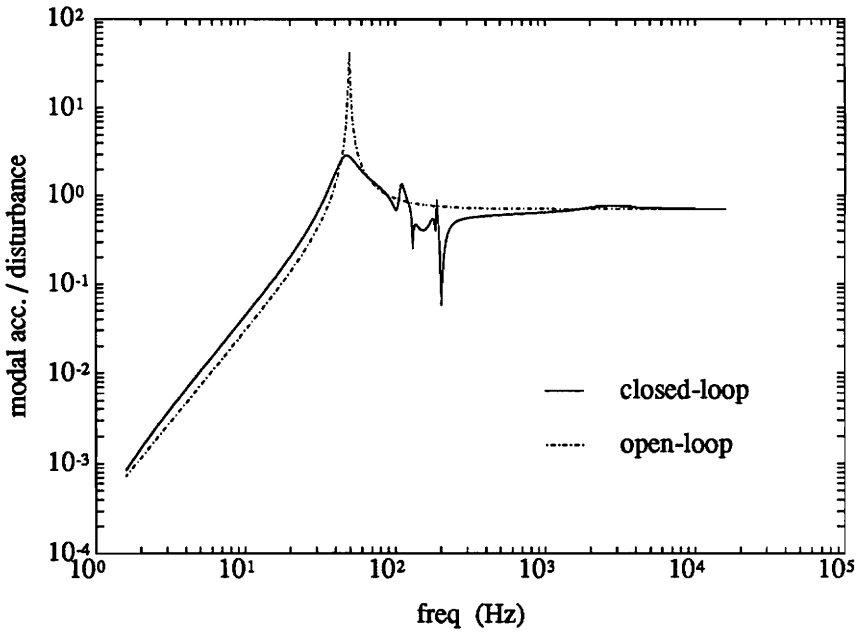

a. Mode 1 : 47 Hz

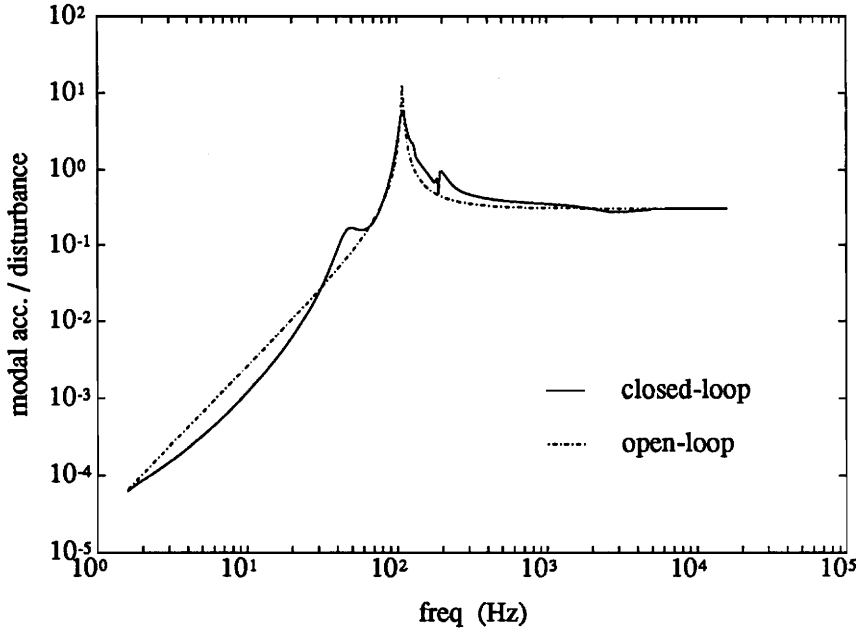

b. Mode 2 : 108 Hz

Figure 3.14: Closed-loop transfer function of modal acceleration to 105 Hz harmonic disturbance, modes 1 and 2, ASAC control.

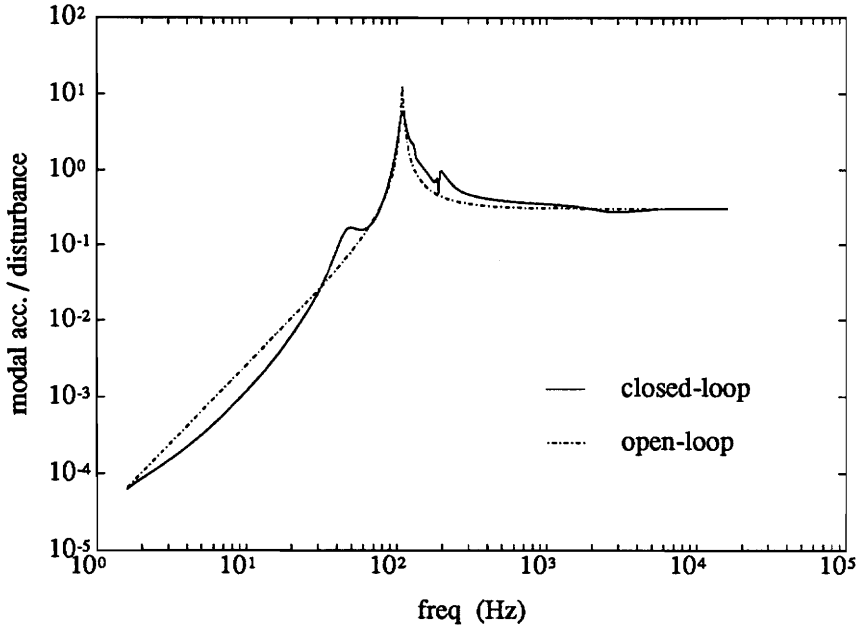

a. Mode 3 : 130 Hz

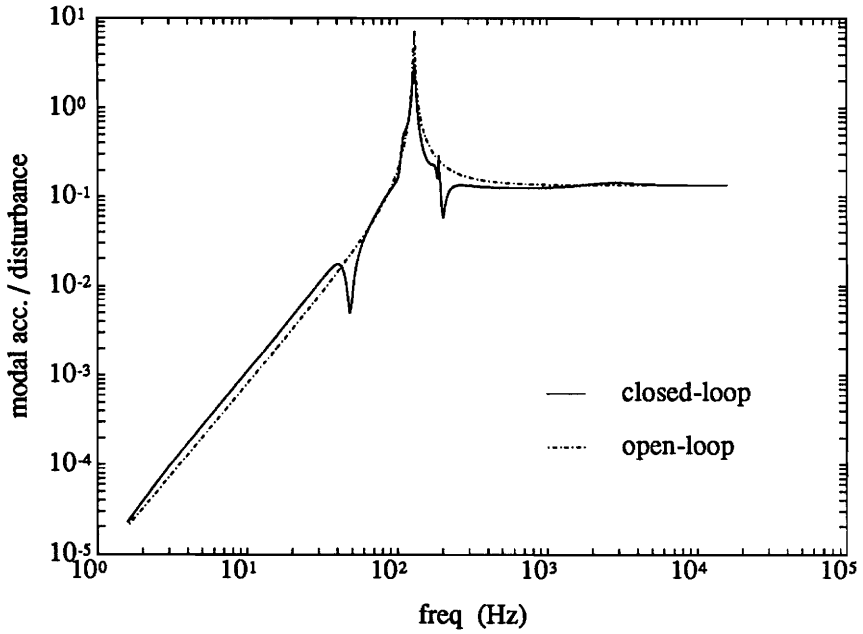

b. Mode 4 : 188 Hz

Figure 3.15: Closed-loop transfer function of modal acceleration to 105 Hz harmonic disturbance, modes 3 and 4, ASAC control.

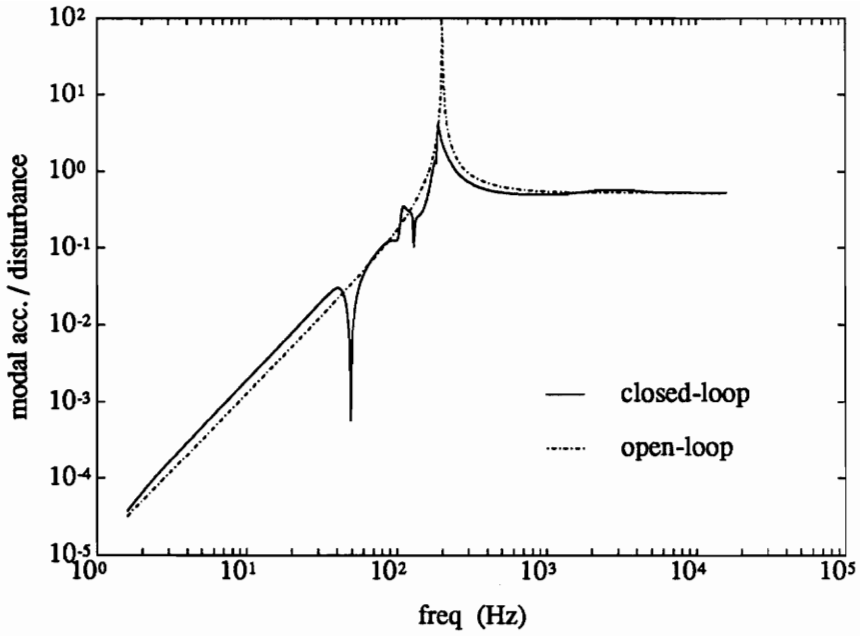

a. Mode 5 : 203 Hz

Figure 3.16: Closed-loop transfer function of modal acceleration to 105 Hz harmonic disturbance, mode 5, ASAC control.

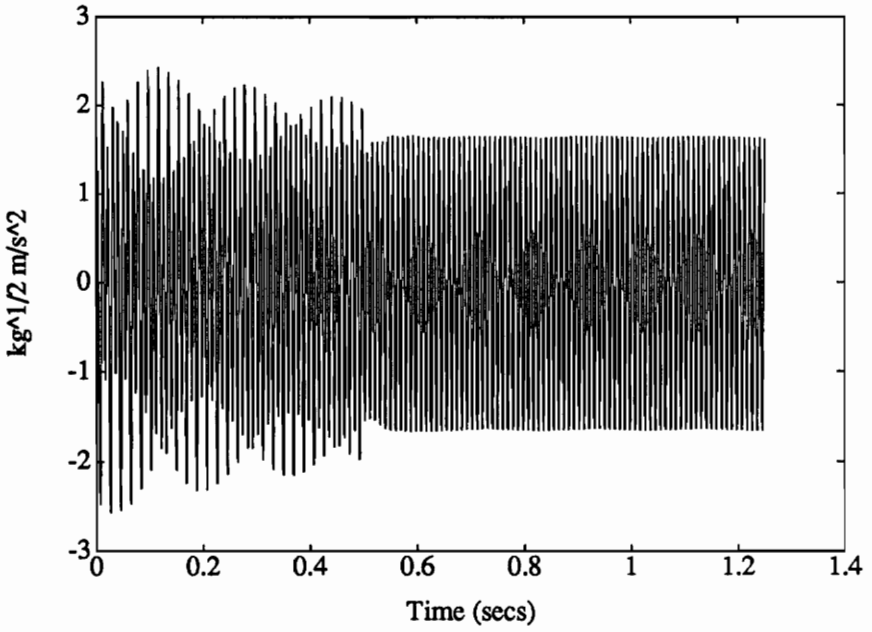

a. ASAC control

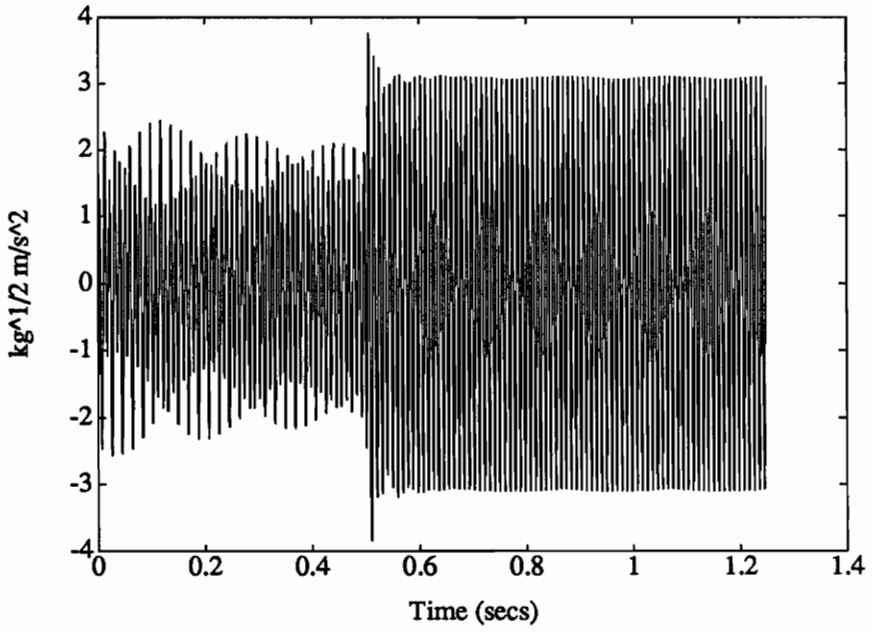

b. Vibration control

Figure 3.17: Time-domain simulation of mode 1 acceleration during vibration control and ASAC control of a $105Hz$ disturbance.

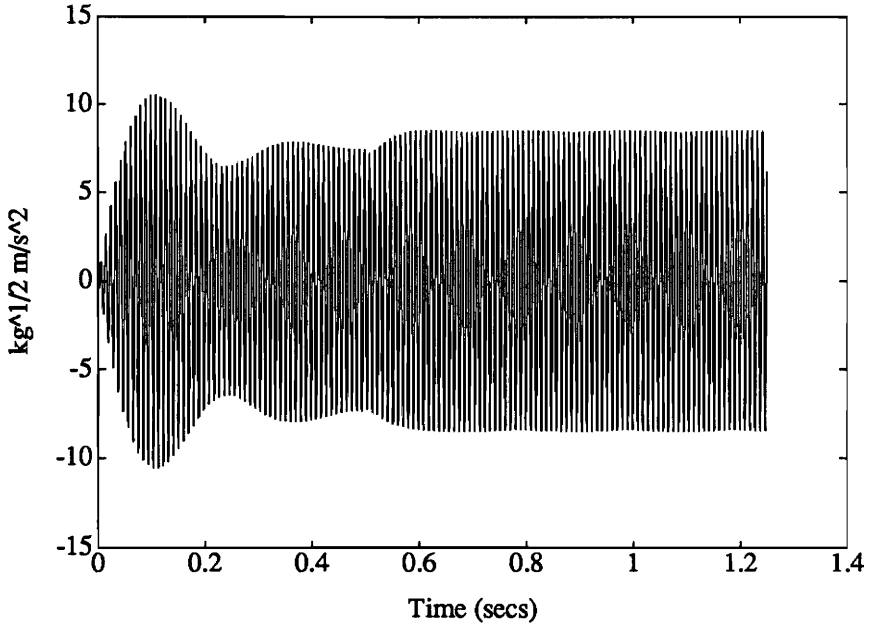

a. ASAC control

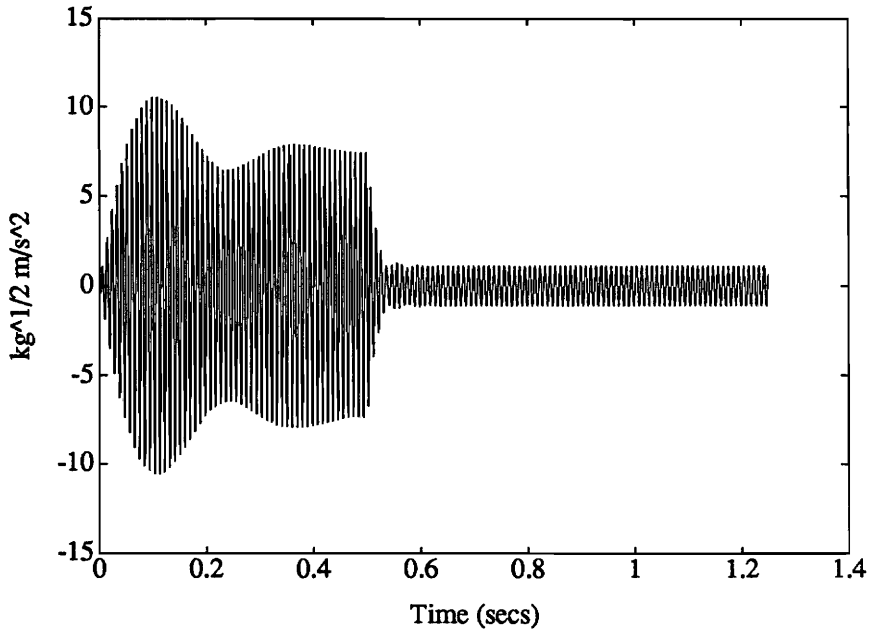

b. Vibration control

Figure 3.18: Time-domain simulation of mode 2 acceleration during vibration control and ASAC control of a $105Hz$ disturbance.

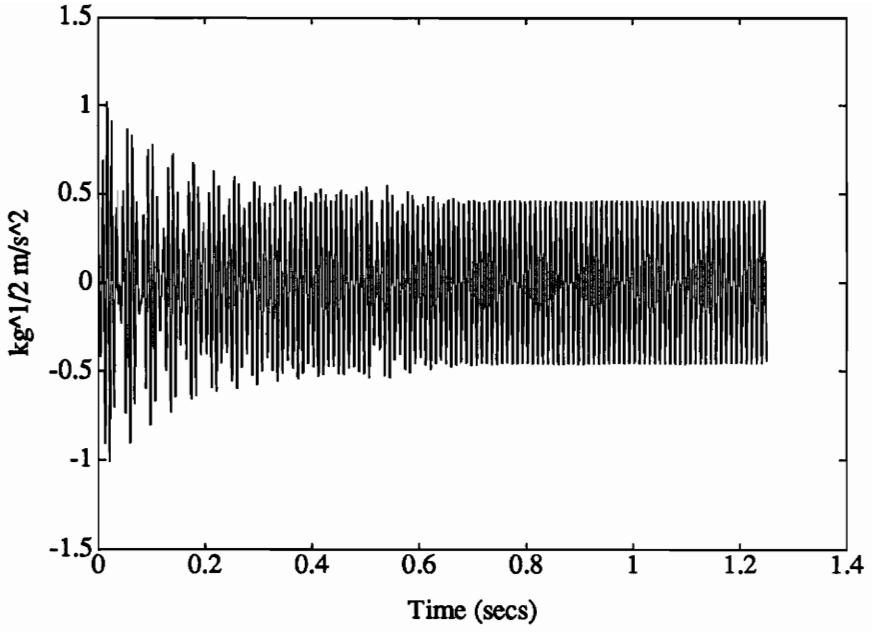

a. ASAC control

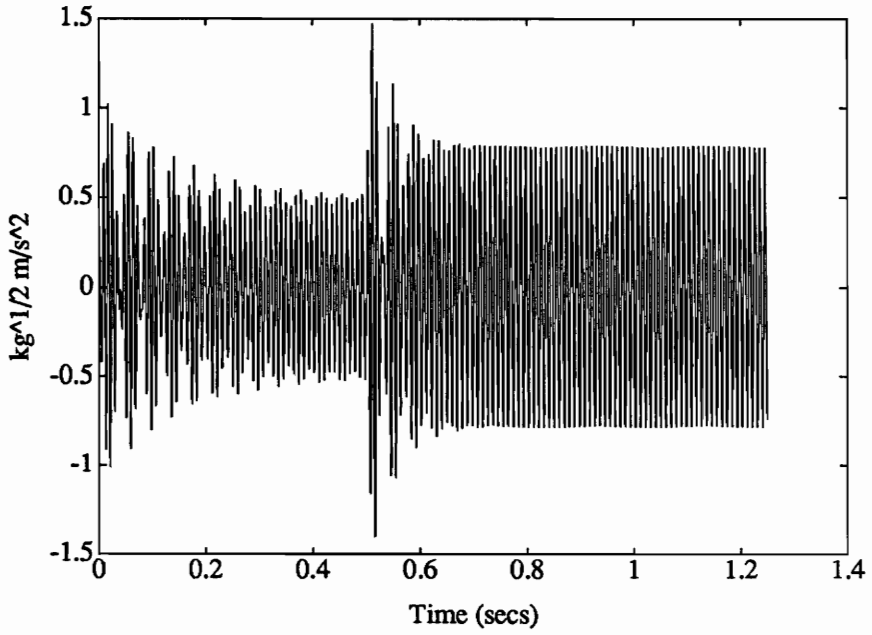

b. Vibration control

Figure 3.19: Time-domain simulation of mode 3 acceleration during vibration control and ASAC control of a $105Hz$ disturbance.

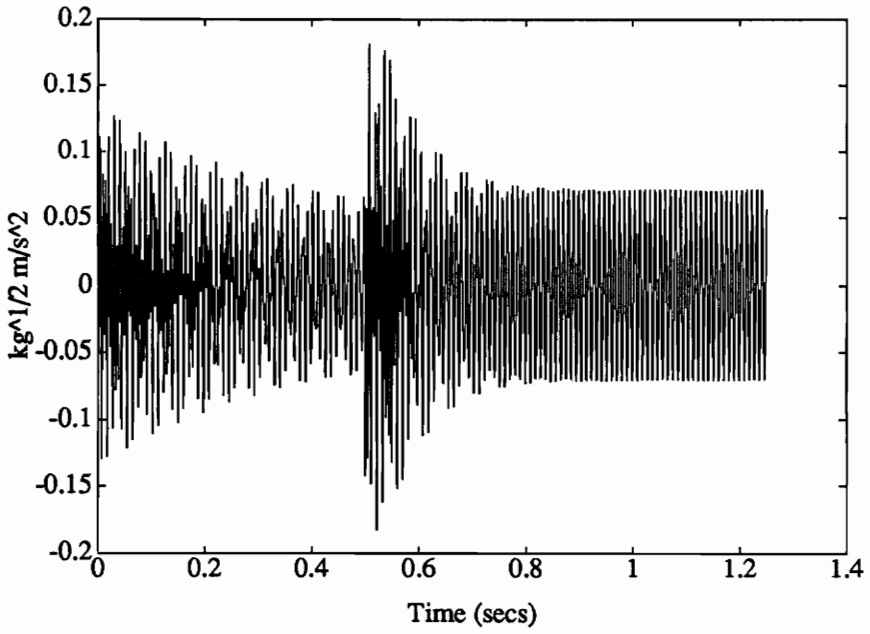

a. ASAC control

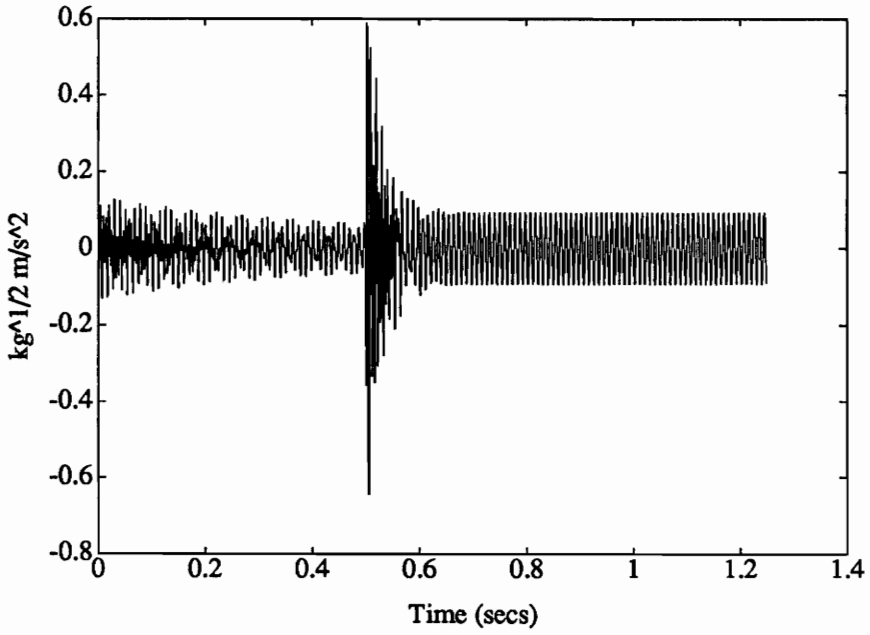

b. Vibration control

Figure 3.20: Time-domain simulation of mode 4 acceleration during vibration control and ASAC control of a $105Hz$ disturbance.

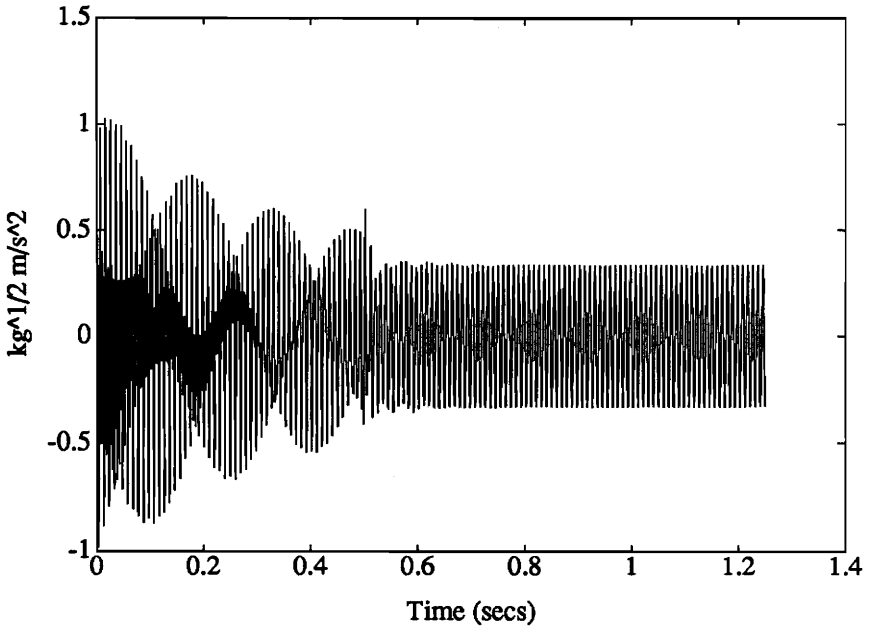

a. ASAC control

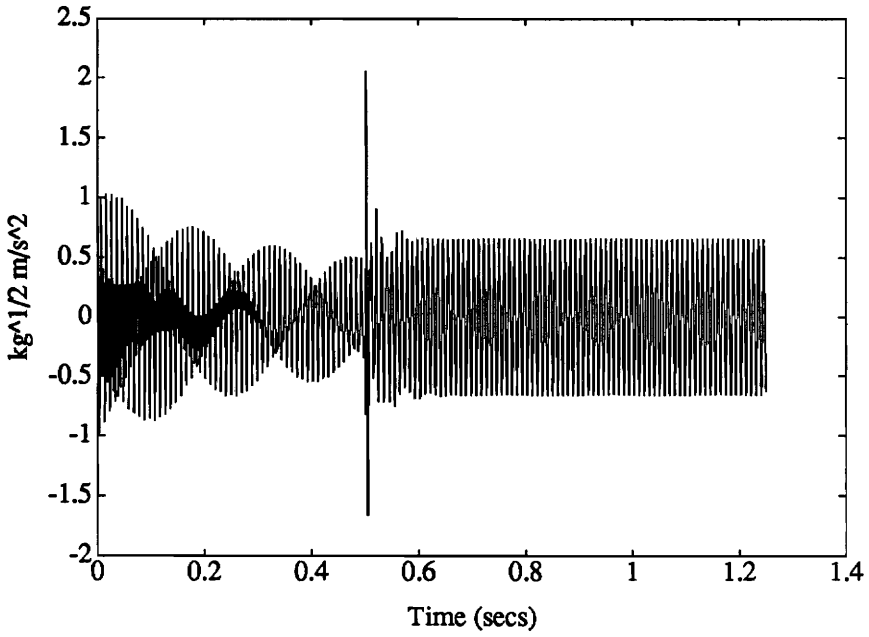

b. Vibration control

Figure 3.21: Time-domain simulation of mode 5 acceleration during vibration control and ASAC control of a $105Hz$ disturbance.

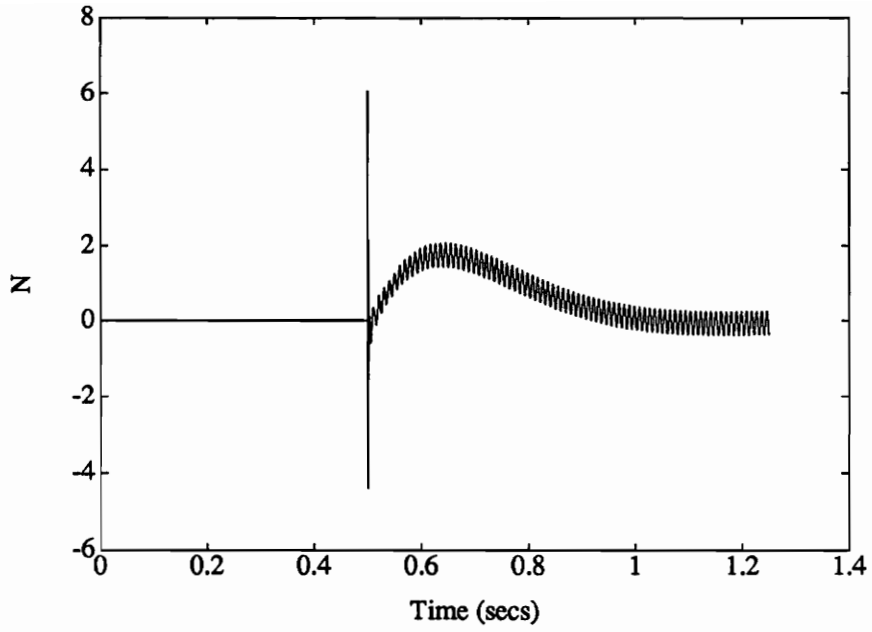

a. ASAC control

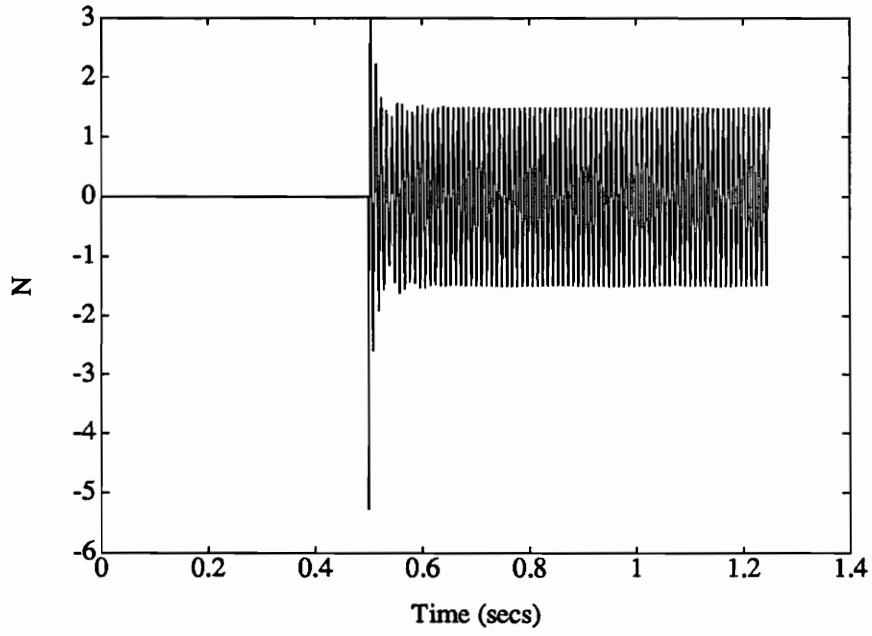

b. Vibration control

Figure 3.22: Time-domain simulation of actuator signal during vibration control and ASAC control of a $105Hz$ disturbance.

than the radiated power during the vibration control simulation over the same time period.

The control signals for the two cases are shown in figure 3.22. During ASAC, the controller delivers a slowly varying "static" force to the plate. This pushing of the actuator was evident in the modal position state variables but does not affect the modal accelerations. As the control gains are lowered, this dc component of the control signal is not observed.

The farfield radiated pressure for the open-loop and closed-loop response is presented in figure 3.23. A comparison between the open-loop radiated pressure, the closed-loop radiated pressure during vibration control and the closed-loop radiated pressure during ASAC is included for the angles $\phi = 0$ and $-\frac{\pi}{2} \; ¡ \; \theta \; ¡ \; \frac{pi}{2}$ and referenced to $R = 1m$. The results show that there is little difference in the closed-loop radiated pressure for the single control actuator placement of the simulated experiment. This is true for vibration and ASAC control. To explain, recall that the closed-loop vibration amplitudes clearly indicated a tendency for the ASAC controller to reduce the efficiently radiating mode 1 instead of suppressing the second mode which dominates the vibration energy. However, the ability to reduce the first mode is limited because there is a single actuator available. The limitation is caused by the relative phasing between mode 1 and mode 2 at the actuator location. The two modes are out of phase at that discrete location. If one of the modes is reduced, then the other mode must increase in amplitude. The dilemma for the ASAC controller is best illustrated by observing the transfer function between the disturbance and the output of the radiation filter for the first two modes. This is shown in 3.24. For the simulation discussed here, the transfer function is the same for the open-loop

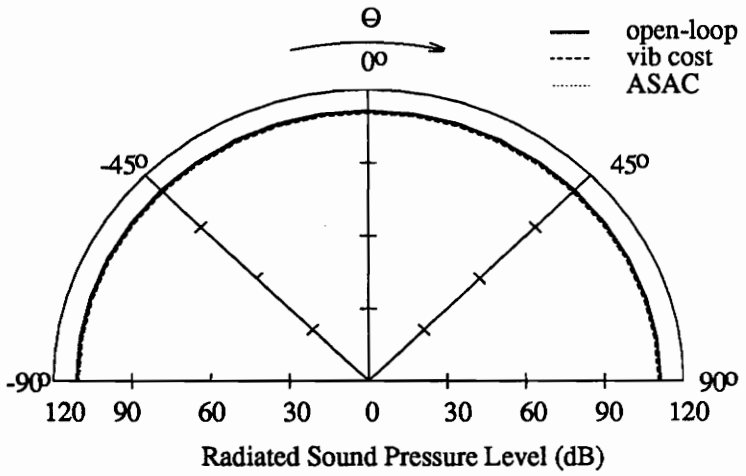

Figure 3.23: Farfield radiated pressure for vibration and ASAC control of 105 Hz disturbance.

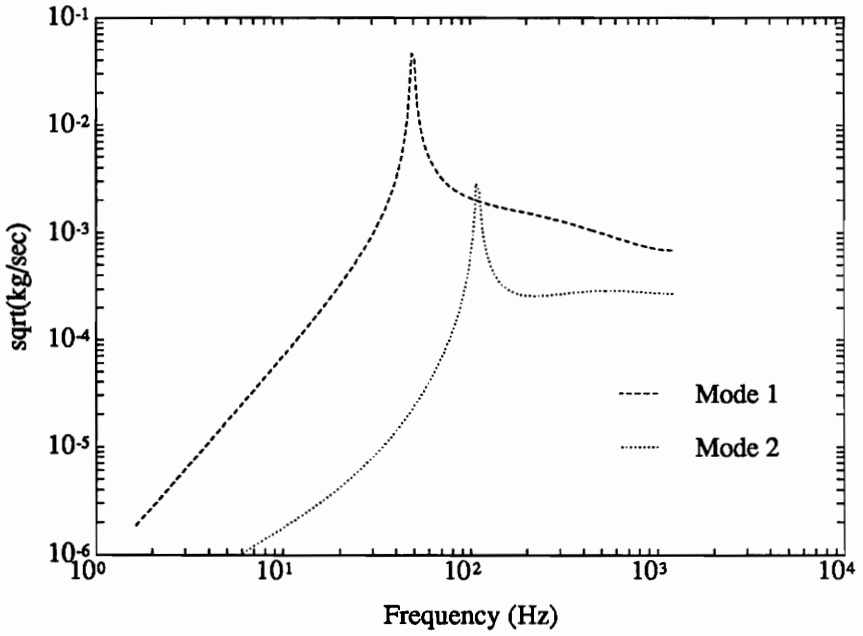

Figure 3.24: Transfer function from disturbance to radiation filter output, modes 1 and 2.

and closed-loop system. This figure highlights the fact that the radiated power from either mode will not be adjusted substantially for the excitation frequency chosen. The ASAC controller is left with the unexciting choice to perform very little control for the case chosen. As discussed earlier, more control actuators would increase the effectiveness of the controllers. In addition, the ASAC controller would be able to focus on the most important radiating modes in the control bandwidth.

Case 2: Broadband disturbance

For this case, the disturbance was generated by passing Gaussian noise through a simple low-pass filter with a cutoff frequency of 250 Hz. The spectral shape of the disturbance is shown in figure 3.25. A disturbance of this spectral shape will excite all of the modelled modes, providing the actuator placement is chosen to do so. For this case of a single control actuator, the controller cannot optimally suppress all the modes but will have to decide which modes contribute to the cost function most significantly. Bode plots of the closed-loop modal accelerance for the vibration cost and the acoustic cost are shown in figures 3.26 through 3.30. Recall that the model for the disturbance dynamics is broadband noise from 0 to 250 Hz.

The difference between the closed-loop transfer functions for the different costs is not as significant for this broadband suppression. However, the ASAC controller does emphasize minimization of mode 1 acceleration and leaves untouched the modes that are relatively less efficient acoustically. Recall that the ASAC controller has the implicit frequency dependent weighting required to minimize the acoustic power within the disturbance bandwidth. The vibration control, which does not have access to the acoustic dynamics, tries to provide suppression at each in-phase mode with-

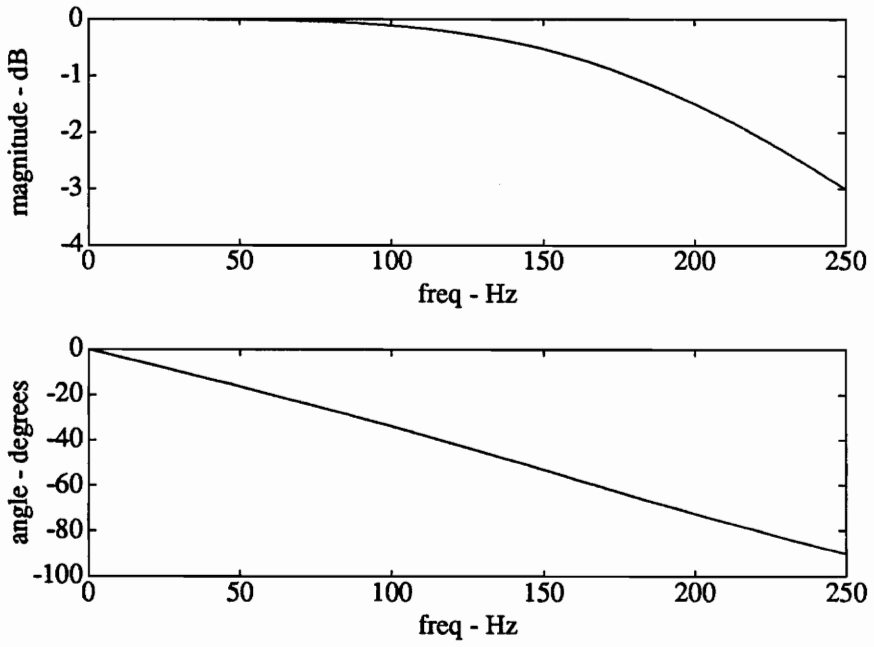

Figure 3.25: Broadband disturbance spectrum, 0 to $250Hz$ lowpass.

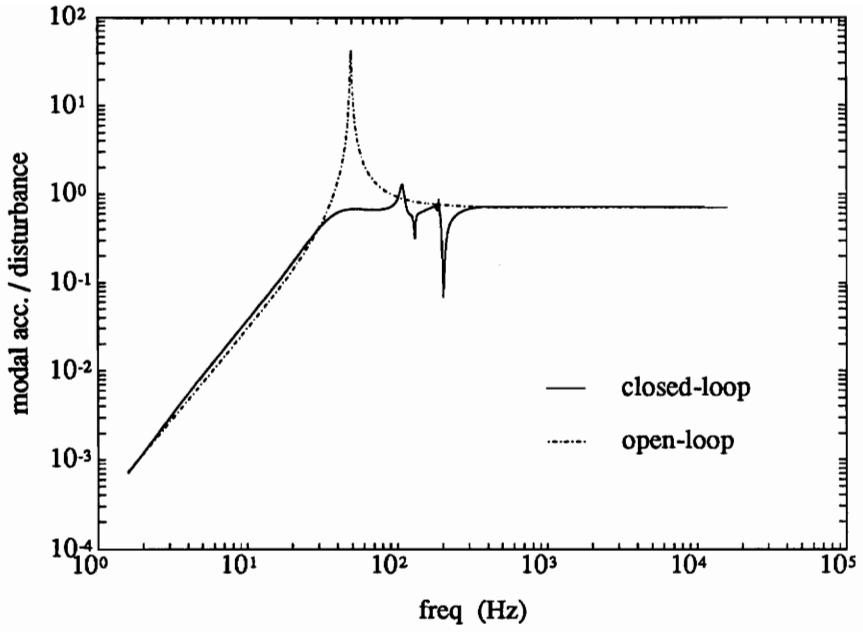

a. ASAC control

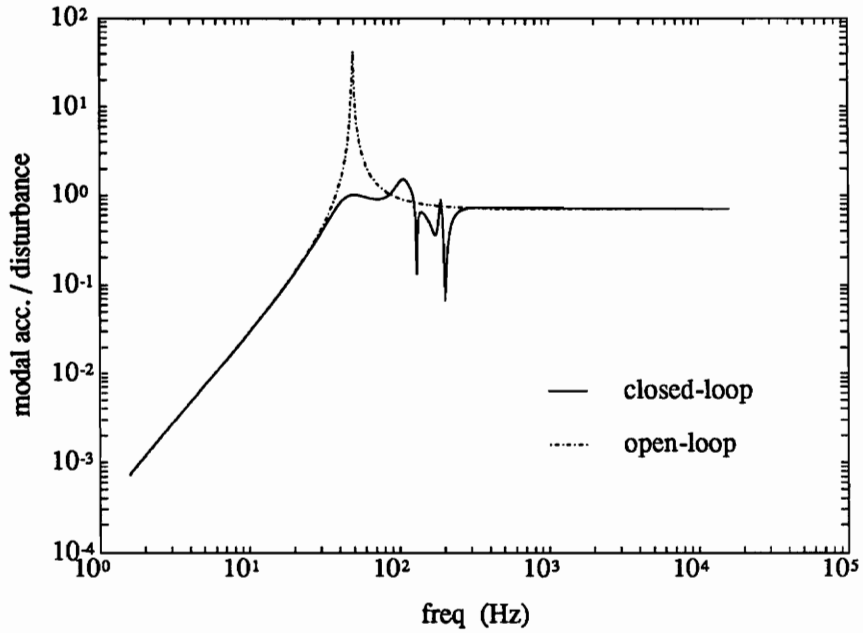

b. Vibration control

Figure 3.26: Frequency-domain simulation of closed-loop transfer function from broadband disturbance to mode 1 acceleration

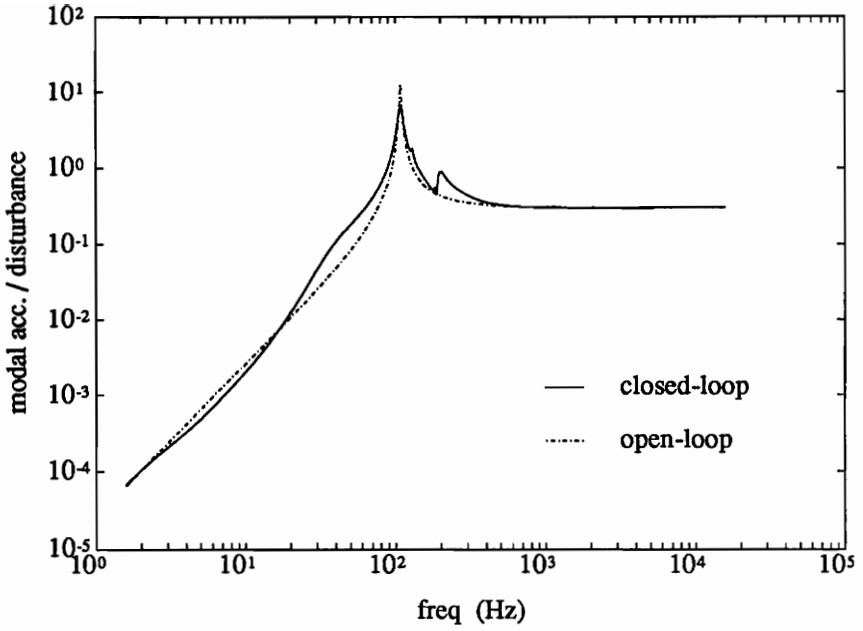

a. ASAC control

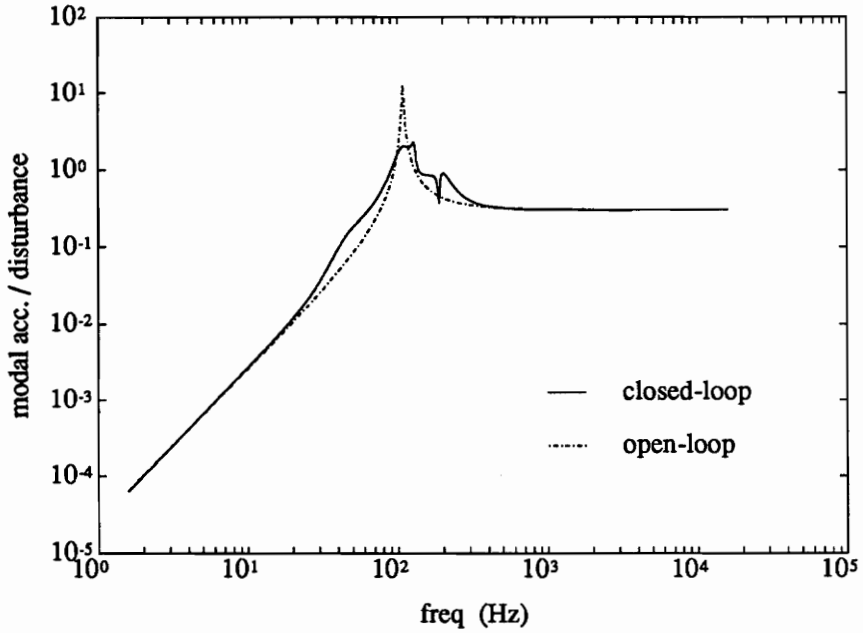

b. Vibration control

Figure 3.27: Frequency-domain simulation of closed-loop transfer function from broadband disturbance to mode 2 acceleration

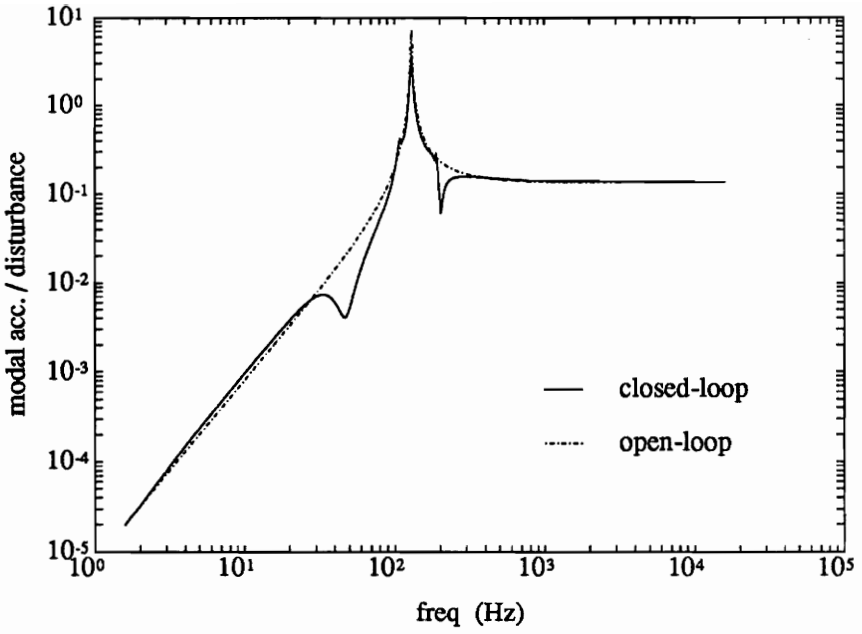

a. ASAC control

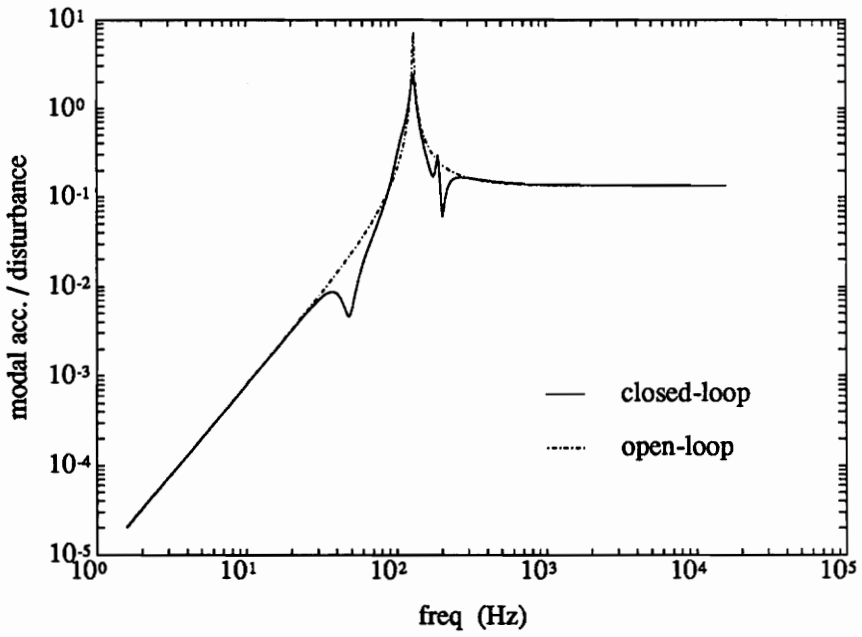

b. Vibration control

Figure 3.28: Frequency-domain simulation of closed-loop transfer function from broadband disturbance to mode 3 acceleration

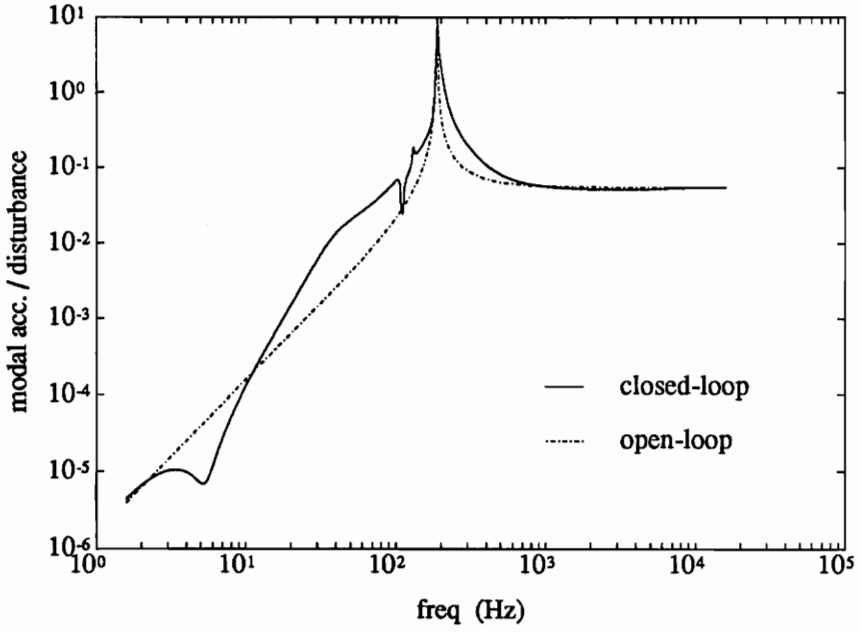

a. ASAC control

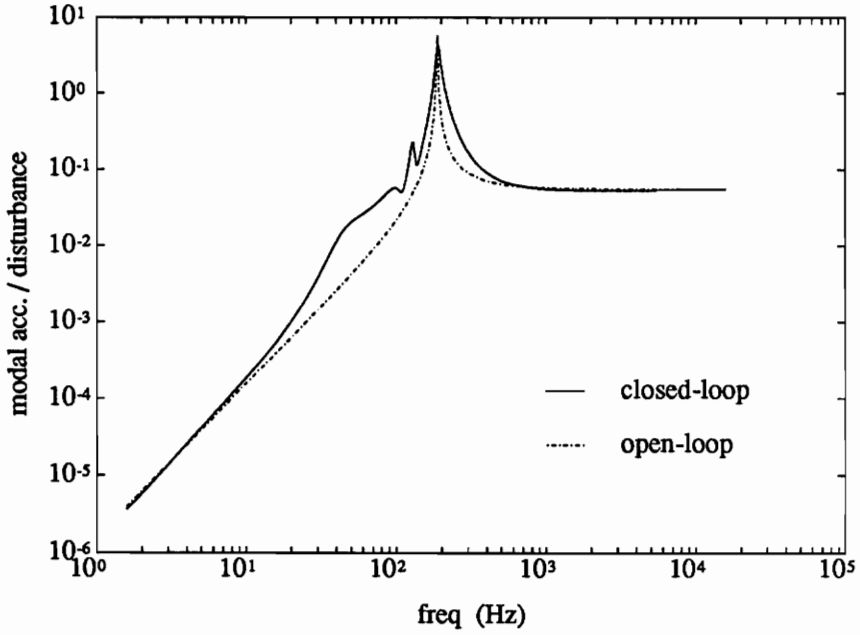

b. Vibration control

Figure 3.29: Frequency-domain simulation of closed-loop transfer function from broadband disturbance to mode 4 acceleration

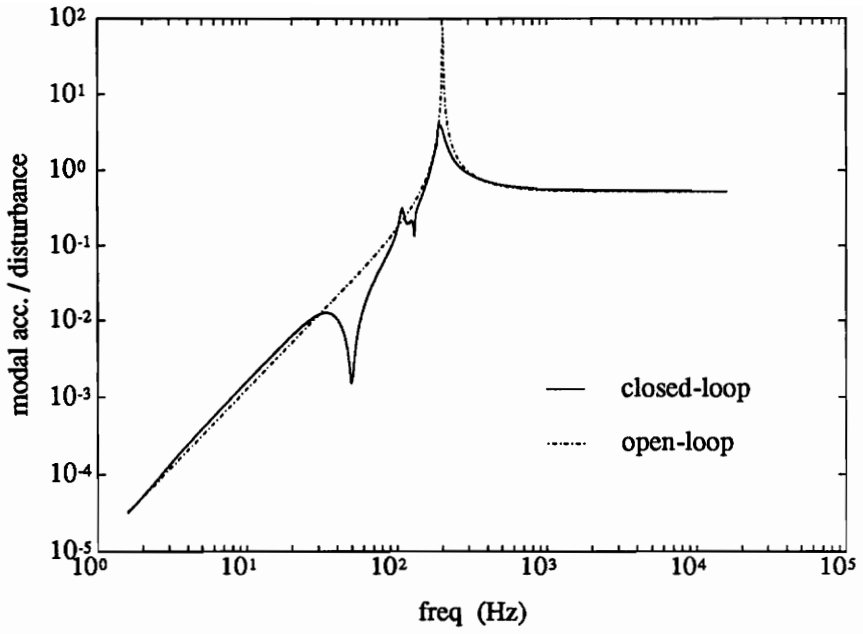

a. ASAC control

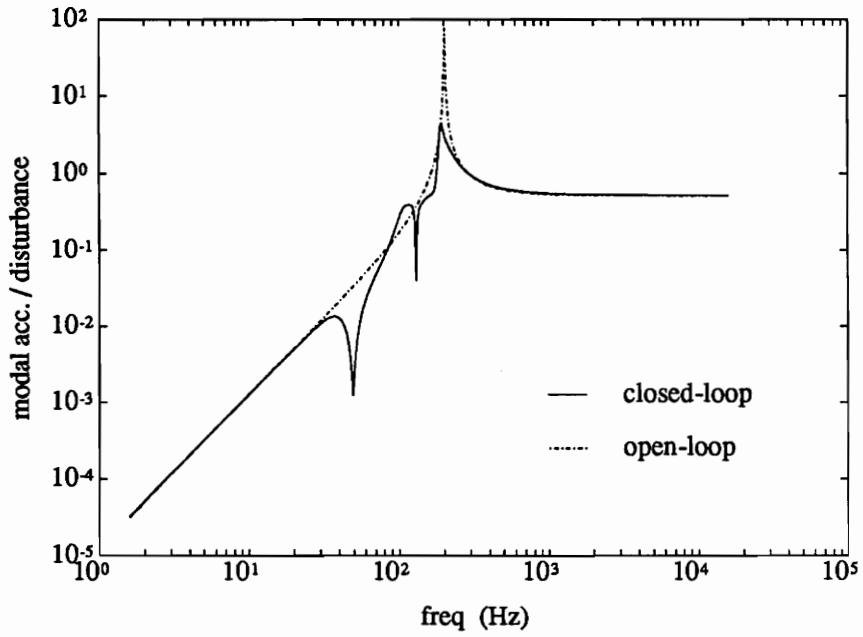

b. Vibration control

Figure 3.30: Frequency-domain simulation of closed-loop transfer function from broadband disturbance to mode 5 acceleration

out preference to its radiation efficiency. If the problem was formulated with more control actuators, the controller would be able to achieve this global suppression. ASAC control essentially reduces the number of modes which must be minimized, since it is trying to reduce a cost function which is affected nearly exclusively by only efficiently radiating modes.

The corresponding time-domain representations of the closed-loop system to the broadband disturbance are provided in figures 3.31 through 3.35. Again, the comparisons of the vibration control and ASAC results was based on equal control energy for both simulations.

Case 3: Impulsive Disturbance

The final simulation for the in-air ASAC controller examines the modal responses to an applied pulse. The applied pulse was 1 msec duration and was applied at accelerometer location five at $t = 0.01$ secs. Two selected plots compare the open-loop and closed-loop response for the vibration controller and the ASAC controller. Figure 3.36 shows that, once again, the ASAC controller penalizes the vibration of the very efficient first mode substantially more than the vibration control does. Referring to figure 3.37, the ASAC control also transfers energy to the very poorly radiating mode 4. As expected, the ASAC control does not attempt to reduce inefficient radiating modes. This theme of ASAC control, which is exactly the purpose for designing ASAC control, will be seen again for the ASAC control of the plate in a heavy fluid.

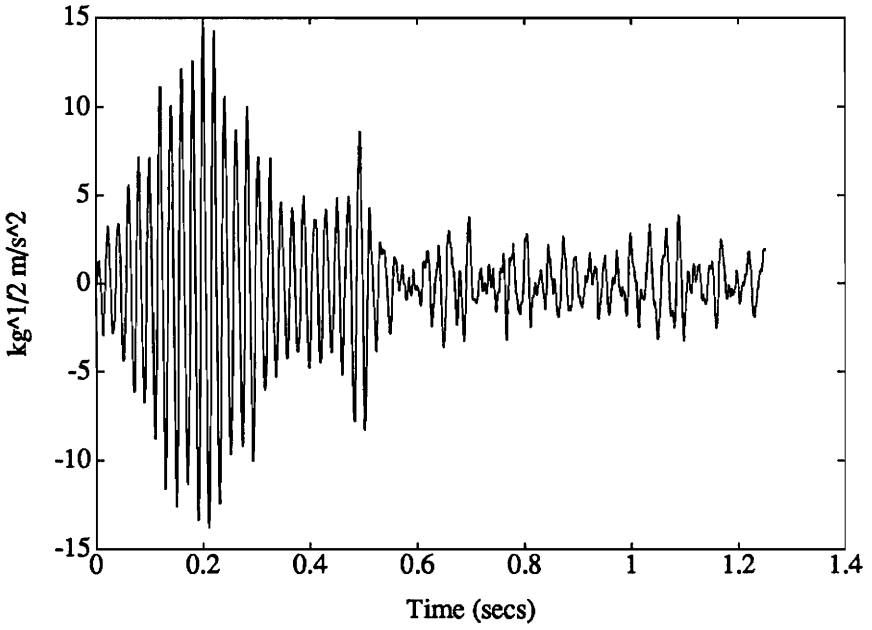

a. ASAC control

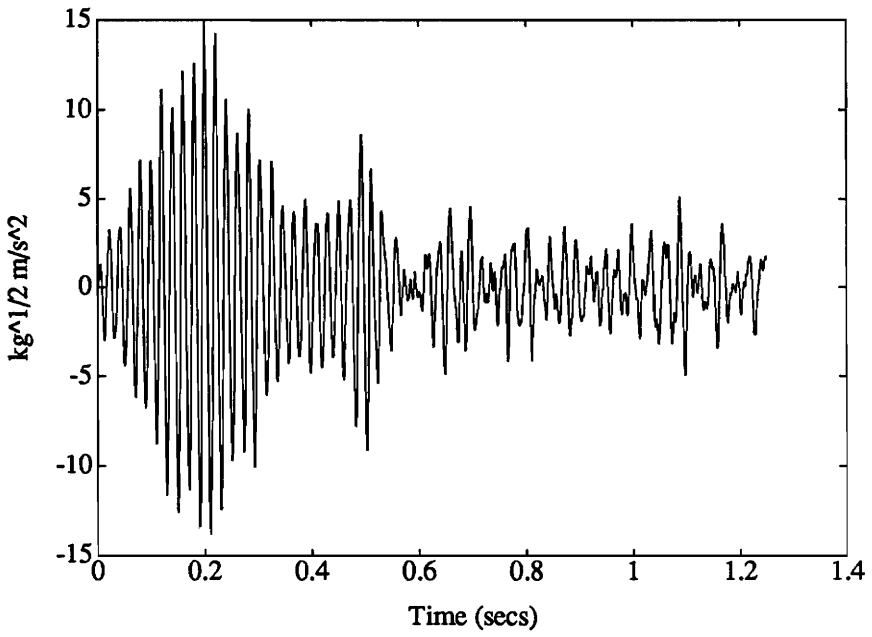

b. Vibration control

Figure 3.31: Time-domain simulation of mode 1 acceleration during vibration control and ASAC control of a broadband disturbance.

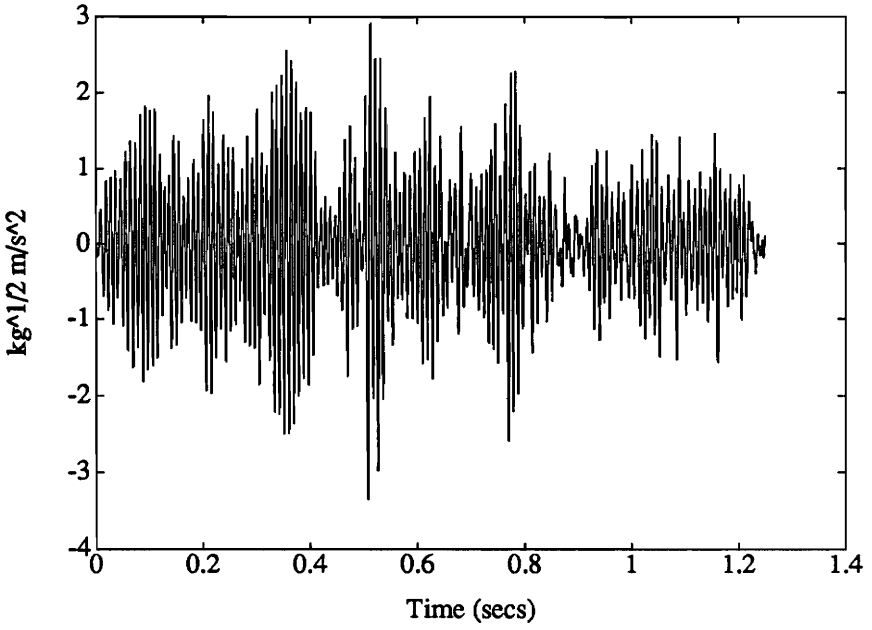

a. ASAC control

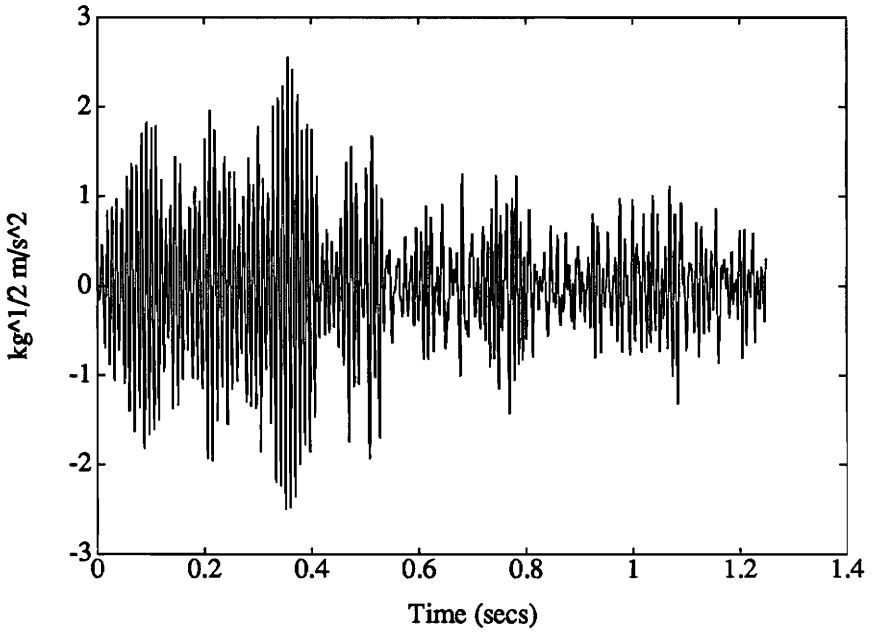

b. Vibration control

Figure 3.32: Time-domain simulation of mode 2 acceleration during vibration control and ASAC control of a broadband disturbance.

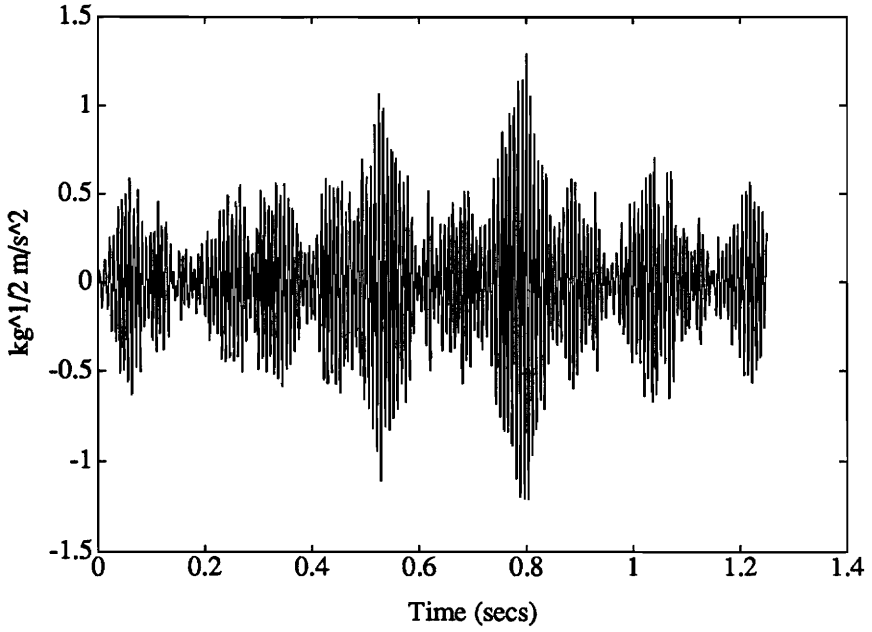

a. ASAC control

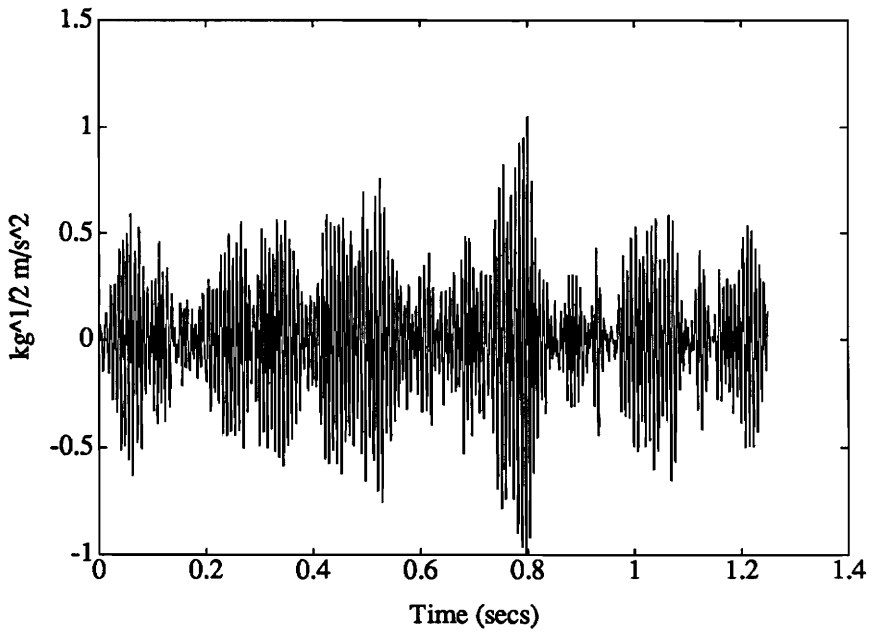

b. Vibration control

Figure 3.33: Time-domain simulation of mode 3 acceleration during vibration control and ASAC control of a broadband disturbance.

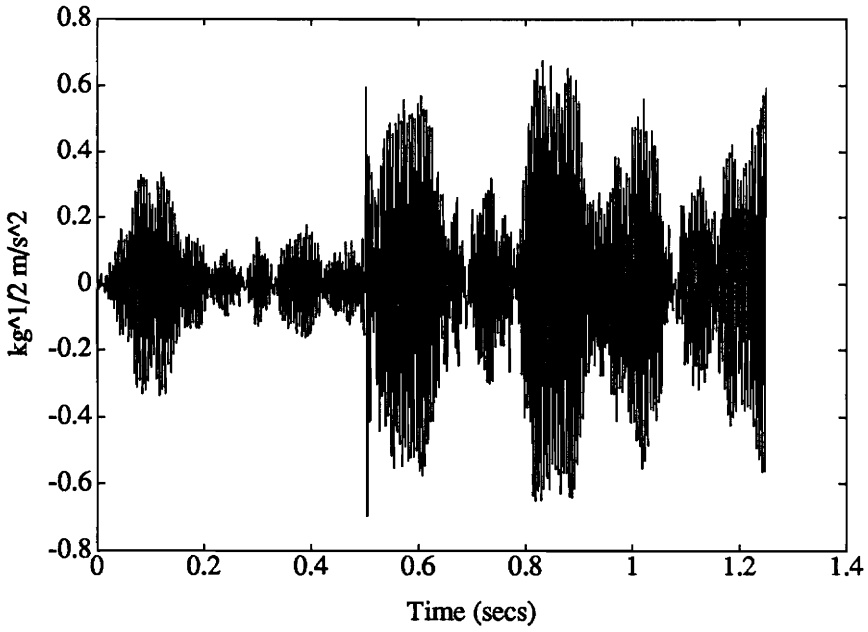

a. ASAC control

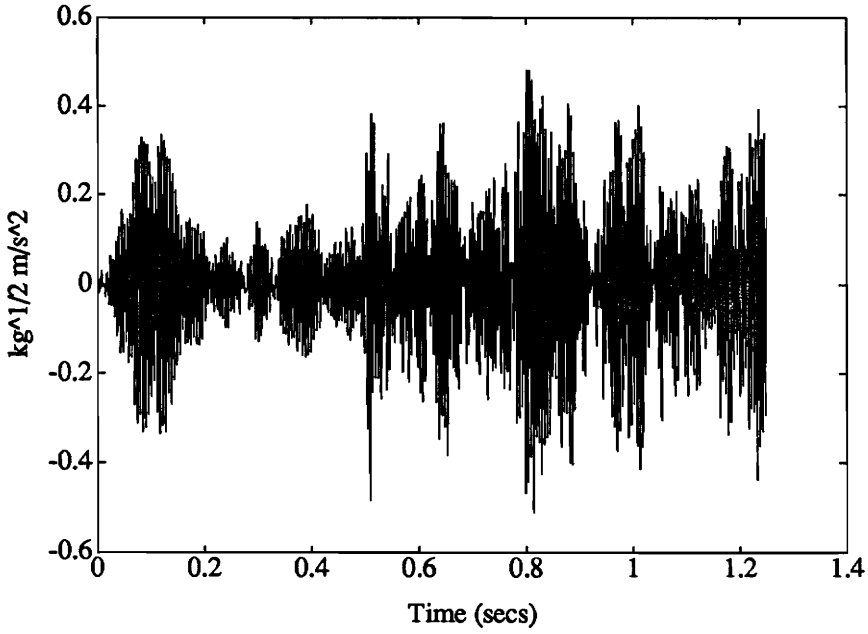

b. Vibration control

Figure 3.34: Time-domain simulation of mode 4 acceleration during vibration control and ASAC control of a broadband disturbance.

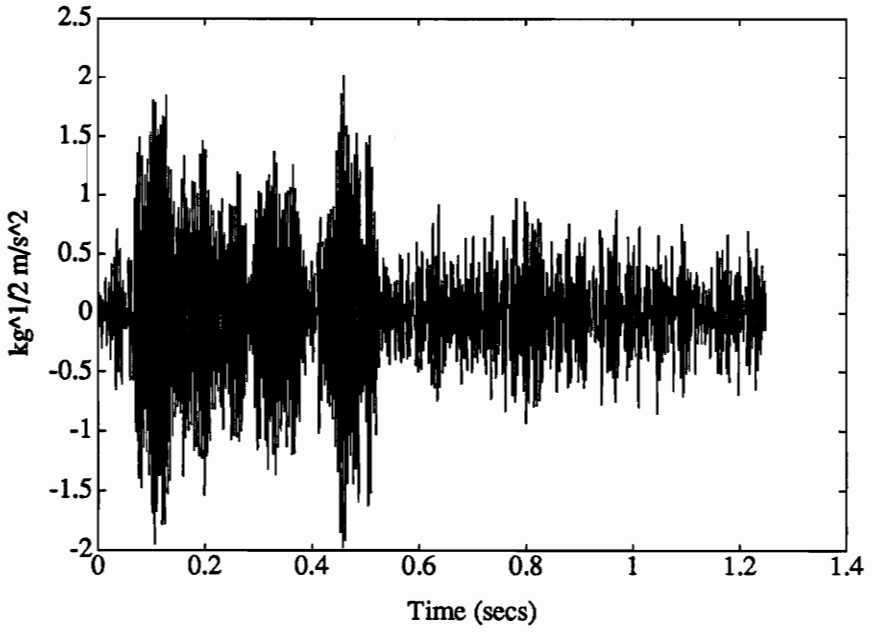

a. ASAC control

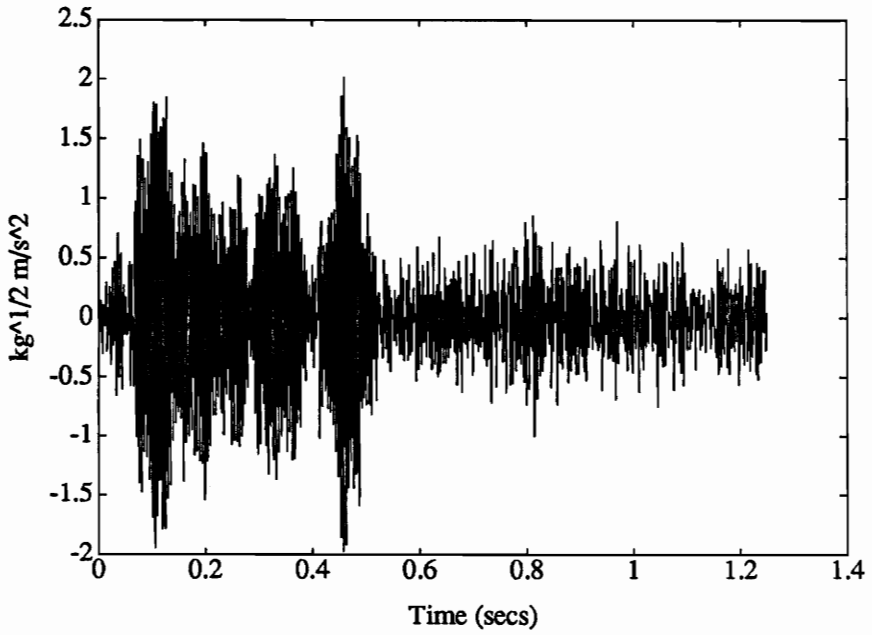

b. Vibration control

Figure 3.35: Time-domain simulation of mode 5 acceleration during vibration control and ASAC control of a broadband disturbance.

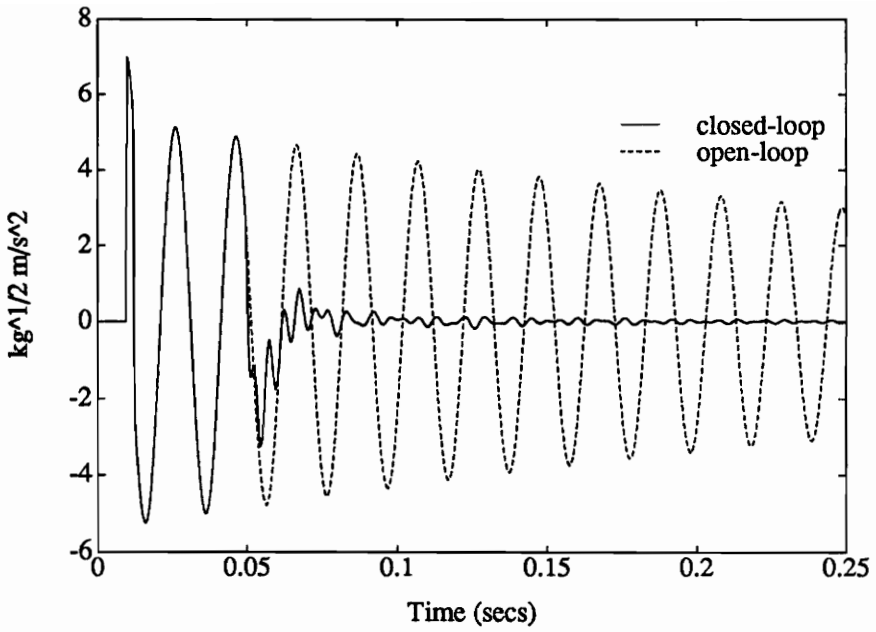

a. ASAC control

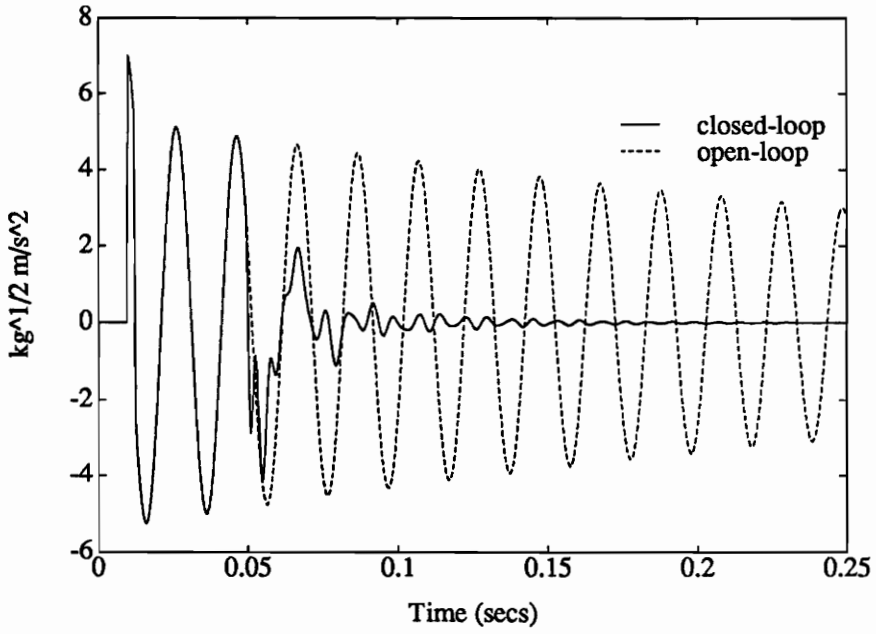

b. Vibration control

Figure 3.36: Time-domain simulation of mode 1 acceleration during vibration control and ASAC control of an impulsive disturbance.

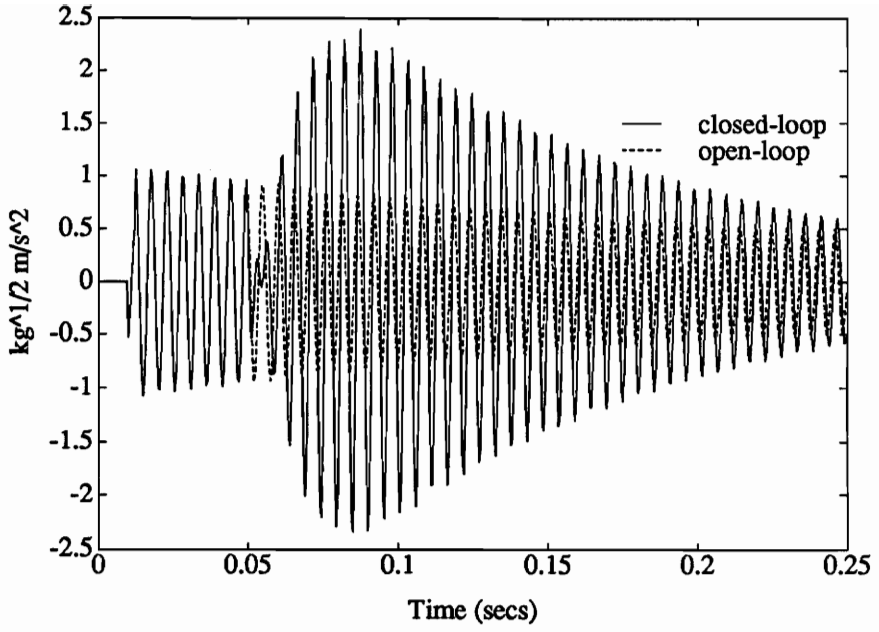

a. ASAC control

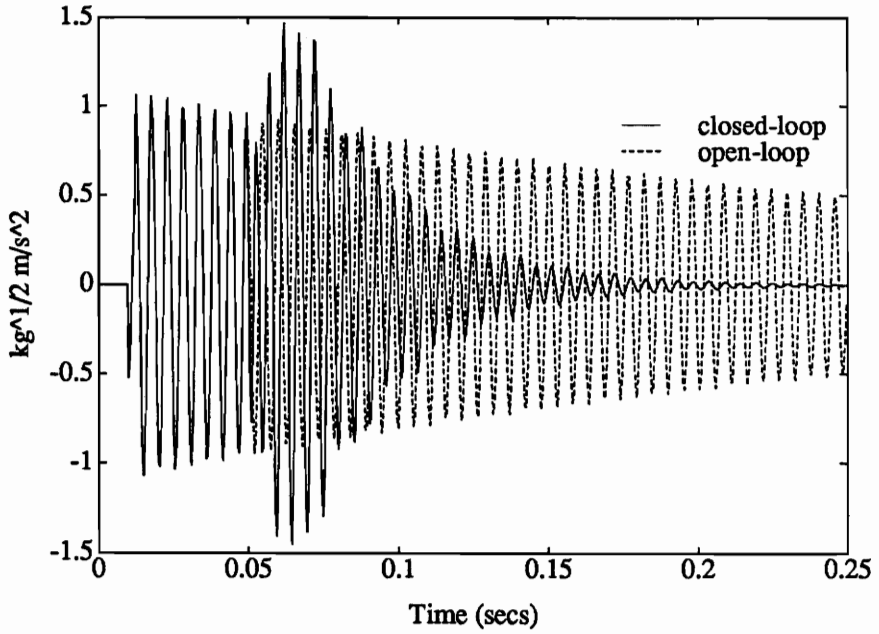

b. Vibration control

Figure 3.37: Time-domain simulation of mode 4 acceleration during vibration control and ASAC control of an impulsive disturbance.

Chapter 4

Heavy Fluid Loading: Structural Acoustic Modelling

As the relationship between the fluid mach number M and the intrinsic fluid loading parameter ϵ changes from $M \gg \epsilon$ to $M \ll \epsilon$ (see section 2.1.1), the formulation of an ASAC controller must include the back-reaction of the fluid on the structure. This additional forcing term leads to the coupled structure-acoustics problem introduced in Chapter 1. The results presented in this chapter will propose a state-space, optimal control for minimization of radiated noise from a submerged plate subject to impulsive, broadband, or harmonic disturbances. This controller form represents a significant advancement in the state-of-the-art of ASAC design methodology.

A simply-supported plate, mounted in a baffle and exposed to water of semi-infinite dimension on one side, will be the open-loop plant for this analysis. The half-space on the other side of the plate may be considered as in-vacuo or air. The in-vacuo modes will form the basis for the fluid-loaded ASAC design. The modelling approach used in this chapter relies on an analytical representation of the plate.

The intention of the work presented in this chapter is to provide an ASAC design

approach for the bandwidth defined by the heavy fluid loading criteria. It is necessary to provide this distinction because of the modal basis chosen for the controller. As stated earlier, a low-frequency control approach will be developed which is valid for subsonic response of the plate modes. Subsonic refers to the situation where $k_{mn} > k_o$ over the majority of the spectral distribution of the excitation. This bandwidth is characterized by radiated pressures generated by relatively sparse numbers of plate modes. As frequency is increased, the radiation approaches supersonic ratios and the order of a controller must increase proportionately with frequency. For this research, the subsonic assumption ensures a practical limit to system order. The effectiveness of model order reduction schemes for high order ASAC controllers remains as an exciting research issue at this time, with the potential for increasing the valid bandwidth of the approach presented next.

4.1 Structural acoustics modelling

The coupled structure-acoustics problem leads to a series of linear, coupled, second-order differential equations with non-constant coefficients. The coefficients are rational functions of the independent variable, which is time for the application physics of this problem. Written in standard form, the type of equations we will obtain may be written

$$\frac{d^2y}{dt^2} + a1(t)\,\frac{dy}{dt} + a2(t)\,y = f(t) \tag{4.1}$$

As discussed by Hildebrand [65], solutions to these types of equations may be obtained by expanding power series about discrete values of the independent variable. In state-space form, this means that the associated state matrix will be time-varying. This requires a solution about specific time points, in a discrete sense. Clearly, this

is not plausible for a controller design. Instead, the vibration of a heavy fluid-loaded plate will be formulated using an algebraic form of the coupled differential equations. The equations will be shown to be of the standard form given in Eq. 4.1. Following the algebraic equation development, a linear system theory approach will be used to develop an approximate method which sidesteps the apparent roadblock to the solution of the coupled equations in the time domain. *This procedure is imperative for the design of a vibration or ASAC controller capable of transient suppression.*

4.1.1 The structural dynamics

We begin with the differential equation of motion for the elastic plate,

$$m_p \frac{\partial^2 w(\bar{e},x,t)}{\partial t^2} + C_d \frac{\partial w(\bar{e},x,t)}{\partial t} + D\nabla^4 w(\bar{e},x,t) = d(\bar{e},x,t) + u(\bar{e},x,t) - p^s(\bar{e},x,t). \tag{4.2}$$

where

$$\begin{aligned} \bar{e} &= (y,z) \\ D &= \frac{Eh^3}{12(1-\nu^2)} \\ C_d &= \frac{c}{A_p} \\ m_p &= \rho_p h \end{aligned}$$

and $w(\bar{e},x,t)$ is the displacement normal to the plate in the x direction, using the same coordinate system introduced by figure 3.1. (The x coordinate will be omitted in the notation for the following derivations unless it becomes necessary for clarification.) Shear deformation is neglected in equation 4.2 because $k_b h < 1$ over the control bandwidth of interest for this problem. The bi-Laplacian operator is

given by

$$\nabla^4 = \frac{\partial^4}{\partial y^4} + \frac{\partial^4}{\partial z^4}$$

and the forcing terms in equation 4.2 are a mechanical disturbance, $d(\bar{e}, t)$, a pressure loading $p^s(\bar{e}, t)$ caused by the back reaction of the radiated acoustic pressure and a control force $u(\bar{e}, t)$. The units of the equation are $\frac{kg}{ms^2}$, or force per unit area.

Before proceeding, it will be helpful to change the detailed form of equation 4.2 to a more general form, using the notation of Meirovitch [66]. Then the dynamics of the open-loop plant may be written

$$Kw(\bar{e}, t) + C\dot{w}(\bar{e}, t) + m_p(\bar{e})\ddot{w}(\bar{e}, t) = d(\bar{e}, t) - p^s(\bar{e}, t) + f(\bar{e}, t) \qquad (4.3)$$

where K and C are stiffness and damping differential operators, respectively. For the following analysis, we specify that K is positive definite (i.e. no rigid body modes) and self-adjoint (i.e. positive real eigenvalues). Also, C is defined as viscous damping, proportional to the stiffness operator K and the mass distribution m_p according to the following:

$$C = \alpha\, K + \beta\, m_p. \qquad (4.4)$$

Now a modal analysis of equation 4.3 will be used to transform the system to a modal coordinate system.

The boundary conditions for the simply-supported plate were given by equations 3.2 and 3.3. A solution of the eigenvalue problem provided the shape functions defined

by equation 3.4. For convenience, the plate eigenvectors will be defined here as

$$\psi_k(\bar{e}) = sin\frac{n\pi y}{L_y} sin\frac{m\pi z}{L_z} \tag{4.5}$$

$$\psi_l(\bar{e}) = sin\frac{r\pi y}{L_y} sin\frac{q\pi z}{L_z} \tag{4.6}$$

The normalization and orthogonality imposed on the eigenvectors for this problem are stated to be

$$\int_0^{L_z}\int_0^{L_y} \psi_k(\bar{e}) m_p \psi_l(\bar{e}) d\bar{e} = \delta_{kl} \quad k = l = 1, 2, 3... \tag{4.7}$$

$$\int_0^{L_z}\int_0^{L_y} \psi_k(\bar{e}) K \psi_l(\bar{e}) d\bar{e} = \omega_k^2 \delta_{kl} \quad k = l = 1, 2, 3... \tag{4.8}$$

$$\int_0^{L_z}\int_0^{L_y} \psi_k(\bar{e}) C \psi_l(\bar{e}) d\bar{e} = 2\zeta_k \omega_k \delta_{kl} \quad k = l = 1, 2, 3... \tag{4.9}$$

where the constants of equation 4.4 have been chosen as $\alpha = \frac{2\zeta_k}{\omega_k}$ and $\beta = 0$ by analogy with a single-degree-of-freedom system, as discussed by Thomson [67].

Applying the modal expansion theorem

$$w(\bar{e}, t) = \sum_{l=1}^{\infty} \psi_l(\bar{e}) w_l(t) \tag{4.10}$$

to equation 4.3, multiplying the result by $\psi_k(\bar{e})$, and integrating over the spatial domain of the plate, the modal form of the plate equation becomes

$$\ddot{w}_k(t) + 2\zeta_k \omega_k \dot{w}_k(t) + \omega_k^2 w_k(t) = d_k(t) - p_k(t) + f_k(t). \tag{4.11}$$

where $k = 1, 2, 3...$ and the generalized forcing terms are given by

$$d_k(t) = \int_0^{L_x} \int_0^{L_y} \psi_k(\bar{e}) d(\bar{e}, t) d\bar{e} \tag{4.12}$$

$$p_k(t) = \int_0^{L_x} \int_0^{L_y} \psi_k(\bar{e}) p^s(\bar{e}, t) d\bar{e} \tag{4.13}$$

$$f_k(t) = \int_0^{L_x} \int_0^{L_y} \psi_k(\bar{e}) f(\bar{e}, t) d\bar{e}. \tag{4.14}$$

This is essentially the algebraic analog of the modal representation of the plate given in equation 3.8. However, the independence of this infinite set of equations cannot be established until the relationship between the generalized surface pressure $p_k(t)$ and the modal velocities $\dot{w}(t)$ is defined. It has been shown by various authors [8, 24, 44, 45] that $p^s(\bar{e}, t)$ in fact spans the space of the in-vacuo modal basis, thus coupling the equations 4.12. It is possible to solve for the exact relationship between $p_k(t)$ and $\dot{w}(t)$ for the simply-supported plate for harmonic disturbances but an exact solution for arbitrary structures and disturbances is not achievable. Because our goal is an ASAC controller capable of transient or persistent disturbance suppression, the following approach to this obstacle will be investigated.

The coupling between the generalized surface pressure created by the $k'th$ mode and the response of every other $l'th \neq k$ mode will be derived using steady-state analysis techniques. This approach was used to generate the radiation filters in Chapter 3. It will be helpful to re-state the concept behind the following development: a filter will be developed which describes the coupling between modal velocities and acoustic surface pressure using steady-state response information. An approximation of the transfer function of the filter will be created from a superposition of frequency

response functions for varying values of ω. Once the transfer function approximation is complete, the response of the system to arbitrary time-domain signals can be realized by applying the input waveform to the filter and observing the output. As before, this approach will require an increase in the order of the resulting ASAC design relative to a comparable vibration controller for a plate with light fluid loading. The development of the transfer function approximation will be discussed next.

4.1.2 The structural-acoustic dynamics

The objective is to determine the relationship between the generalized surface pressure of equation 4.13 and the modal velocities $\dot{w}_k$. For the baffled, simply-supported plate excited by a harmonic disturbance a function may be derived which achieves this. It should be mentioned here that, in general, this impedance function may not be easy to describe and may be impossible using any exact solution method. However, numerical approaches to this phase of the controller design may be developed which provide the required transfer function approximation for this ASAC design approach. No investigation of candidate numerical methods is included in this work. The emphasis here is on the overall design approach. Now, a brief description of the acoustic boundary value problem for the plate is provided.

The acoustic velocity field in the medium with a phase velocity c_o is modelled by the wave equation

$$\nabla^2 \Psi(\bar{e}, x, t) = \frac{1}{c_o^2} \frac{\partial^2 \Psi(\bar{e}, x, t)}{\partial t^2}, \qquad x > 0 \tag{4.15}$$

where ∇^2 is the three-dimensional Laplacian operator and $\Psi(\bar{e}, x, t)$ is the velocity

potential. As before, we suppress x except when required for clarity. The acoustic pressure in the fluid derives from the Navier-Stokes equations

$$p(\bar{e},t) = -\rho_o \frac{\partial \Psi(\bar{e},t)}{\partial t} \tag{4.16}$$

where ρ_o is the mass density of the fluid. The condition for continuity of velocity at the plate-fluid interface is

$$\frac{\partial \Psi(\bar{e},x=0,t)}{\partial x} = \dot{w}(\bar{e},x=0,t), \quad on\ the\ plate \tag{4.17}$$

$$= 0, \qquad off\ the\ plate \tag{4.18}$$

Equations 4.15 through 4.18 comprise the boundary value problem which must be solved for the fluid.

A transform solution for the boundary value problem associated with rectangular sound radiators was illustrated by Junger and Feit [8]. They obtained an explicit expression for the pressure in terms of the acceleration. A similar approach will be used here and is based on harmonic excitation of the plate. The steady-state information will then be used to synthesize an input-output relationship between modal velocity and surface pressure which is valid for arbitrary input disturbance waveforms.

For the following steady-state analysis, the notation $g(t) = \tilde{g}e^{-j\omega t}$ will be employed for any harmonic time-dependent function. Thus, for $\Psi(t) = \tilde{\Psi}e^{-j\omega t}$ it may be shown that the wave equation becomes the Helmholtz equation

$$\left(\nabla^2 + k_o^2\right)\Psi(\bar{e},x,t) = 0 \tag{4.19}$$

Defining the double Fourier transform pair as follows:

$$\hat{f}(k_x, k_y) = \int\int_{-\infty}^{\infty} f(x,y)\, exp[-i(k_x x + k_y y)]dxdy, \tag{4.20}$$

$$f(x,y) = \frac{1}{(2\pi)^2}\int\int_{-\infty}^{\infty} \hat{f}(k_x, k_y)\, exp[i(k_x x + k_y y)]dk_x dk_y, \tag{4.21}$$

the transform on the spatial distribution of the velocity potential yields the relationship between the acoustic wavenumber and the trace wavenumbers of a propagating wave in the fluid, namely

$$k_o^2 = k_x^2 + k_y^2 + k_z^2 = k_x^2 + k_b^2 \tag{4.22}$$

where k_b is the bending wavenumber of the plate.

The similarly transformed interface condition becomes

$$jk_x\Psi(\bar{k}, t) = \dot{w}(\bar{k}, t), \quad x = 0 \tag{4.23}$$

Using equation 4.22 we find an expression which relates the velocity potential to the velocity of the plate at the interface

$$\Psi(\bar{k}, t) = -j\frac{\dot{w}(\bar{k}, t)}{\sqrt{k_o^2 - k_b^2}} \tag{4.24}$$

Modifying equation 4.16 for the known harmonic excitation and doubly transforming spatially, a relationship between acoustic pressure and the velocity potential may be written as

$$p(\bar{k}, t) = -j\rho_o c_o k_o \Psi(\bar{k}, t) \tag{4.25}$$

Substituting equation 4.24 into equation 4.25 gives the desired relationship between the surface pressure and the plate velocity

$$p(\bar{k},t) = -\rho_o c_o k_o \frac{\dot{w}(\bar{k},t)}{\sqrt{k_o^2 - k_b^2}} \tag{4.26}$$

The form of equation 4.26 is such that we have derived the specific acoustic impedance for the simply-supported plate. At the interface, the impedance determines the pressure loading on the plate and is seen to be a complex quantity with real and imaginary parts depending on the ratio of k_o and k_b. Defining the radiation impedance,

$$\mathcal{Z}_{rad} = \frac{\rho_o c_o k_o}{\sqrt{k_o^2 - k_b^2}} \tag{4.27}$$

we may examine in a general sense the physics of $\mathcal{Z}_{rad}$ by separating the real part and factoring an ω from the imaginary part so that

$$\begin{aligned} p(\bar{k},t) &= \mathcal{Z}_{rad}\dot{w}(\bar{k},t) && (4.28)\\ &= (C_{rad} + j\omega M_{rad})\,\dot{w}(\bar{k},t) && (4.29)\\ &= C_{rad}\dot{w}(\bar{k},t) + M_{rad}\ddot{w}(\bar{k},t). && (4.30) \end{aligned}$$

This shows that the radiation impedance provides a term proportional to the plate velocity and subsequently a damping force related to energy lost by the structure in the form of radiated energy. The imaginary term, proportional to plate acceleration, is related to the inertial force associated with the entrained mass of the fluid adjacent to the plate. So the inclusion of the surface pressure on the right side of equation 4.4 would be expected to modify the mass and damping matrices of the in-vacuo system in some manner during the structural acoustics modelling process.

Now the surface pressure must be related to a modal velocity. Using the expansion

$$\dot{w}(\bar{e},t) = \sum_{l=1}^{\infty} \psi_l(\bar{e}) \dot{w}_l(t) \tag{4.31}$$

we can write the wavenumber transform of the plate velocity as

$$\dot{w}(\bar{k},t) = \int_{A_p} \sum_{l=1}^{\infty} \psi_l(\bar{e}) \dot{w}_l(t) e^{j\bar{k}\cdot\bar{e}} d\bar{e}. \tag{4.32}$$

A compact notation for the velocity transforms is defined as

$$\dot{w}(\bar{k},t) = \sum_{l=1}^{\infty} S_l(\bar{k}) \dot{w}_l(t) \tag{4.33}$$

with the definition of $S_l(\bar{k})$ following from equation 4.32 and a reminder that $\dot{w}(t) = \tilde{\dot{w}} e^{-j\omega t}$.

Introducing equation 4.33 into the expression for the surface pressure,

$$p(\bar{k},t) = \frac{\rho_o c_o k_o}{\sqrt{k_o^2 - k_b^2}} \sum_{l=1}^{\infty} S_l(\bar{k}) \dot{w}_l(t) \tag{4.34}$$

and then carrying out the inverse Fourier transform back to spatial coordinates, we get an expression for the surface pressure in modal coordinates

$$p(\bar{e},t) = \int_{-\infty}^{\infty} \int_{-\infty}^{\infty} \frac{\rho_o c_o k_o}{\sqrt{k_o^2 - k_b^2}} \sum_{l=1}^{\infty} S_l(\bar{k}) \dot{w}_l(t) e^{j\bar{k}\cdot\bar{e}} d\bar{k} \tag{4.35}$$

Finally, we need to substitute 4.35 for the surface pressure into the generalized

surface pressure of equation 4.13.

$$p_k(t) = \int_{-\infty}^{\infty}\int_{-\infty}^{\infty} \frac{\rho_o c_o k_o}{\sqrt{k_o^2 - k_b^2}} \sum_{l=1}^{\infty} S_l^*(\bar{k}) S_k(\bar{k}) d\bar{k} \;\; \dot{w}_l(t) \tag{4.36}$$

A compact notation for equation 4.36 may be written as

$$p_k(t) = \sum_{l=1}^{\infty} \mathcal{Z}_{kl}(\omega) \dot{w}_l(t) \tag{4.37}$$

where $\mathcal{Z}_{kl}(\omega)$ follows from equation 4.36 and is the weighted acoustic impedance which maps the l_{th} modal velocity to the surface pressure forcing the k_{th} mode. Recalling the harmonic time dependence specified at the beginning of the section, it is clear that $\mathcal{Z}_{kl}(\omega)$ is defined for a specific frequency. *If the frequency is stepped over the bandwidth of interest for the ASAC design, the filtering characteristics of the impedance matrix will be specified completely.* The characteristics of $\mathcal{Z}_{kl}(\omega)$ have been the subject of substantial research as highlighted in Chapter 2. It is important to emphasize the physics associated with the impedance matrix from the perspective of control design. This will be accomplished next.

4.1.3 The radiation impedance matrix

An exact solution to the integral of equation 4.36 has not been achieved but asymptotic solutions have been reported by Davies [21]. Sandman and Vieira [22] and Lomas and Hayek [23] presented numerical solutions for simply-supported plates. A numerical approach was used for this research, also. Details of the procedure used to generate a radiation impedance matrix from the infinite series of equations will be presented.

We begin by truncating the system of equations for the radiation impedance to a

finite number. The number of modes to retain in the representation must be sufficient to allow an accurate calculation of the open-loop system response over the bandwidth of interest. For this research, an approximate control bandwidth from 0 to 100 Hz is desired for the heavy fluid-loaded case. Since the frequencies of the fluid-loaded plate are known only approximately a priori, the first nine modes of the plate were retained in the radiation impedance calculations. A solution of the eigenvalue problem for the in-vacuo resonances of the plate, using equation 4.2, provides the frequencies of the first nine plate modes. The values are shown in table 4.1 along with the modal indices m and n corresponding to the notation of equation 4.2.

Table 4.1: In-vacuo resonances of the simply-supported plate

m	n	Freq (Hz)
1	1	47.8
2	1	106.6
1	2	132.5
2	2	191.3
3	1	204.6
1	3	273.6
3	2	289.3
2	3	332.4
4	1	341.8

Referring back to equation 4.36, the task is to solve the double integral for the coupling of the k_{th} mode to every l_{th} mode in the summation. Fortunately, the problem is reduced by observing that the product of the shape functions in the integrand $S_l^*(\bar{k})S_k(\bar{k})$ is non-zero only when the indices associated with k and l have the same parity. For example, for two modes of indices (m,n) and (q,r), (m and q) and (n

and r) must both be even or both be odd. Thus, each mode couples at most to only a quarter of all other modes. This reduces the computational task significantly. In addition, it may be shown that the non-zero inner product of the integral is an even function which allows a change of the lower limit of integration in equation 4.36 to zero, with the proper scaling.

Solutions for the real part and the imaginary part of the integral $\mathcal{Z}_{kl}(\omega)$ require integrations over different ranges of the wavenumber space $\bar{k}$. The real part is associated with the supersonic wavenumbers, as indicated by the denominator of equation 4.36. The imaginary part is calculated over the subsonic space. Finally, the numerical integrations which must be completed are defined for the real and imaginary parts. Writing the complex impedance

$$\mathcal{Z}_{kl}(\omega) = C_{kl}(\omega) - jM_{kl}(\omega) \tag{4.38}$$

and dropping the notation for ω, we can define the radiation impedance matrix by the following:

$$[\mathcal{Z}]_{rad} = [C_{rad}] - j\,[M_{rad}] \tag{4.39}$$

where

$$C_{rad}(k,l) = \int_0^{k_o}\int_0^{k_o} \frac{\rho_o c_o k_o}{\sqrt{k_o^2 - k_b^2}} S_l^*(\bar{k}) S_k(\bar{k}) d\bar{k} \tag{4.40}$$

and

$$M_{rad}(k,l) = \int_{k_o}^{k_x\to\infty}\int_{k_o}^{k_y\to\infty} \frac{\rho_o c_o k_o}{\sqrt{k_o^2 - k_b^2}} S_l^*(\bar{k}) S_k(\bar{k}) d\bar{k} \tag{4.41}$$

A three-point Newton-Cotes closed numerical integration was used to evaluate the

integrals of equations 4.40 and 4.41. The fluid properties were assigned values corresponding to water: $\rho = 1000\frac{kg}{m^3}$ and $c = 1500\frac{m}{sec}$. A sine dwell over the bandwidth of interest for all k, l modes of the required parity provided a representation of $[\mathcal{Z}_{rad}]$ at each frequency. The frequencies of the stepped sine evaluations were chosen to begin at $10Hz$ and continue through the coincidence frequencies of the various modes.

Some results of the numerical calculations are shown in figures 4.1 and 4.2. It was shown by equations 4.30 that the real part of the impedance corresponds to a radiation damping effect on the plate while the imaginary part of the impedance is associated with the entrained mass of the plate during vibration. Historically, acousticians have taken such an approach in dealing with the effects of fluid loading introduced by the impedance matrix. This form has a nice interpretation in that it is clear that the real part is in phase with velocity (hence a damping force) and the imaginary part is in phase with acceleration (hence an inertial force). This representation of the impedance matrix will be dealt with briefly in the following discussion.

The curves shown in figure 4.1 represent the self radiation resistance for the first five individual modes $k = l$ and appear along the diagonal in the radiation damping matrix $[C_{rad}]$. The units of the data are $\frac{1}{sec}$ because of the mass normalization chosen for the basis of the problem. Of course, this is consistent with the units of the viscous damping model chosen for the structure. Figure 4.2 shows the generalized added mass matrix for the diagonal terms of $[M_{rad}]$. The matrix is dimensionless which it must be if it is a mass in the formulation developed earlier. At the lower frequencies, the terms are a constant and are consistent with approximate equations for added mass of a fluid-loaded plate. The approximation derives from wave

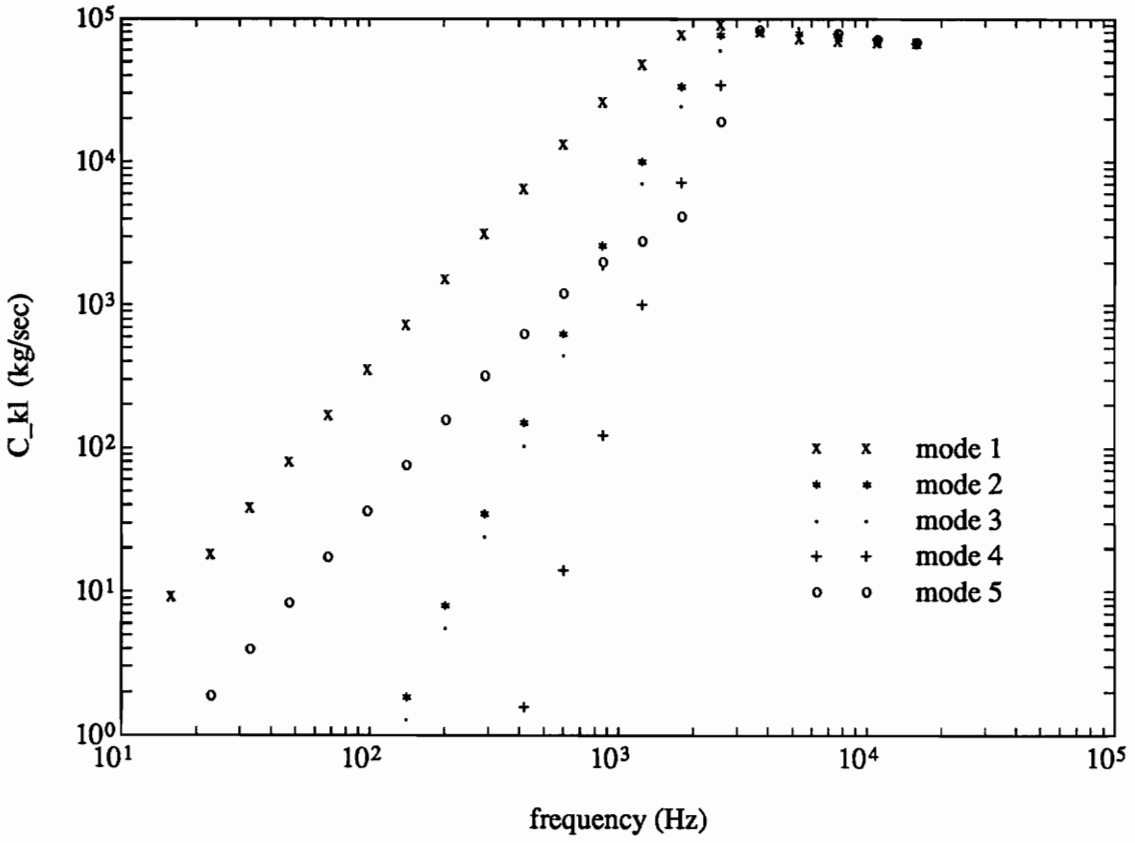

Figure 4.1: Self radiation resistances for the first five plate modes, (steel plate in water)

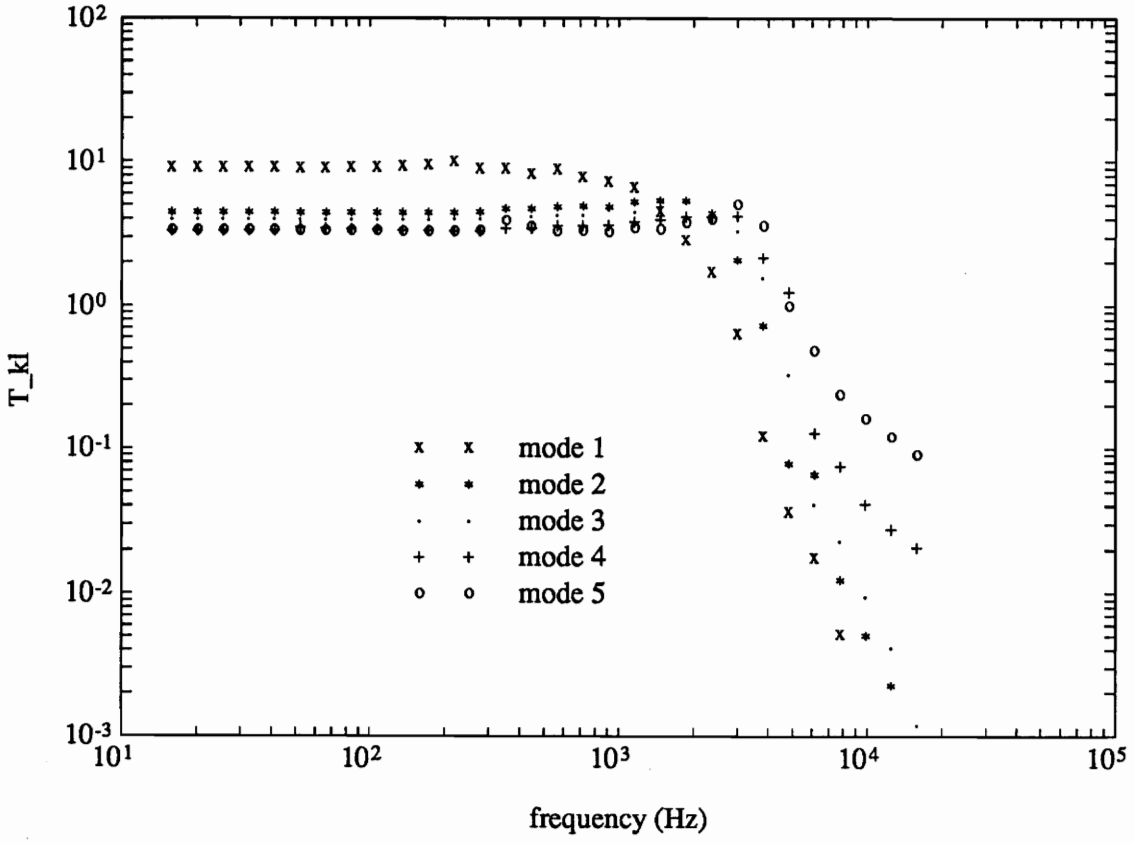

Figure 4.2: Self inertial coupling for the first five plate modes, (steel plate in water)

impedance considerations and is provided by Fahy [10]:

$$\omega_l^f = \frac{\omega_l}{\sqrt{1 + \frac{\rho_o}{m_p k_l}}} \tag{4.42}$$

where ω_l^f is the reduced fluid-loaded resonant frequency and ω_l represents the corresponding in-vacuo resonant frequency. A comparison of the reduction in the first five natural frequencies of the steel plate predicted by the approximate expression of 4.42 and the reduction due to the added mass values of $[M_{rad}]$ is shown in table 4.2. The expression for the submerged natural frequencies follows from substitution

Table 4.2: Submerged natural frequencies for a steel plate, approximate results and numerical results.

Approx. (Hz)	Numerical (Hz)
18.8	14.6
49.4	46.6
64.1	58.0
99.1	93.0
107.3	112.3

of equations 4.30 into equation 4.11. As expected, for these low-order plate modes the approximate result underestimates the inertial loading of the fluid on the plate. However, the purpose of the comparison was simply to show that the numerical integration results for $[M_{rad}]$ were representative of added mass.

The decomposition of the impedance matrix shown in equation 4.39 is acceptable for physical interpretation of the acoustic principles and steady-state analysis of the plate response. However, the goal of this derivation is to generate state equations which are practical for both transient and persistent disturbances. Recall that the augmentation method of chapter 3 relied on a rational approximation of the radiated

power operator matrix. This allowed a characterization of the power output for any arbitrary time signal. The question now is whether a similar approach may be used for the heavy fluid loading case. This question will be addressed in the following section.

Rational approximation of the radiation impedance matrix

It will be shown that a state augmentation approach may be used to realize a state space representation of the coupled fluid-structure equations. First, the link between the form of the matrix $[\mathcal{Z}_{rad}]$ and a causal system representation will be discussed. The result is that the complex form must be dealt with directly. Next, the procedure for deriving the state space realization of the radiation impedance dynamics will be detailed. Finally, the simplified state equations are presented for subsequent augmentation to the open-loop plant equations.

Traditional steady-state analysis techniques suggest the individual treatment of the real and imaginary terms of Z_{rad} above. For the state-space representation, a rational approximation of the frequency response shown for each term in figure 4.1 is required. The constant inertial loading terms do not require dynamic modelling. Because the radiation loading terms are real, it is not possible to approximate a stable transfer function for the zero phase system. However, if the terms of $[\mathcal{Z}_{rad}]$ are dealt with in their complex form, the individual terms behave like simple high pass filters to a first approximation. Figure 4.3 shows the Z_{rad} magnitudes for the first five plate modes, including any coupling terms which arise in this modal grouping. Notice that the parity requirements for coupling are met only by mode 1 and mode 5 for this case. The phase of the loading curves are provided in figure 4.4. A close

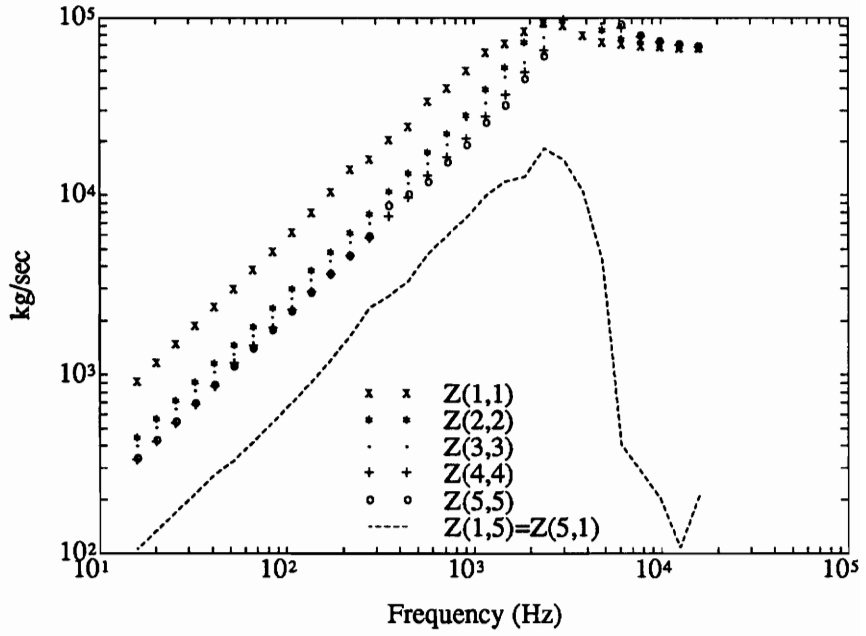

Figure 4.3: Z_{rad} magnitude, modes 1 - 5

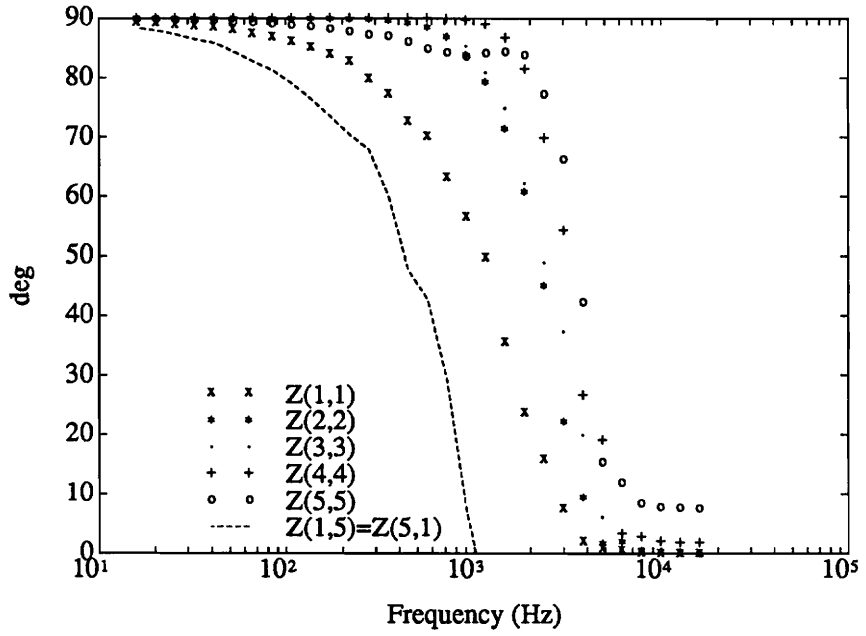

Figure 4.4: Z_{rad} phase, modes 1 - 5

examination of the mode 1 magnitude and phase indicates that a transfer function for a simple high pass filter $\frac{s}{s+a}$ should approximate the curve adequately. This approximation is shown for the first mode in figure 4.5. The approximation of the $Z(5,5)$ term, corresponding to the fifth mode, is shown in figure 4.6. The curve-fits indicate that higher order dynamics are required to provide an accurate estimate over the entire bandwidth shown. This is evident mostly in the phase matching. In order to keep the order of the fluid loading model low, a design specification was chosen as follows: Accurate modelling of the fluid loading was specified for a bandwidth of 0 to 500 Hz only. This criteria was used while modelling each individual term of figures 4.3 and 4.4.

Rational approximations for the fluid loading matrix were determined using MATLAB software. Proper transfer functions for the self and cross terms were designed and then combined in a MIMO state space representation. The transfer functions for each element are provided in table 4.3. A state-space minimal realization was computed for the polynomial impedance matrix. The input to the system is modal velocity and the output is modal surface pressure. Thus, the state vector formulation may be written as:

$$\dot{p} = F_{rad}p + G_{rad}\dot{w} \tag{4.43}$$

$$Z = C_{rad}p + D_{rad}\dot{w} \tag{4.44}$$

$$\tag{4.45}$$

where Z is the resultant fluid loading force vector. Each variable in Z is associated with a specific mode. This state-space equation, in combination with the state-space form of the in-vacuo plate equation, represents the solution to the coupled structure-

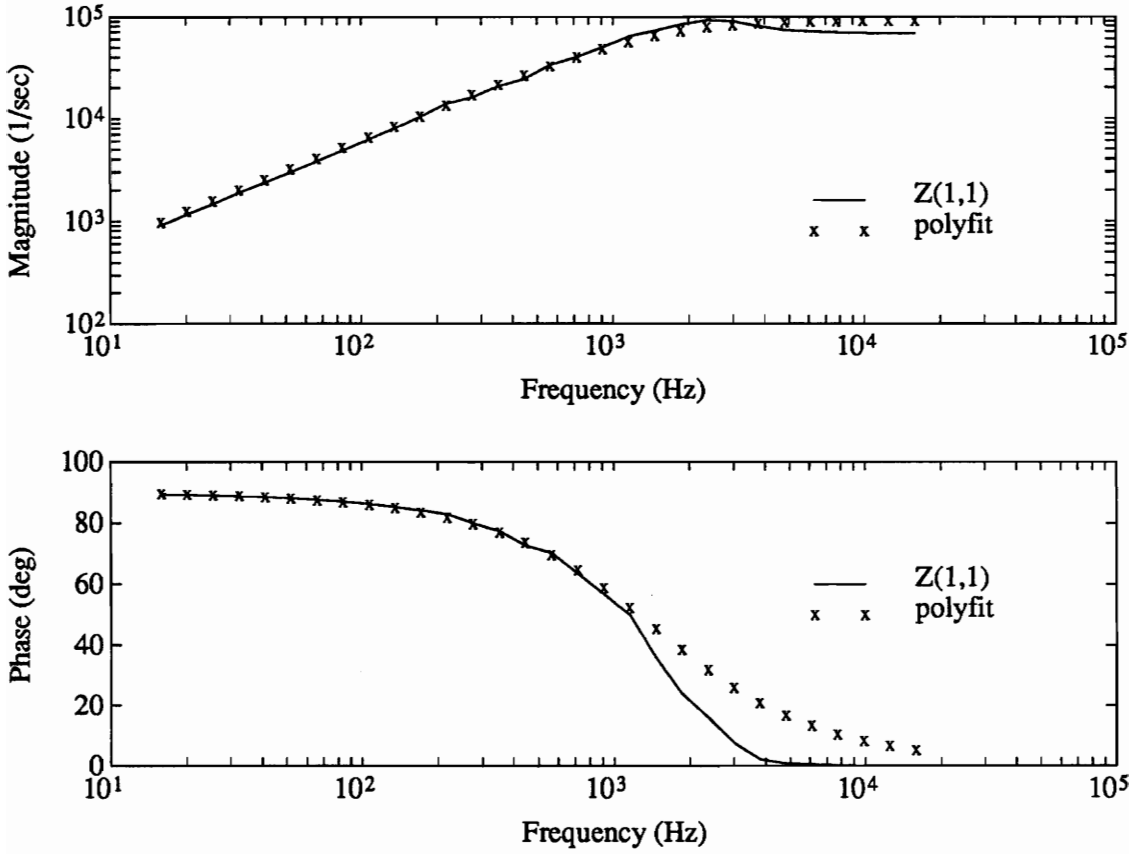

Figure 4.5: Z_{rad} mode 1 rational approximation

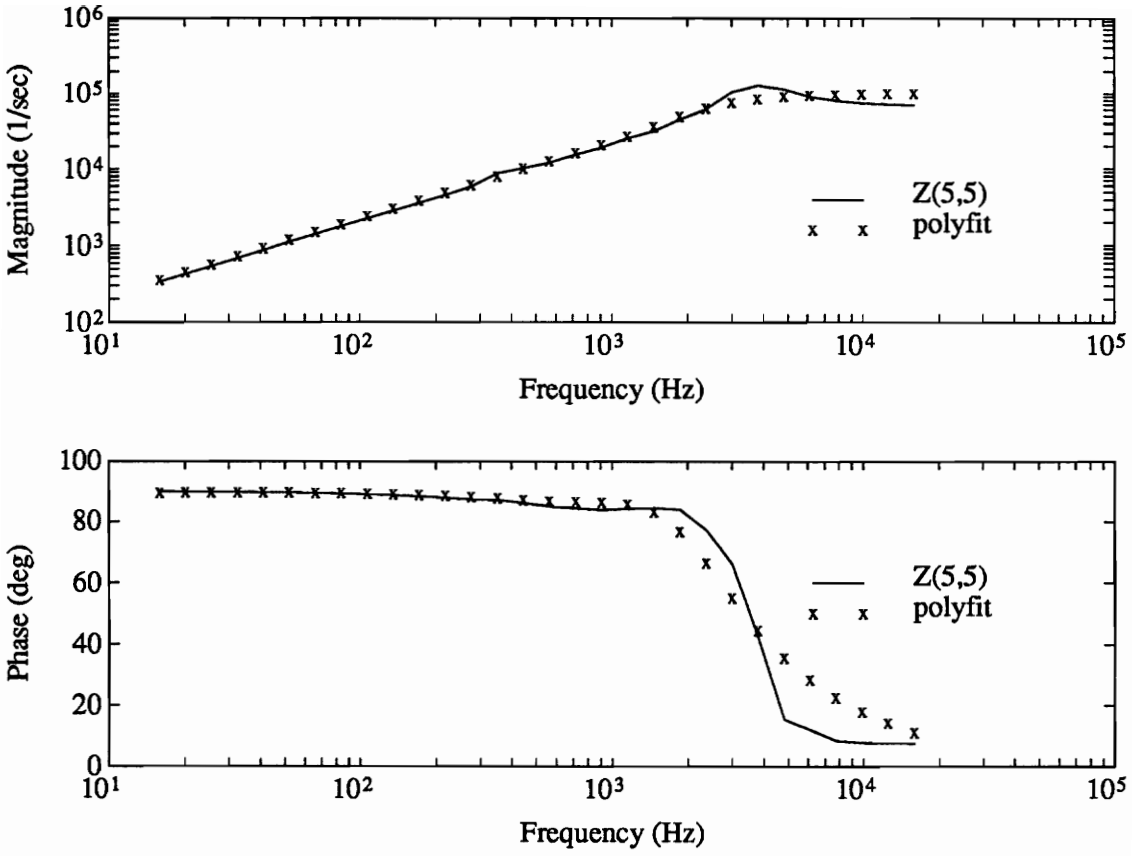

Figure 4.6: Z_{rad} mode 5 rational approximation

Table 4.3: Rational approximations for the fluid loading impedance matrix, Z

$$
\begin{aligned}
Z(1,1) &= \frac{9.0e^4(s+0.01)(s+13000}{(s+11000)(s+11000)} \\
Z(2,2) &= \frac{9.7e^4(s+1)(s+6400 \pm j*4780)}{(s+6980 \pm j*6980)(s+15000)} \\
Z(3,3) &= \frac{9.7e^4(s+1)(s+6420 \pm j*4760)}{(s+6970 \pm j*6970)(s+15100)} \\
Z(4,4) &= \frac{1.0e^5(s+1)(s+6000 \pm j*5780)}{(s+8400 \pm j*8400)(s+15200)} \\
Z(5,5) &= \frac{1.0e^5(s+1)(s+6500 \pm j*6380)}{(s+8600 \pm j*8900)(s+15350)} \\
Z(1,5) &= \frac{1.8e^{12}(s+1)(s+4500 \pm j*4080)}{(s+4100 \pm j*4100)(s+8000 \pm j*8000)(s+15000)} \\
Z(5,1) &= \frac{1.8e^{12}(s+1)(s+4510 \pm j*4090)}{(s+4130 \pm j*4130)(s+8020 \pm j*8020)(s+15100)}
\end{aligned}
$$

fluid boundary value problem. The open-loop and closed-loop system equations for the simply-supported plate will be developed in the next chapter. Simulated plate responses to various input disturbances will be calculated and discussed vibration and ASAC control.

Chapter 5

Heavy Fluid Loading: ASAC Design

Assembly of the modelled structural and acoustic dynamics into state-space equations will be completed to provide a plant model for the heavy fluid-loaded plate. Open-loop response to persistent disturbances or transient mechanical loads may be simulated using the open-loop plant equations. Another advantage of the state variable representation for the fluid-loaded case is evident in the ability to predict the frequencies of resonant response. The classical steady-state approach to this problem does not allow such calculations. This will be discussed in more detail in this chapter. Controller design for vibration control and ASAC control will be demonstrated. Once again, the LQG paradigm is used to design the controllers for the heavy fluid case. Continuous-time and discrete-time control concepts will be used to present the performance of vibration control and ASAC control for the simply-supported plate in water.

5.1 Open-loop equations for heavy fluid loading

Dynamics for the fluid-loaded structural acoustic plant were described in Chapter 4. Following the approach of Chapter 3, dynamics for the necessary smoothing filters and the "expected" disturbance dynamics will be stated without further discussion. Thus, the individual dynamic equations become:

1. Fluid-loaded plate dynamics

$$\dot{w} = Fw + Gu + Ld - Z \tag{5.1}$$

$$y = Cw + D_c u + D_d d + \theta \tag{5.2}$$

2. Fluid Loading dynamics:

$$\dot{p} = F_{rad} p + G_{rad} w \tag{5.3}$$

$$Z = C_{rad} p + D_{rad} w \tag{5.4}$$

3. Disturbance dynamics:

$$\dot{s} = F_d s + G_d \eta \tag{5.5}$$

$$d = C_d s \tag{5.6}$$

4. Smoothing filter dynamics:

$$\dot{r} = F_f r + G_f \tilde{u} \tag{5.7}$$

$$u = C_f r \tag{5.8}$$

The selection of the state equations for the disturbance dynamics and the smoothing filter dynamics follows the discussion presented in chapter 3 on the same topic. It is apparent that equations 5.1 through 5.8 are nearly identical to equations 3.45 through 3.52 of section 3.3. Variable names have been changed slightly for clarity but the state equations for the component dynamics are of the same form for the light fluid loading and the heavy fluid loading, except for the surface pressure z in equation 5.1. In other words, the fluid-structure equations are coupled by the output of the fluid loading filters. The coupling will be more evident once the augmented equations are expanded. To do this, the state variables are augmented to a system state vector

$$W_a = \begin{bmatrix} w \\ \dot{w} \\ p \\ s \\ r \end{bmatrix} \tag{5.9}$$

where the state vector associated with the plate's modal vibration is written in expanded form for illustrative purposes only. Using the augmented state vector, the augmented system equations become:

$$\dot{W}_a = \begin{bmatrix} \dot{w} \\ \ddot{w} \\ \dot{p} \\ \dot{r} \\ \dot{s} \end{bmatrix} = \begin{bmatrix} 0 & I & 0 & 0 & 0 \\ -\mathcal{K} & -(\mathcal{C} + D_{rad}) & -C_{rad} & GC_f & LC_d \\ 0 & G_{rad} & F_{rad} & 0 & 0 \\ 0 & 0 & F_f & 0 & 0 \\ 0 & 0 & 0 & 0 & F_d \end{bmatrix} \begin{bmatrix} w \\ \dot{w} \\ p \\ r \\ s \end{bmatrix} + \begin{bmatrix} 0 \\ 0 \\ 0 \\ G_f \\ 0 \end{bmatrix} \tilde{u} + \begin{bmatrix} 0 \\ 0 \\ 0 \\ 0 \\ G_d \end{bmatrix} v \tag{5.10}$$

$$y = \begin{bmatrix} -\mathcal{K} & -(\mathcal{C} + D_{rad}) & -C_{rad} & D_c C_f & D_d C_d \end{bmatrix} \begin{bmatrix} w \\ p \\ r \\ s \end{bmatrix} + \theta \tag{5.11}$$

or

$$Z = \begin{bmatrix} D_{rad} & C_{rad} & 0 & 0 \end{bmatrix} \begin{bmatrix} w \\ p \\ r \\ s \end{bmatrix} + \theta \tag{5.12}$$

The "closed-loop,open-loop" dynamics for the heavy fluid-loaded problem are evident in equation 5.10. The surface pressure loads the modal velocities via the C_{rad} and D_{rad} matrices. These are the coupling terms in the plate acceleration equation which introduce the fluid inertial forces and the radiation damping forces caused by the non-negligible surface pressure for this case. To condense the notation, the following equations will be used to refer to the augmented dynamics described by equations 5.10 through 5.12:

$$\dot{W}_a = F_a W_a + G_a \tilde{u} + L_a \eta \tag{5.13}$$

$$y = C_v W_a + \theta \tag{5.14}$$

$$Z = C_a W_a + \theta \tag{5.15}$$

where C_v refers to the augmented output matrix used for the plate acceleration measurement and C_a refers to the output matrix which maps the states to acoustic

surface pressure. The augmented state equation 5.13 and the two output equations 5.14 or 5.15 are in an acceptable form for the LQG controller formulation discussed in chapter 3. First, some interesting features of the open-loop plant equations will be highlighted.

The augmented state matrix F_a for the heavy fluid-loaded plate contains an accurate model of the coupled structure-fluid dynamics over the control bandwidth 10 to $500Hz$. For the in-vacuo case of chapter 3, the eigenvalues of the augmented state matrix were a summation of the eigenvalues corresponding to the individual structural poles and radiation filter poles. Now, the coupling of the two systems produces eigenvalues which are indicative of the fluid-structure interaction. There must be n eigenvalues of the state matrix F_a which correspond to the fluid-loaded plate resonances. The eigenvectors associated with these eigenvalues are weighted almost exclusively on the structural states w. A comparison of the eigenvalues of F_a with the in-vacuo plate modes shows the same information which was presented in table 4.2. The plate resonances are lowered by the inertial loading. It is worth mentioning that the classical approach to this fluid-loaded plate problem does not allow a direct calculation of the submerged resonances. The approach typically used in the past was to generate some drive-point impedance and visually locate the peaks in that function. A distinct advantage of the state-space formulation presented earlier is the ability to predict precisely where these resonances will occur. Of course, significant computational effort is required to calculate the values of the fluid loading filters. Thus, a trade-off exists between the difficulty of the traditional and the state-space approach for prediction of fluid-loaded resonant frequencies.

Finally, several representative modal accelerance plots for the fluid-loaded plate are provided in figures 5.1 through 5.3. The accelerance magnitudes for the first five plate modes are shown. For the controller developed later, five modes were retained in the model. Thus, coupling existed between the (1,1) and the (3,1) mode only. The open-loop transfer functions show that the plate response is generally lower in water and the frequencies are lower. This is typically the case for plates in a heavy fluid.

The open-loop results demonstrate that the dynamics of the coupled fluid-structure plant were adequately characterized by the methods discussed earlier. Next, the LQG ASAC and vibration controllers will be designed using the general approach discussed in Chapter 3.

5.2 Closed-loop equations for heavy fluid loading

The closed-loop system equations for the heavy fluid case appear to have identical augmented state equations, however it should be clear that the dynamics of the heavy fluid state matrix are quite different. In other words, the form of F_a is substantially different for the heavy fluid than for the light fluid. For now, only the form of the following equations is important. Recalling equations 5.13 through 5.15

$$\dot{W}_a = F_a W_a + G_a \tilde{u} + L_a \eta \tag{5.16}$$

$$y = C_v W_a + \theta \tag{5.17}$$

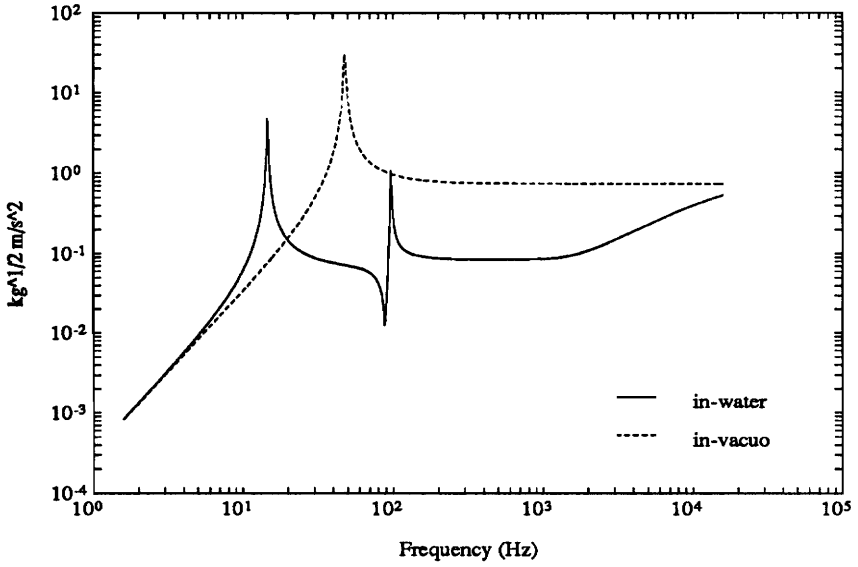

a. Mode 1 accelerance: magnitude

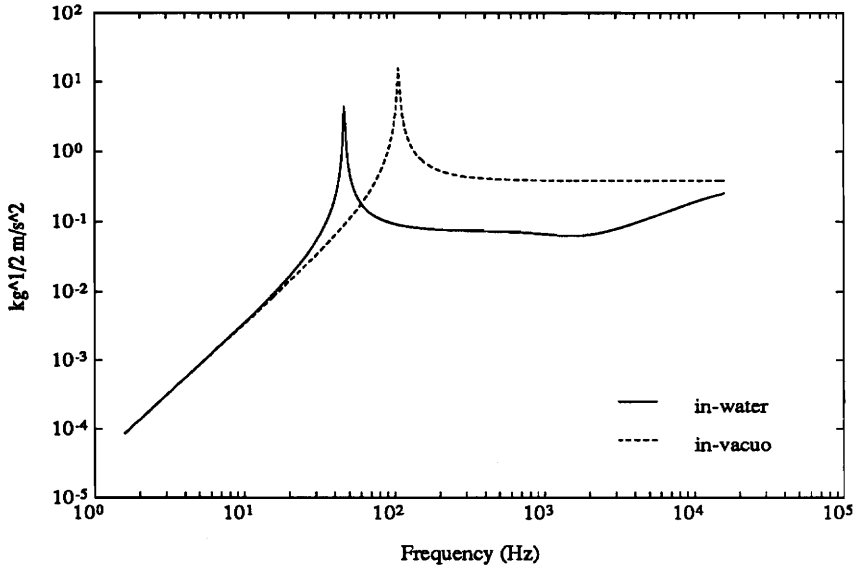

b. Mode 2 accelerance: magnitude

Figure 5.1: A comparison between the modal accelerance for the in-vacuo versus fluid-loaded simply-supported plate (modes 1 and 2).

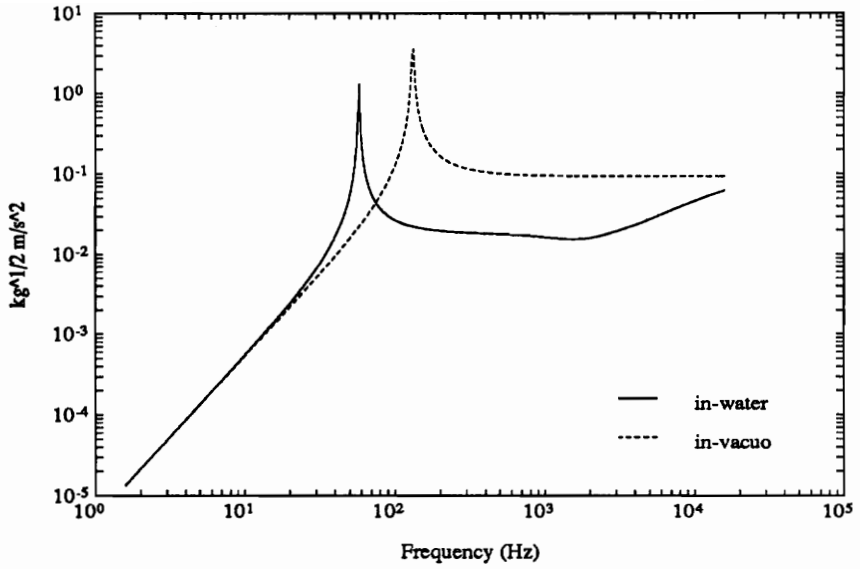

a. Mode 3 accelerance: magnitude

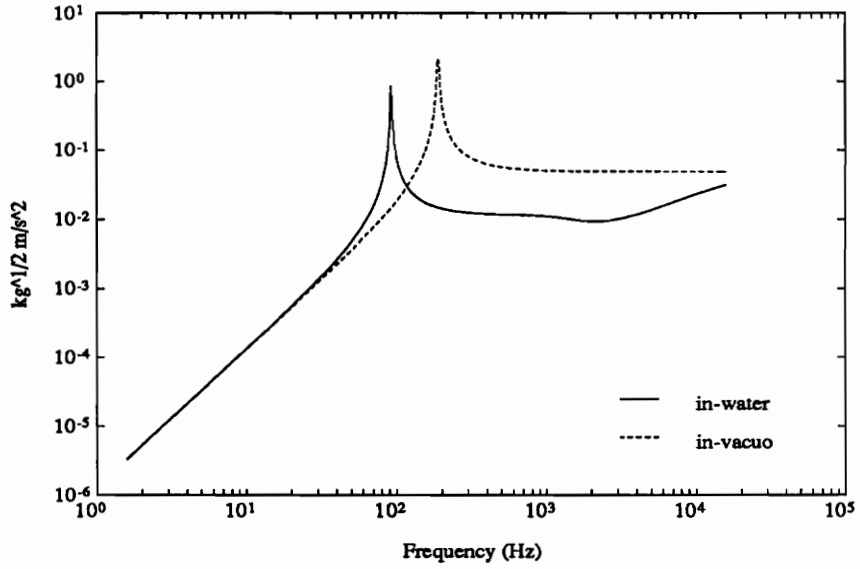

b. Mode 4 accelerance: magnitude

Figure 5.2: A comparison between the modal accelerance for the in-vacuo versus fluid-loaded simply-supported plate (modes 3 and 4).

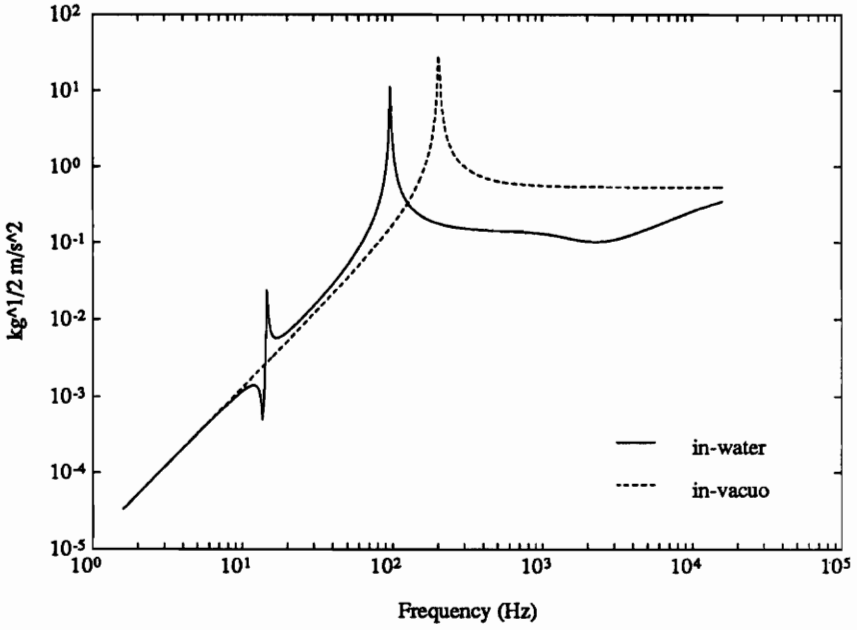

a. Mode 5 accelerance: magnitude

Figure 5.3: A comparison between the modal accelerance for the in-vacuo versus fluid-loaded simply-supported plate (mode 5).

$$Z = C_a W_a + \theta, \tag{5.18}$$

we need only define the cost functions required for design of the vibration and acoustic controllers for the fluid-loaded plant. The cost for the vibration is straightforward and follows from Chapter 3:

$$J_v = \int_{-\infty}^{\infty} (y^T y + \tilde{u}^T R \tilde{u}) dt \tag{5.19}$$

The acoustic cost for the heavy fluid ASAC controller is more interesting and is discussed next.

5.2.1 The acoustic cost function

We wish to estimate the power flow to the acoustic farfield from the plate. A quadratic cost function may then be expressed in terms of radiated acoustic power. This step is critical to the ASAC design approach and provides the controller with the ability to expend control energy exclusively on the plate motions which radiate sound efficiently. A specific goal for the cost function is to utilize the radiation loading dynamics already included in the state vector. Using energy conservation principles, it is clear that the power dissipated from the structure in the form of radiation damping must equal the power radiated to the farfield. The issue becomes how to isolate the component of the velocity which is in phase with the surface pressure.

It will be helpful to define the instantaneous power for the plate as

$$\Pi(t) = \int_{A_p} p(\bar{e}, o, t) \dot{w}(\bar{e}, t) d\bar{e} \tag{5.20}$$

A representation of the instantaneous power transmitted to the fluid by the plate is shown for the harmonic case in figure 5.4. The reactive power is associated with kinetic energy transferred back and forth between the plate and the fluid. Over a half-cycle or cycle, the net power transfer is zero for the reactive portion. The resistive power, representing the power radiated away to the farfield is some finite value over the same cycle. Thus, for some time averaged measure of power given by

$$\bar{\Pi}(t) = \frac{1}{T}\int_0^T p(\bar{e}, o, t)\dot{w}(\bar{e}, t)dt \tag{5.21}$$

only the resistive power contributes to the integral. Extending this concept to the transient case and employing Fourier analysis, it is clear that it is possible to generate an estimate of the total radiated farfield power by using a time averaged representation. Within a constant, this is the form of the cost function for the standard linear quadratic problem introduced in Chapter 3. It remains to solve for the exact cost function for the ASAC design.

As the time $T \rightarrow \infty$ the total radiated power from the plate becomes the cost to be minimized:

$$J = \int_0^\infty p(\bar{e}, o, t)\dot{w}(\bar{e}, t)dt \tag{5.22}$$

After introducing the modal expansion to the surface pressure and the velocity of equation 5.22, and accounting for the orthogonality of the shape functions the cost becomes

$$J = \int_0^\infty \dot{w}_k^*(t)p_k(0, t)dt. \tag{5.23}$$

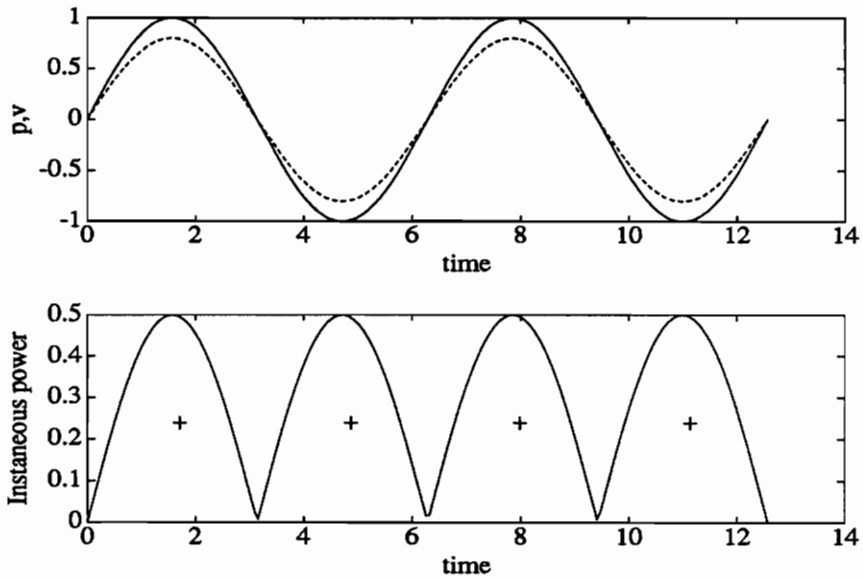

a. Resistive power

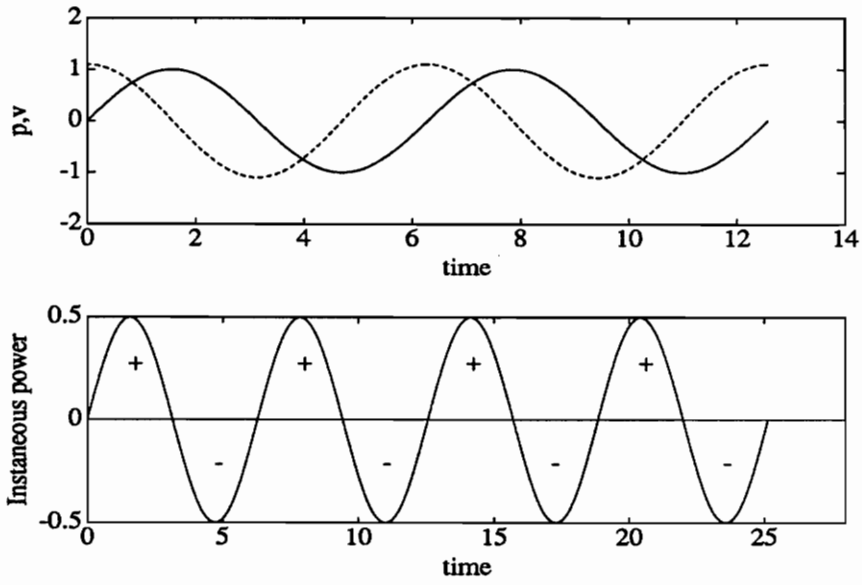

b. Reactive power

Figure 5.4: Representation of reactive and resistive power transmitted to the fluid.

Referring to equation 4.37 for the generalized surface pressure, we write

$$J = \int_0^\infty \dot{w}_k^*(t) \sum_{l=1}^{\infty} \mathcal{Z}_{kl}(\omega) \dot{w}_l(t) \tag{5.24}$$

It is important to recognize here that all of the variables of equation 5.24 are available from the state. This is an important result of the heavy fluid ASAC controller design. It means that it is not necessary to augment radiation filters to the system equations as in the light fluid ASAC design. Thus, the system order for the light and heavy fluid ASAC designs will be approximately the same. Physically, it is the radiation damping component of the fluid loading filters which provides the measure of acoustic energy radiated away. In some sense, this fluid-loaded solution is almost advantageous because the acoustic state is observable on the structure. Recall that this was not true for the light fluid loading problem. Proceeding with the development of the cost, the state-space representation of the surface pressure term in equation 5.24 will be used in conjunction with the augmented state vector to write

$$J = \int_0^\infty \dot{w}^* Z dt \tag{5.25}$$

Using equation 4.45 for Z, define a matrix C_{xp} which maps the state to the surface pressure. Similarly, define a matrix C_{xv} which maps the modal velocity state variables from the augmented state vector W_a. Then, the weighting matrix Q for the heavy fluid ASAC design becomes

$$J = \int_0^\infty W_a^T C_{xv}^T C_{xp} W_a dt \tag{5.26}$$

The matrix product $C_{xv}^T C_{xp}$ does not meet the symmetry requirements for the LQR

solution. Thus, we define a symmetric Q for the ASAC cost function as

$$Q = \frac{\left[C_{xv}^T C_{xp}\right]^T \left[C_{xv}^T C_{xp}\right]}{a} \tag{5.27}$$

where a is an arbitrary scalar which scales the control effort in conjunction with the weighting matrix R for this formulation. Now the ASAC control gains can be calculated in the manner described in chapter 3. Next, simulations of the vibration and ASAC controllers for the heavy fluid-loaded simply-supported plate will be presented.

5.3 Simulation results

Vibration control and ASAC control simulation results are presented for the heavy fluid-loaded plate following the format used for the in-air plate simulations. Two cases are included: a harmonic disturbance force at $59Hz$ and an impulsive disturbance force. For brevity, only time-domain results will be presented here. An exhaustive case study is not necessary to highlight the important features of ASAC for the heavy fluid loading case. As before, any comparison between vibration control and ASAC control is based on equal control energy basis for the two control methods.

A discrete-time compensator was designed for the control simulations presented below. During the design of the sampled-data system equations, two difficulties arose. Both were related to the poor condition numbers of the system matrices. First, the continuous-to-discrete transformation resulted in an open-loop unstable system for sample speeds less than approximately $7000Hz$. The exact mechanism of the insta-

bility was not examined in detail but must be numerical in origin. As a result, all of the simulations below were conducted at a sample frequency of $7000Hz$. Second, the MATLAB Ricatti solution methods encountered numerical difficulties if the system was not numerically balanced beforehand. The procedure used was to generate the augmented system matrices, balance, perform the discrete transformation, generate the compensator gains, and transform the system back to its original coordinate system. MATLAB balancing routines were used for this process. Better balancing methods may be possible but were not explored here.

Case 1: Harmonic disturbance at $59Hz$

A single disturbance force was located at the plate coordinates corresponding to the first accelerometer location ($y = 0.12m, z = 0.12m$). A single control actuator was located at the accelerometer location five ($y = 0.24m, z = 0.25m$). The controller was turned on at $t = 0.5$ secs. The disturbance frequency $59Hz$ coincides with the third resonance of the plate. Based on the in-air ASAC results, we would expect the vibration controller to suppress the third resonance without regard to spillover into efficiently radiating modes. This is the case for the heavy fluid ASAC controller, also. Figures 5.5 through 5.9 compare the controlled response for the vibration and acoustic costs. Once again, the ASAC control concentrates on the first mode vibration while the vibration controller heavily suppresses mode 3, the structural resonance most excited by the disturbance force. Notice that the efficiently radiating mode 5 is also minimized more by the ASAC controller.

The radiated pressure for the controlled harmonic disturbance is provided in figure 5.10. The small reduction in radiated pressure may be explained using the arguments discussed in Chapter 3 for the light fluid loading problem. Again, more

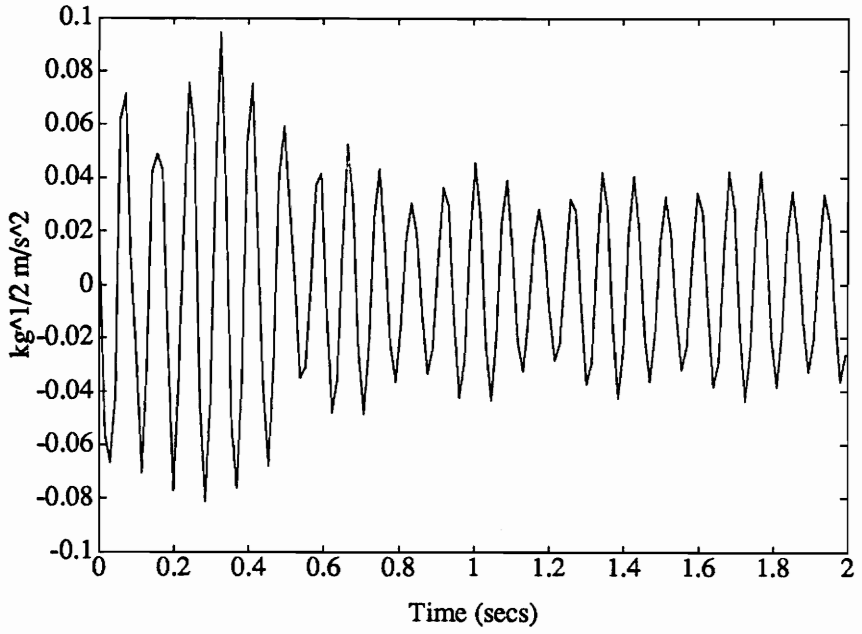

a. ASAC control

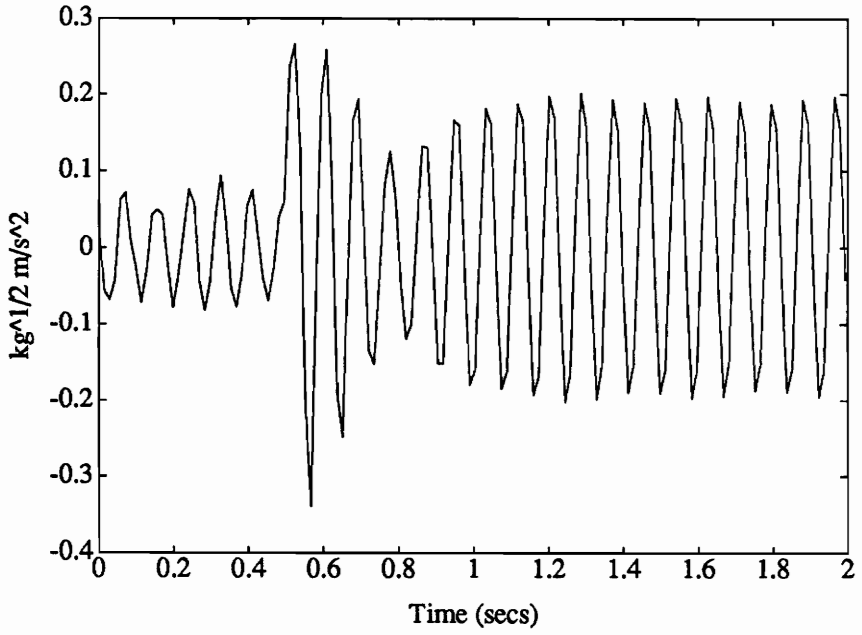

b. Vibration control

Figure 5.5: Time-domain simulation of mode 1 acceleration during vibration control and ASAC control of $59Hz$ disturbance.

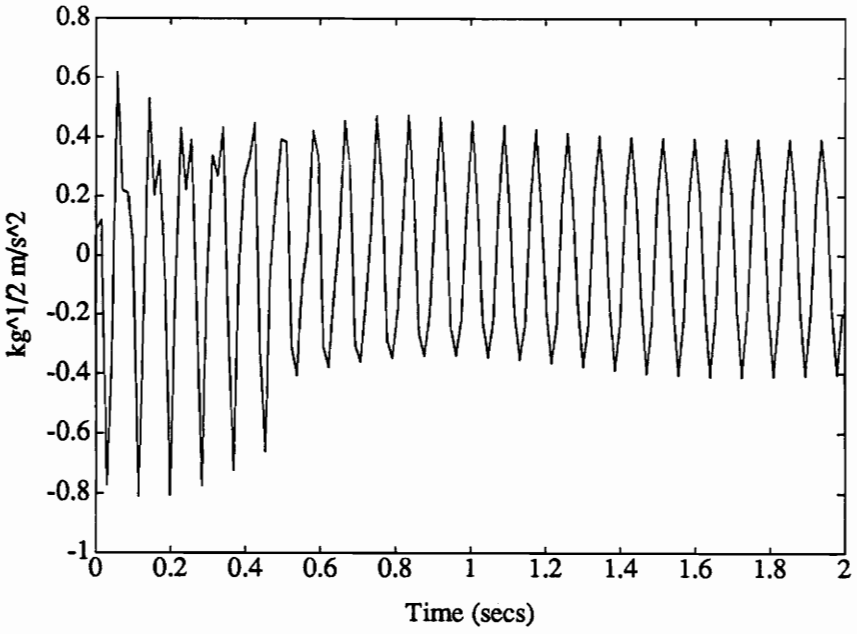

a. ASAC control

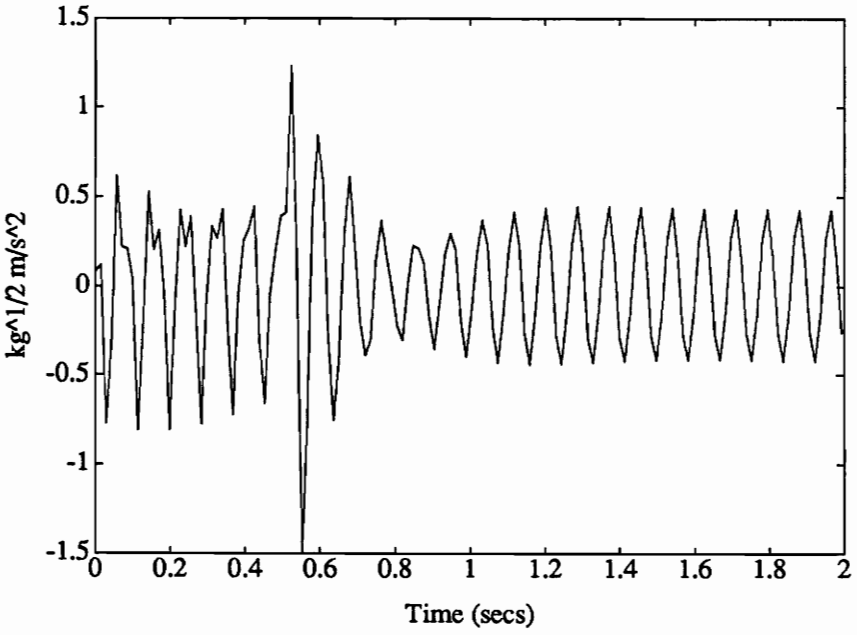

b. Vibration control

Figure 5.6: Time-domain simulation of mode 2 acceleration during vibration control and ASAC control of $59Hz$ disturbance.

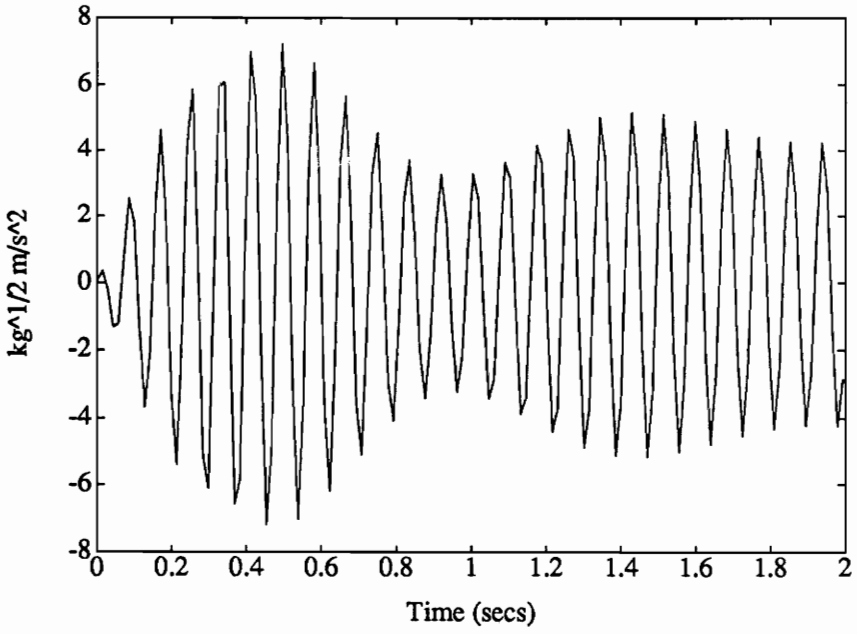

a. ASAC control

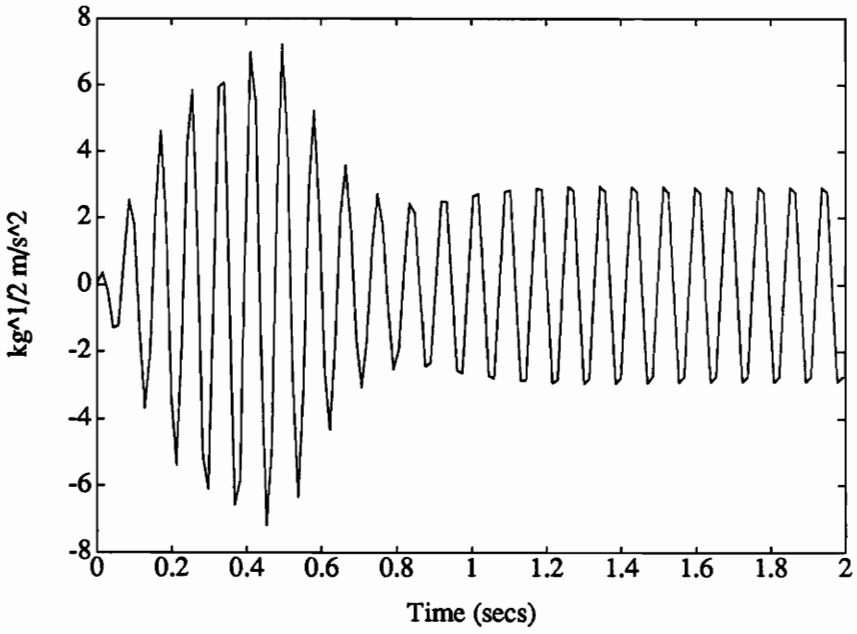

b. Vibration control

Figure 5.7: Time-domain simulation of mode 3 acceleration during vibration control and ASAC control of $59Hz$ disturbance.

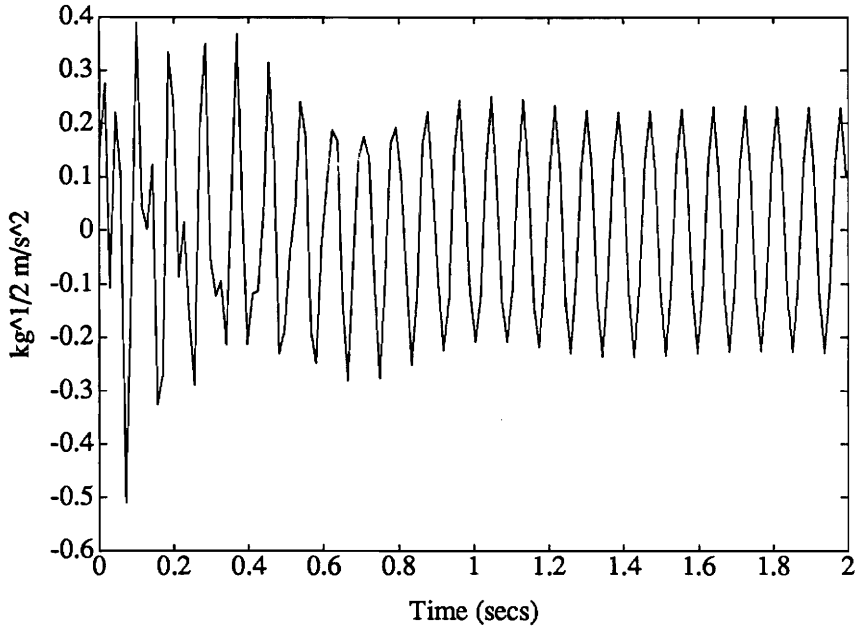

a. ASAC control

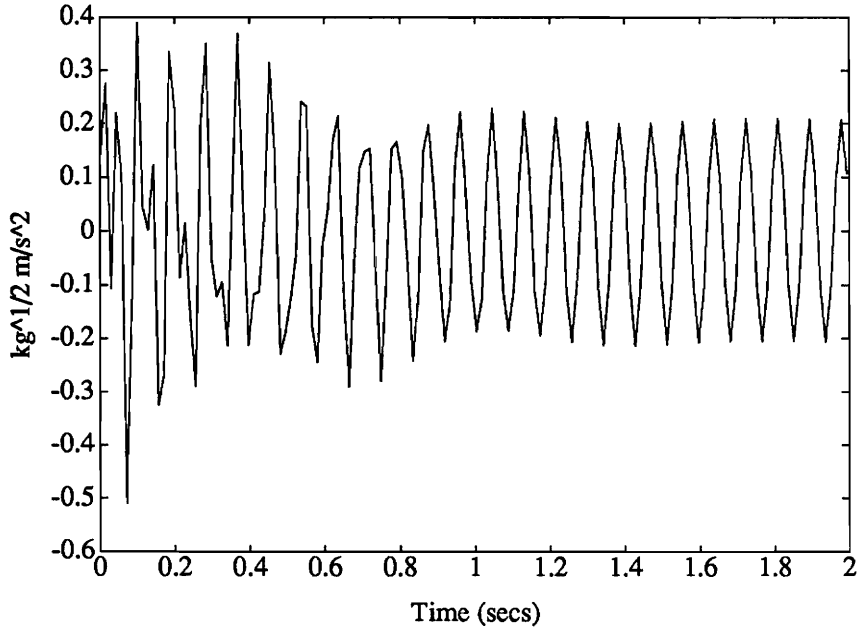

b. Vibration control

Figure 5.8: Time-domain simulation of mode 4 acceleration during vibration control and ASAC control of $59Hz$ disturbance.

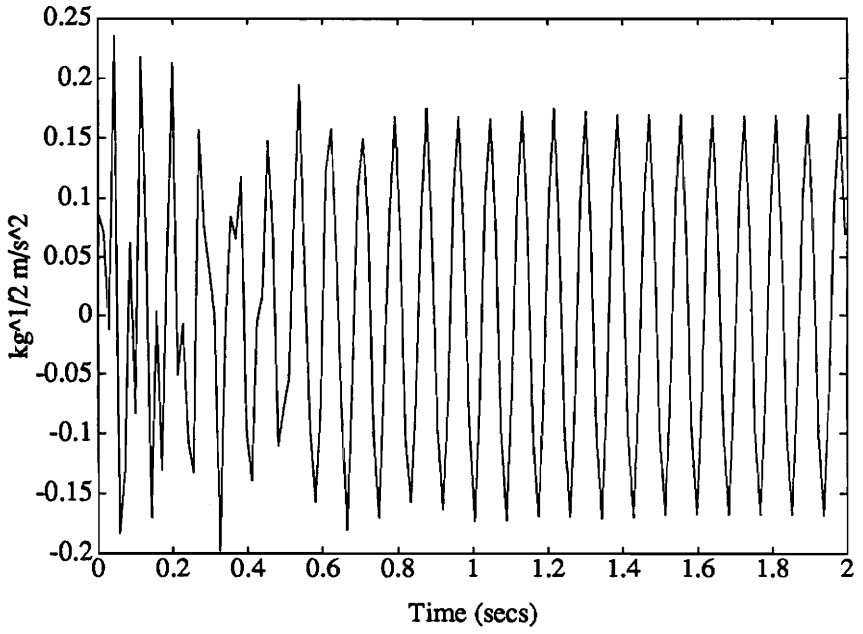

a. ASAC control

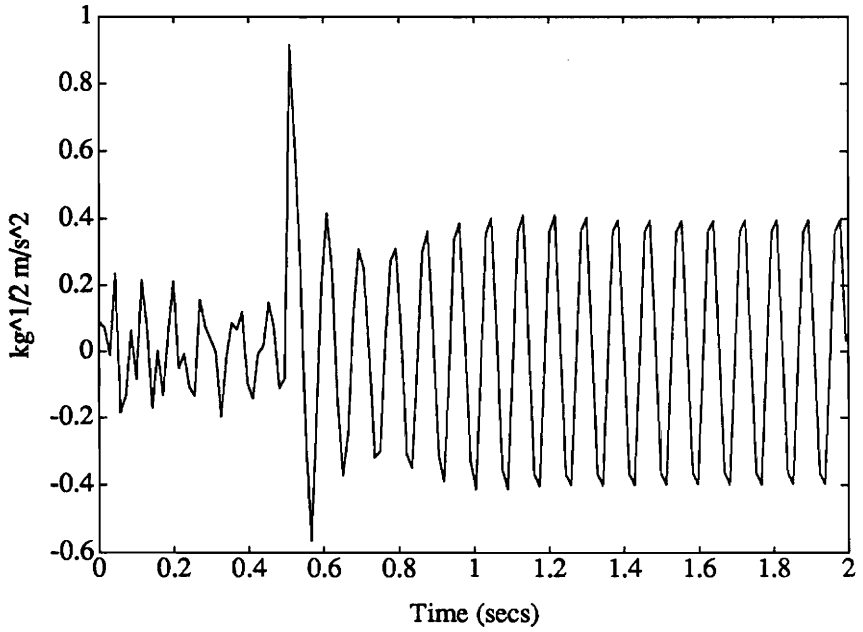

b. Vibration control

Figure 5.9: Time-domain simulation of mode 5 acceleration during vibration control and ASAC control of $59Hz$ disturbance.

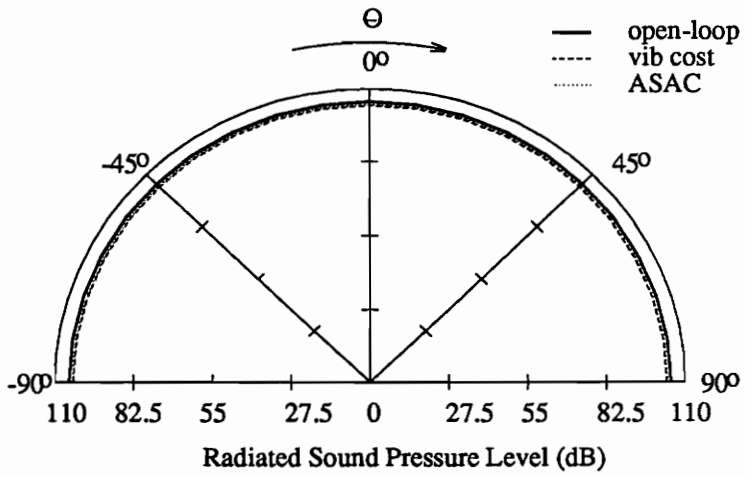

Figure 5.10: Farfield radiated pressure for vibration and ASAC control of 59 Hz disturbance.

control actuators would increase the performance of the controller.

Case 2: Impulsive disturbance

The plate coordinates of the control actuator are the same as the previous case and the impulsive load is assumed to be a discrete pulse which enters the plate at accelerometer location one. The pulse duration is 17 msec and is applied at $t = 0$. Figures 5.11 through 5.15 compare the results for the vibration control and the ASAC control. The ASAC controller adds the most damping to the important radiating modes, as expected.

The minimization of the efficiently radiating modes in the subsonic frequency regime was a central feature of the ASAC design for both the in-air and in-water simply-supported plate. The heavy fluid-loaded plate ASAC design demonstrated that the inclusion of the structural acoustic dynamics in the plant equations is necessary for discrimination between a minimization of vibrational and acoustic energy.

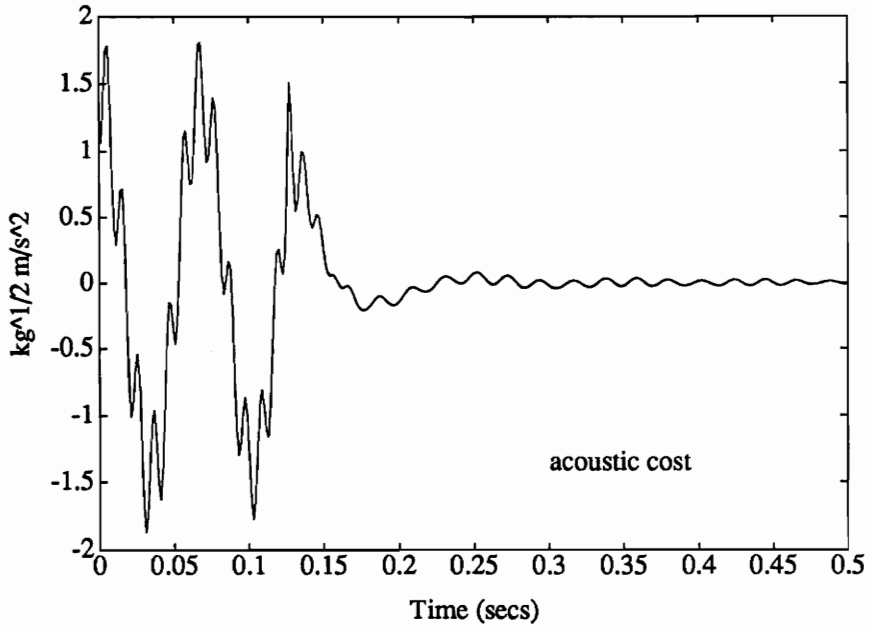

a. ASAC control

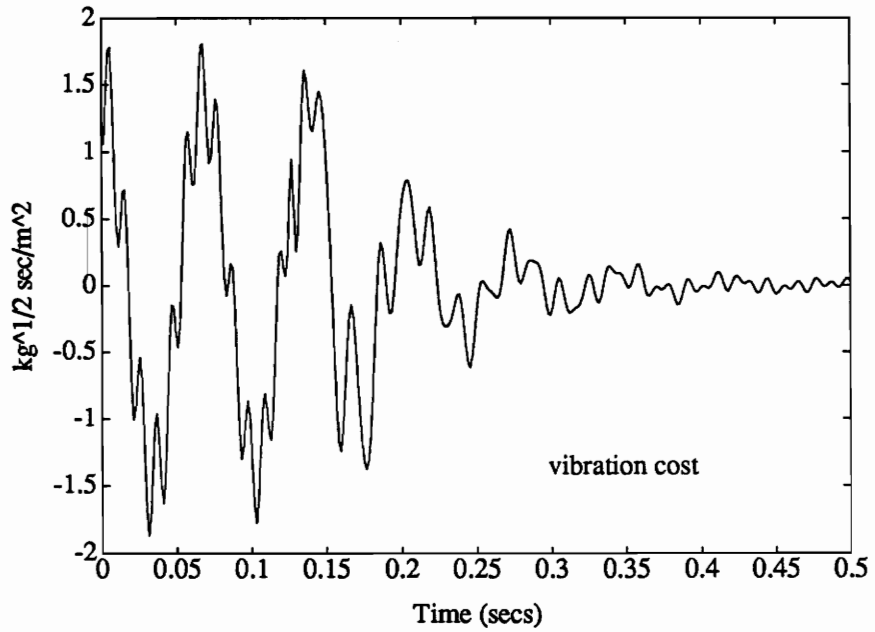

b. Vibration control

Figure 5.11: Time-domain simulation of mode 1 acceleration during vibration control and ASAC control of impulsive disturbance.

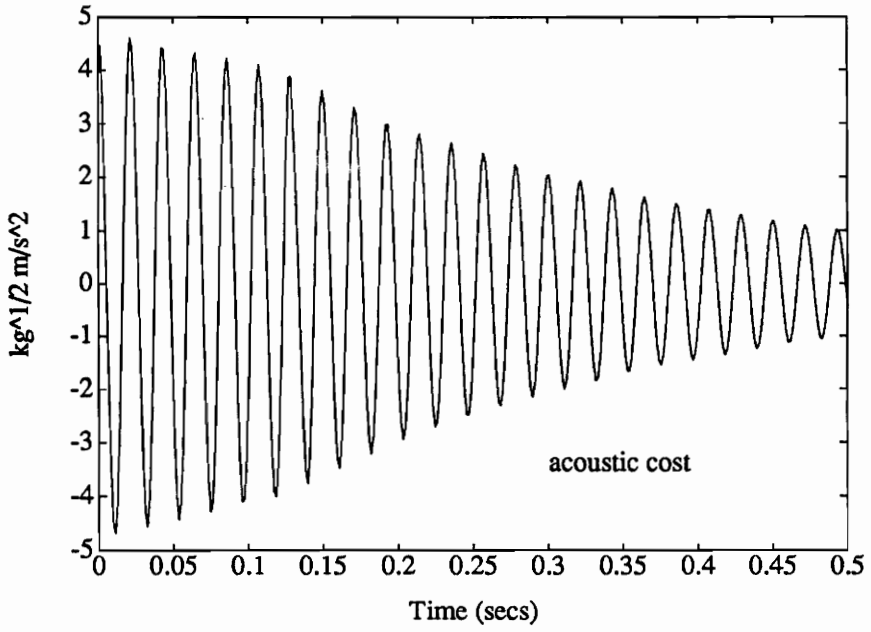

a. ASAC control

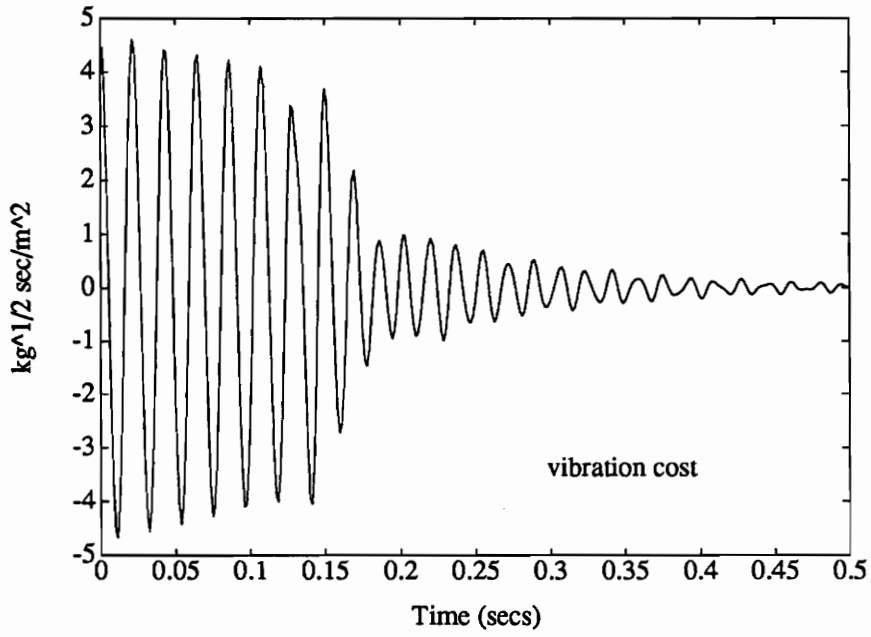

b. Vibration control

Figure 5.12: Time-domain simulation of mode 2 acceleration during vibration control and ASAC control of impulsive disturbance.

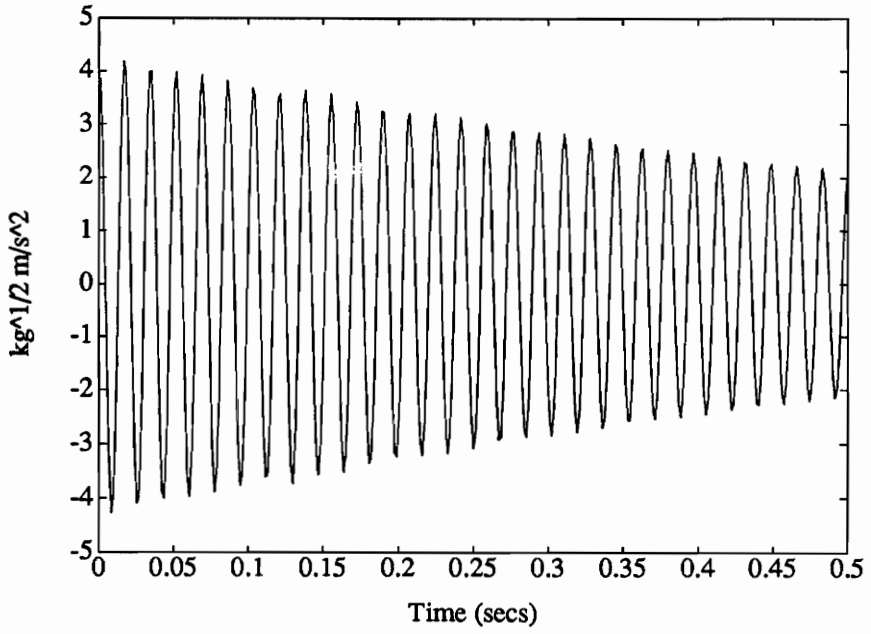

a. ASAC control

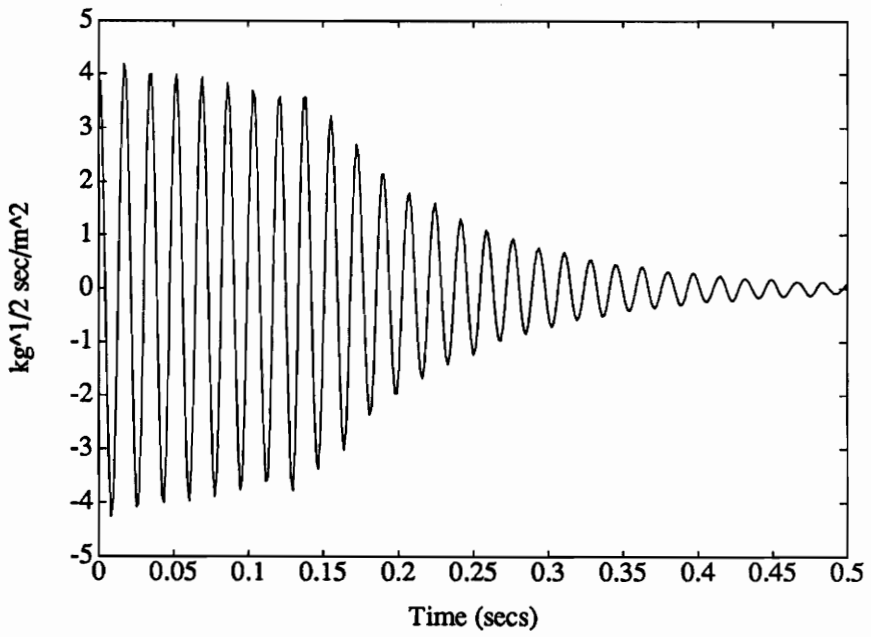

b. Vibration control

Figure 5.13: Time-domain simulation of mode 3 acceleration during vibration control and ASAC control of impulsive disturbance.

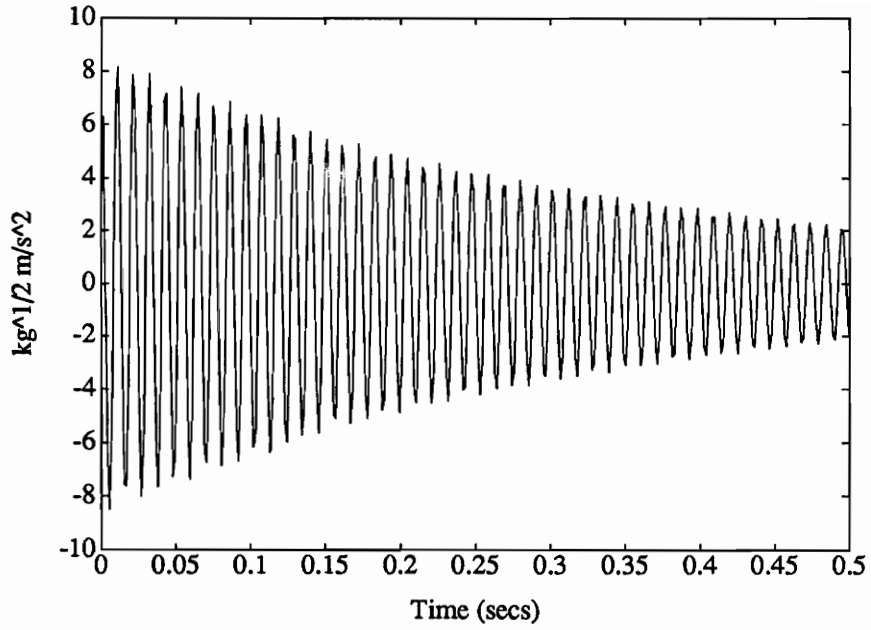

a. ASAC control

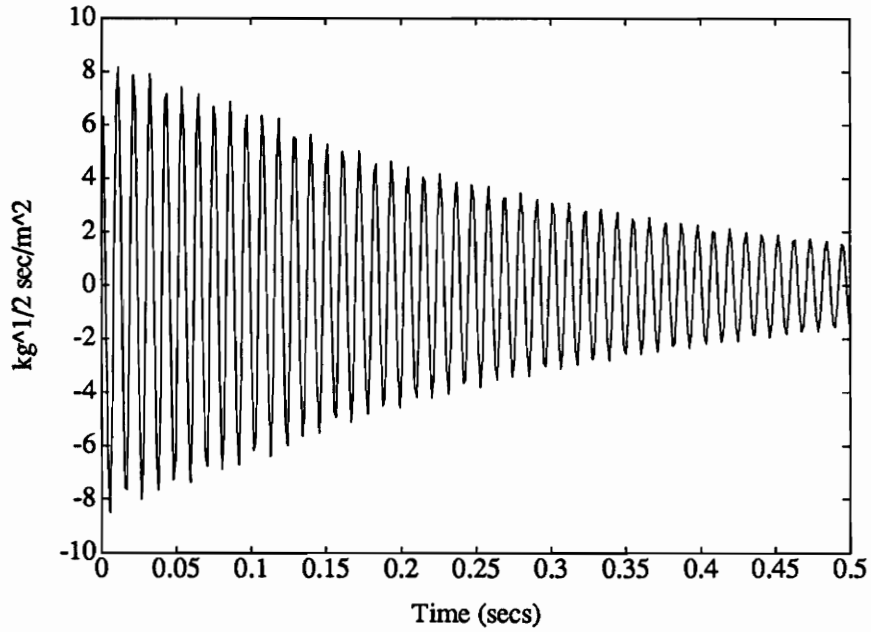

b. Vibration control

Figure 5.14: Time-domain simulation of mode 4 acceleration during vibration control and ASAC control of impulsive disturbance.

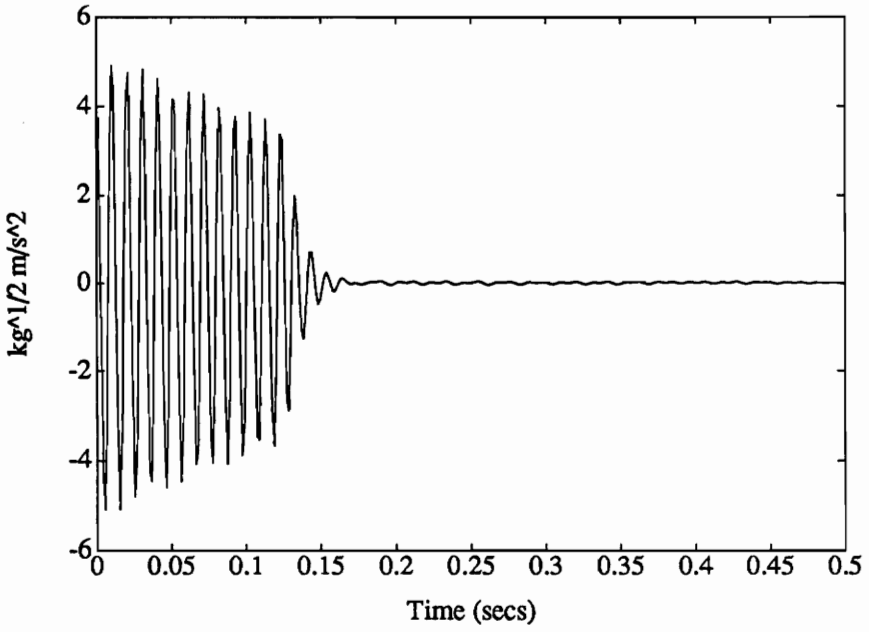

a. ASAC control

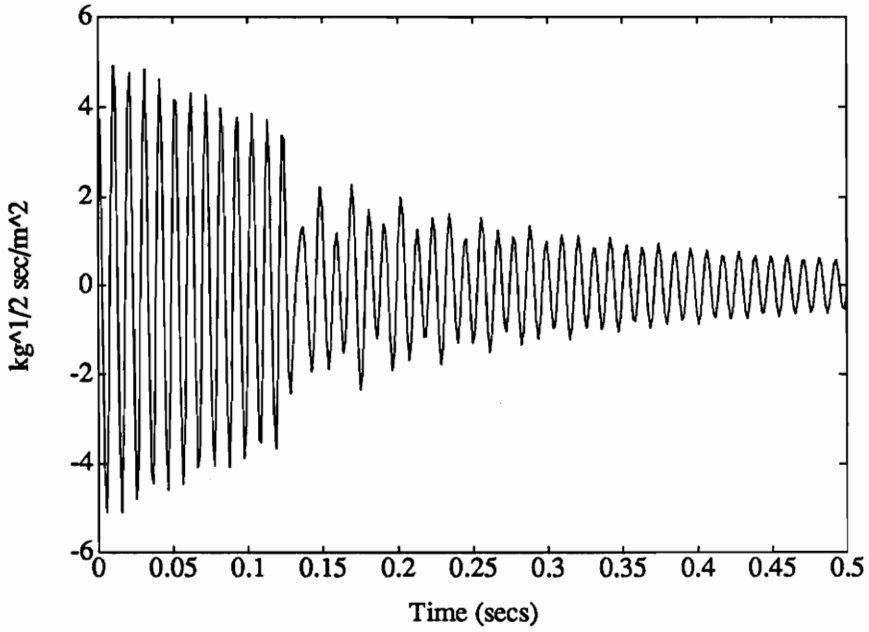

b. Vibration control

Figure 5.15: Time-domain simulation of mode 5 acceleration during vibration control and ASAC control of impulsive disturbance.

Chapter 6

Conclusions and Recommendations

6.1 Conclusions

The recent introduction of ASAC to the noise and vibration control community is an exciting contribution. This research extends the modern control approach to ASAC for light and heavy fluid-loaded structures. Most importantly, the theoretical development of Chapters 4 and 5 introduces the first ASAC controller capable of both persistent and transient disturbance suppression for a heavy fluid-loaded structure. The problem was posed using the in-vacuo modes of a simply-supported plate in a baffle. This choice of structural model simplified the calculation of the fluid loading filters for this effort. However, it is suggested that this approach to ASAC may be extended to any fluid-loaded structure for which the in-vacuo modes form an admissible basis. Future research may also indicate that a purely numerical approach to the coupled structure-acoustic control problem is possible using the fluid loading filter concepts presented here.

Several specific conclusions, based on the formulation of the ASAC control laws and the simulation results for both in-air and submerged operation, can be stated. The

system order for ASAC controllers increases over comparable vibration controllers. This is a somewhat obvious conclusion when one considers that the ASAC objective requires acoustic modelling which the vibration controller does not. The minimum number of states introduced by the light fluid ASAC paradigm was shown to be dependent on the radiation efficiencies of the modelled modes. The desired accuracy of the radiation filters across a specified bandwidth will also affect the number of additional states in the ASAC controller. For the heavy fluid, similar arguments apply. However, it is promising that the heavy fluid ASAC formulation introduced by this research requires approximately the same system order as the light fluid ASAC design.

Several advantages of the ASAC controller were highlighted by this research. It was shown that ASAC control is more efficient in reducing farfield radiated power than vibration control on an equal control energy basis. This occurs because the acoustic modelling in the ASAC approaches provides the controller with the ability to preferentially suppress efficient radiating modes. In addition, no farfield measurements are required for feedback to the controller. Finally, the prediction of resonances for the fluid-loaded plate follows from the state-space approach used to describe the fluid-structure coupled system equations.

Design of ASAC compensators using the methods presented in this research relies on modelling of the dynamic systems which comprise the plant. In a sense, the ASAC objective places an additional burden on the modelling of the open-loop plant. Because ASAC is a special case of the active vibration control problem, all of the system identification/robustness issues associated with vibration control are a problem for ASAC controllers, also. However, the acoustic modelling implicit in the

ASAC approach adds a second major source of uncertainties which must be dealt with by the control engineer. Adaptive methods may be used to refine the structural model in an iterative, on-line fashion. However, the lack of acoustic measurements will make adaptation of the structural acoustic plant very difficult. It is emphasized here that the reliance of ASAC controllers on relatively accurate acoustic modelling is a shared problem for feedforward and feedback controller design. (Again, it is assumed that farfield sensors are impractical.)

It is concluded that the development of the control theory presented here is adequate for active structural acoustic control for a variety of applications. Certainly, the complexity of the approach for disturbance rejection of a single harmonic excitation is probably not warranted. Adaptive signal processing controllers are proven, efficient tools for such situations. However, increasing bandwidth of the disturbance forces quickly adds complexity to the feedforward approach. As mentioned earlier, acoustic modelling may be required for ASAC feedforward methods, also. Thus, the simplicity of the feedforward control approaches is compromised by more stringent design objectives. The ultimate roles of feedback and feedforward controllers in ASAC methods cannot be predicted. Clearly, the robustness of modern control theory ASAC approaches to disturbance waveform makes it an attractive and exciting research area.

6.2 Recommendations

The final effort of a dissertation is often spent preparing the candidate for the reality of engineering research in the "real world" - proposing technical research issues for *someone else to work on.* As is typically true, the research solutions presented here

provided seed for many more interesting investigations. A brief summary of several proposals and recommendations which arise from this research is discussed next.

A simple structure and radiation model was chosen to demonstrate a modern control approach to ASAC. The methods of the research presented here may be slowly extended. For the light fluid, the critical juncture of the design method is the synthesis of radiation filters. Radiation filters were successfully demonstrated in this work for a Rayleigh integral acoustic model and a simple, uniform plate structure. A general approach for complex structures may be sought by using existing finite element codes in conjunction with numerical approaches to the radiation problem. This should be a straightforward extension using the concepts presented here. For the heavy fluid, the fluid loading filters provide the necessary coupling between the structure and the fluid. The description of the filters depends on a representation of the surface pressure and interface velocity. It appears likely that this method will be feasible for more complex structures, also. Future work should investigate a completely numerical approach to the ASAC design for fluid loaded structures. Additionally, an approach which formulates the ASAC control for the fluid-loaded structure using the submerged or "wet" modes as the basis needs to be established.

Numerical difficulties were encountered during various procedures of the design methods investigated in this research. The computation of the radiation filters for the in-air case, the Ricatti equation solutions for the compensator gains and even the continuous-to-discrete transformation encountered numerical problems. Because of the relative speeds of the structural and acoustic systems, poor numerical condition numbers will be encountered. System balancing is not only helpful, it is necessary for accurate computations. The most serious problem is the high sample frequen-

cies required for stable discrete-time simulations and subsequently implementations. More effective balancing routines need to identified for the structural acoustic state-space models which result from the modern control approaches.

The requirement for system models may seem to place a prohibitive cost on the modern control theory approach, particularly for larger, more complex structures. Unlike feedforward controller designs, the feedback ASAC approach requires a priori system characterization. However, the present advantages of feedback ASAC design provide important incentives to continue development of modern control theory approaches to this problem. Most importantly, feedback control provides transient suppression of arbitrary disturbance waveforms. The present inability of feedforward control to handle the transient case may be significant for a variety of acoustic problems. For example, turbulent boundary layer induced flow noise and the classical scattering problem may introduce time scales which are very difficult for the adaptive feedforward approach. The modern control ASAC theory presented in this research showed robustness to structural-acoustic excitations of any type. Continuing advancements in the modern control theory approach to ASAC may require serious progress in system identification/modelling tasks in structural acoustics. For example, the heavy radiation damping which exists for certain fluid-structure problems makes experimental validation of system models quite difficult. The distinct roles which the structural dynamic models and the acoustic dynamic models play in the ultimate performance of ASAC designs needs to be assessed.

Bibliography

[1] Meirovitch, L. and Thangjitham, S. "Active Control of Sound Radiation Pressure" ASME Journal of Vibration and Acoustics, Vol.112, No.2, April, 1990, pp.237-244.

[2] Meirovitch, L. and Thangjitham, S. "Control of Sound Radiation from Submerged Plates" J. Acoust. Soc. Am. **88**(1), July, 1990, pp.402-407.

[3] Baumann, W.T., Saunders, W.R., and Robertshaw, H.H. "Active Suppression of Acoustic Radiation from Impulsively Excited Structures" Accepted for publication in J. Acoust. Soc. Am.

[4] Brogan, W.L. **Modern Control Theory**, Prentice-Hall, Inc. New Jersey, 1985.

[5] J.W. Strutt Lord Rayleigh **Theory of Sound**, New York:Dover, 1945, 2nd ed., vol.II.

[6] Lax, M. "The Effect of Radiation on the Vibration of a Circular Diaphragm" J. Acoust. Soc. Am. Vol. 16, 1944 pp. 5-13.

[7] Cremer, L., Heckl, M., and Ungar, E.E. **Structure-Borne Sound**, Springer-Verlag, New York, 1972, 2nd ed.

[8] Junger, M.C., and Feit D. **Sound, Structures, and Their Interaction**, The MIT Press, Cambridge, Mass., 1972, 2nd ed.

[9] Fahy, F. **Sound and Structural Vibration**, Academic Press Inc. (London) Ltd., 1985.

[10] Ross, D. **Mechanics of Underwater Noise**, Pergammon Press Inc., Elmsford, New York, 1976.

[11] Kinsler, and Frey, **Fundamentals of Acoustics** John Wiley & Sons, New York, 1962.

[12] Mackertich, S.S. and Hayek, S.I. "Acoustic Radiation from an Impulsively Excited Elastic Plate," J. Acoust. Soc. Am. Vol. 69, 1981, pp. 1021-1028.

[13] Mackertich, S.S. "Transient Acoustic Radiation from Excited Plates," J. Acoust. Soc. Am. Vol. 87, 1990, pp. 2551-2556.

[14] Everstine, G. NASHUA code

[15] Schenck, A. and Benthien, G.W. "Numerical Solution of Acoustic-Structure Interaction Problems" NOSC TR 1263, 1989, pp.1-36.

[16] Smith, "Coupling of Sound and Panel Vibration below the Critical Frequency" J. Acoust. Soc. Am. Vol. 36, No. 8, 1962, pp. 1516-1520.

[17] Maidanik, G. "Response of Ribbed Panels to Reverberant Acoustic Fields" J. Acoust. Soc. Am., Vol. 34, No. 6, 1962, pp.809-826.

[18] Wallace, C.E. "Radiation Resistance of a Rectangular Panel" J. Acoust. Soc. Am., Vol. 51, No. 3, 1972, pp. 946-952.

[19] Wallace, C.E. "The Acoustic Radiation Damping of the Modes of a Rectangular Panel" J. Acoust. Soc. Am., Vol. 81, No.6, 1987, pp.1787-1794.

[20] Crighton, D.G. and Innes D. "The Modes, Resonances and Forced Response of Elastic Structures Under Heavy Fluid Loading" Proc. R. Soc. Lond. A**312**, 1984, pp.295-341.

[21] Davies, H.G. "Low Frequency Random Excitation of Water-Loaded Rectangular Plates" J. Sound and Vib. **15**(1), 1971, pp.107-126.

[22] Sandman, B.E. and Vieira, J. "The Experimental and Theoretical Dynamics of Fluid-Loaded Plates" Dev. Mech. 8, Proc. 13th Midwest Conf., 1975, pp. 295-311.

[23] Lomas, N.S. and Hayek, S.I. "Vibration and Acoustic Radiation of Elastically Supported Rectangular Plates" J. Sound and Vib. **52**(1), 1977 pp.1-25.

[24] Laulagnet, B. and Guyader, J.L. " Modal Analysis of a Shell's Acoustic Radiation in Light and Heavy Fluids" J. Sound and Vibration 131(3), 1989 pp.397-415.

[25] Franklin, G.F, Powell, J.D. and Emami-Naeini, A. **Feedback Control of Dynamic Systems** Addison-Wesley Publishing Company, Inc. 1986.

[26] Takahashi, Y. Rabins, M.J. and Auslander, D.M., **Control and Dynamic Systems**, Addison-Wesley, Reading, Massachusetts, 1970.

[27] Dorf, R.C., **Modern Control Systems**, Addison-Wesley, Reading, Mass., 1967.

[28] Elgerd, O.I., **Control Systems Theory** McGraw-Hill, New York, 1967.

[29] Kirk, D.E., **Optimal Control Theory** Prentice-Hall, Englewood Cliffs, New Jersey, 1970.

[30] Anderson, B.D. and Moore, J.B., **Linear Optimal Control**, Prentice-Hall, Englewood Cliffs, New Jersey, 1971.

[31] Kalman, R.E. "A New Approach to Linear Filtering and Prediction Problems" ASME Journal of Basic Engineering, 1960, pp. 35-45.

[32] Kalman, R.E. and Bucy, R. "New Results in Linear Filtering and Prediction Theory" ASME Journal of Basic Engineering, 1961, pp. 95-108.

[33] Widrow, B. and Stearns, S.D. **Adaptive Signal Processing** Prentice Hall, Englewood Cliffs, NJ, 1985.

[34] Redman-White, W., Nelson, P.A. and Curtis, A.R., "Experiments on the active control of flexural wave power flow", J. Sound and Vib., (112)1, 1987, pp. 187-191.

[35] vonFlotow, A.H. and Schafer, B., "Wave-absorbing controllers for a flexible beam", J. of Guidance, Control and Dynamics, Vol.9, No.4, 1986, pp. 673-680.

[36] Meirovitch, L. and Baruh, H., "Control of self-adjoint distributed-parameter systems", J. of Guidance and Control, Vol. 5, No.1, 1982, pp.60-66.

[37] Meirovitch, L. and Baruh, H., "On the problem of observation spillover in self-adjoint distributed-parameter systems", J. of Optimization Theory and Applications, Vol.39, No.2, 1983, pp.269-291.

[38] Rubenstein, S.P., Saunders, W.R., Ellis, G.K., Robertshaw, H.H. and Baumann, W.T. "Demonstration of a LQG Vibration Controller for a Simply-Supported Plate" Proceedings of Recent Advances in Active Noise and Vibration Control Conference at VPI & SU, April 1991.

[39] Karpel, M., "Design for active flutter suppression and gust alleviation using state-space aeroelastic modeling", J. Aircraft, Vol.19, No.3, 1982, pp.221-227.

[40] Roger, K.L., Hodges, G.E. and Felt, L., "Active flutter suppression - a flight test demonstration", J. of Aircraft, Vol.12, 1975, pp.551-556.

[41] Edwards, J.W., "Unsteady aerodynamic modeling and active aeroelastic control", SUDDAR 504, Stanford Univ., 1977.

[42] Edwards, J.H., "Applications of Laplace transform methods to airfoil motion and stability calculations", AIAA Paper 79-0772, April, 1979.

[43] Karpel, M., "Reduced size first-order subsonic and supersonic aeroelastic modeling", AIAA Paper 1154-CP, 1990, pp.1405-1416.

[44] Inman, D.J. **Vibration with Control, Measurement and Stability** Prentice Hall, Englewood Cliffs, NJ, 1988.

[45] Chen, C.T. **Introduction to Linear System Theory** Holt, Rinehart & Winston, 1970.

[46] Rubenstein, S.P. "An experiment in State-Space Vibration Control of Steady Disturbances on a Simply-Supported Plate" , Masters Thesis, VPI &SU, August, 1991.

[47] Fuller, C.R. and Jones, J.D. "Experiments in Reduction of Propeller Induced Interior Noise by Active Control of Cylinder Vibration" J. Sound and Vib. 112(2), 1987, pp.389-395.

[48] Jones, J.D. and Fuller, C.R. "Active Control of Sound Fields in Elastic Cylinders by Vibration Inputs" Proceedings of Noise-Con 1987, 1987, pp.413 -418.

[49] Burdisso, R.A. and Fuller, C.R. "Theory of Feed-Forward Controlled System Eigenproperties" J. Acoust. Soc. Am., Vol. 88(S1), 1990.

[50] Clark, R.L. and Fuller, C.R. "Experiments on Active Control of Structurally Radiated Sound Using Multiple Piezoceramic Actuators" submitted to the J. Acoust. Soc. Am., 1990.

[51] Fuller, C.R., Hansen C.H. and Snyder, S.D. "Active Control of Sound Radiation from a Vibrating Rectangular Panel by Sound Sources and Vibration Inputs: An Experimental Comparison" J. Sound and Vib. **145**(2) 1991, pp. 195-215.

[52] Fuller, C.R. and Burdisso, R.A. "A Wave Number Domain Approach to the Active Control of Structure-Borne Sound" J. Sound and Vib. **148**(2), 1991, pp. 355-360.

[53] Baumann, W.T., Ho F., Robertshaw, H.H. "Active Acoustical Control of Broadband Structural Disturbances" Presented at the 120th Meeting of the Acoust. Soc. Am.

[54] Gu, Y. and Fuller, C., "Active control of sound radiation from discontinuities on a fluid loaded plate I. Far-field pressure", J. Acoust. Soc. Am., 1991.

[55] Gu, Y. and Fuller, C., "Active control of sound radiation from discontinuities on a fluid loaded plate II. Plate Vibration", in preparation.

[56] Gu, Y. and Fuller, C., "Active control of sound radiation from a fluid loaded rectangular uniform plate", Submitted for publication to J. Acoust. Soc. Am.

[57] Mann, J.A., Tichy, J. and Romano, A.J. "Instantaneous and time-averaged energy transfer in acoustic fields" J. Acoust. Soc. Am. **82**(1), 1987 pp.17-30.

[58] Lathi, B.P. **Signals, Systems and Communication**, John Wiley, NY, 1965.

[59] Yousri, S. and Fahy, F. "Acoustic Radiation by unbaffled cylindrical beams in multi-modal transverse vibration", J. Sound and Vib **40**(3), 1975, pp.299-306.

[60] Francis, B.A., **A Course in H_∞ Control Theory**, Lecture Notes in Control and Information Sciences, Springer-Verlag, 1988

[61] Stengel, R.F. **Stochastic Optimal Control**, John Wiley & Sons, 1986.

[62] Ridgely, D.B., and Banda, S.S., "Introduction to Robust Multivariable Control", AFWAL-TR-85-3102, Wright-Patterson AFB, Flight Dynamics Laboratory, 1986.

[63] Ackermann, J. **Sampled-Data Control Systems** Springer-Verlag, 1985, pp. 270-274.

[64] Sievers, L. and vonFlotow, A. "Comparison and Extension of Control Methods for Narrowband Disturbance Rejection", *Presented at the 1990 ASME Winter Annual Meetings.* Nov, 1990.

[65] Hildebrand, F.B. **Advanced Calculus for Applications**, Prentice-Hall, Inc., Englewood Cliffs, NJ, 1976, 2nd ed. pp 400-402.

[66] Meirovitch, L. **Dynamics and Control of Structures** John Wiley and Sons, Inc., 1990.

[67] Thomson, W.T. **Theory of Vibration with Applications** Prentice Hall, Englewood Cliffs, NJ, 1988.

[68] Ellis, G.K. "H_∞ and LQG Optimal Control for the Rejection of Persistent Disturbances: Analysis, Design and Experiment" PhD Dissertation, Dept. of Mech. Eng. VPI &SU, 1992.

Appendix A

A derivation of the basic equations used in classical acoustics is presented. The intention of including this derivation is to provide the reader with the fundamental assumptions which are implicit in the wave equation. It is assumed that the reader is familiar with basic fluid mechanics. The following development of the wave equation treats acoustic signals as small, fluctuating disturbances.

ASSUMPTIONS AND GOVERNING EQUATIONS

First, the assumptions inherent in the wave equation are stated:

Assumptions:

- inviscid, irrotational, isotropic, homogeneous, and continuous fluid
- linear, reversible, adiabatic process
- no external (body) forces
- steady translation of fluid medium only
- relative compression is very small ($\Delta\rho \ll \rho_o$)
- no local sources of sound

- spatial variations of properties are relatively small

Next, the definition of acoustic signals as small, fluctuating values about the ambient fluid property values may be shown expressed for a particular property as

$$p(x,y,z,t) = p_o(x,y,z,t) + p'(x,y,z,t), \tag{A.1}$$

where p_o is the ambient value and p' is the acoustic component.

Now the governing fluid mechanic equations are the momentum equation for inviscid flow (Euler's equation)

$$\rho\left(\frac{\partial \mathbf{v}}{\partial t} + \mathbf{v}\cdot\nabla\mathbf{v}\right) = -\nabla p \tag{A.2}$$

and the continuity equation

$$\frac{\partial \rho}{\partial t} + \mathbf{v}\cdot\nabla\rho + \rho\nabla\cdot\mathbf{v} = 0. \tag{A.3}$$

A relationship between static pressure, density and temperature derives from the energy equation in the general sense. Here, the functional relation between any three thermodynamic properties may be used to write an expression for the pressure in terms of density and entropy:

$$\rho = \rho(p, S) \tag{A.4}$$

Differentiating, we get

$$d\rho = \frac{1}{c^2} dp + \left(\frac{\partial \rho}{\partial S}\right)_p dS \tag{A.5}$$

where $c^2 = \frac{1}{\left(\frac{\partial \rho}{\partial p}\right)_S}$.

For an isentropic process, the previous equation relates the two substantial derivatives of the pressure and density via the coefficient c^2. By the last assumption, this coefficient may be assumed to be constant. Integrating the isentropic form from the background state, we get the equation of state for an acoustic disturbance

$$p' = p - p_o = c^2(\rho - \rho_o) = c^2 \rho'. \tag{A.6}$$

Rewriting the continuity equation using the acoustic variables defined earlier, the expression becomes

$$\frac{\partial \rho'}{\partial t} + \mathbf{v}' \cdot \nabla(\rho_o + \rho') + (\rho_o + \rho')\nabla \cdot \mathbf{v} = 0. \tag{A.7}$$

Applying the governing assumptions, the acoustic form of the continuity equation becomes

$$\frac{\partial \rho'}{\partial t} + \rho_o(\nabla \cdot \mathbf{v}) = 0. \tag{A.8}$$

Similarly, the acoustic form of the momentum equation may be shown to be

$$\rho_o \frac{\partial \mathbf{v}'}{\partial t} = -\nabla p'. \tag{A.9}$$

ACOUSTIC WAVE EQUATION

The acoustic forms of the continuity, momentum and state equations may be combined to form a second-order equation relating the temporal and spatial fluid property fluctuations about their ambient values. Taking the divergence of the momentum equation and the partial derivative of the continuity equation yields the following two expressions

$$\frac{\partial^2 \rho'}{\partial t^2} + \rho_o \left(\nabla \cdot \frac{\partial \mathbf{v}}{\partial t} \right) = 0 \tag{A.10}$$

and

$$\rho_o \left(\nabla \cdot \frac{\partial \mathbf{v}}{\partial t} \right) = -\nabla^2 p'. \tag{A.11}$$

Substituting the for the common term, we get

$$\frac{\partial^2 \rho'}{\partial t^2} - \nabla^2 p' = 0. \tag{A.12}$$

This expression can now be written using either acoustic density or pressure. The form used throughout this report uses pressure, thus the acoustic wave equation may be written as

$$\nabla^2 p' - \frac{1}{c^2} \frac{\partial^2 p'}{\partial t^2} = 0. \tag{A.13}$$

Vita

William R. Saunders was born in Washington, D.C. on May 3, 1955. He grew up in the town of Fairfax, Virginia, in an era when cows roamed abundant pasture land and Tyson's Corner was actually just a corner of a well-travelled rural crossroad. He graduated from Fairfax High School in 1973. A year of hard work convinced him to enroll in nearby George Mason University where he completed two years of general undergraduate course requirements. William transferred to Florida Atlantic University in Boca Raton, Florida where he entered the Ocean Engineering Department. He received a bachelor's degree in Ocean Engineering in June, 1981. After returning to the Washington, D.C. area for employment at the David Taylor Research Center, William married Constance Fitzsimmons. He continued his education on a part-time basis, completing his master's degree in Ocean and Marine Engineering at George Washington University in December, 1985. William and Connie had three children, Emily, Laura and Benjamin between the years of 1984 and 1988. William began to pursue his doctorate at VPI&SU in the fall of 1988. William and Connie separated in June, 1990. William continued a dual role as student and active father, blessed with the children three days of the week. He graduated with a PhD in Mechanical Engineering in December, 1991. Upon graduation he accepted a job as a Research Associate at VPI&SU.